

SEMICONDUCTOR NANOPARTICLES AND THEIR INTERACTION WITH ORGANIC DYES

A DISSERTATION

*Submitted in partial fulfillment of the
requirements for the award of the degree*

of

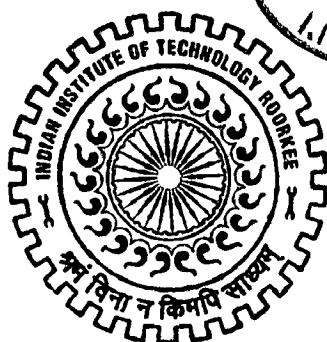
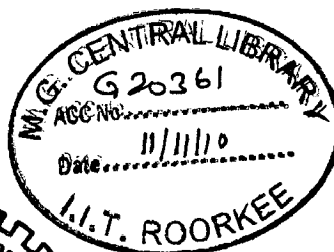
MASTER OF TECHNOLOGY

in

NANOTECHNOLOGY

By

U. RAJESH KUMAR



CENTRE OF NANOTECHNOLOGY
INDIAN INSTITUTE OF TECHNOLOGY ROORKEE
ROORKEE-247 667 (INDIA)

JUNE, 2010


Candidate Declaration

I hereby certify that the work presented in dissertation entitled **“SEMICONDUCTOR NANOPARTICLES AND THEIR INTERACTION WITH ORGANIC DYES”** in partial fulfillment of the requirements for the award of the degree of **Master of Technology** submitted at the **Centre of Nanotechnology, Indian Institute of Technology Roorkee** is an authentic record of my own work carried out during the period from July 2009 to June 2010 under the supervision of **DR. K. R. Justin Thomas**

Date: 30/06/10.


(U. Rajesh Kumar)

This is to certify that the above statement made by the candidate is correct to the best of my knowledge and belief.


30/6/10
Dr. K. R. Justin Thomas
Assistant Professor
Department of Chemistry
Indian Institute of Technology
Roorkee

Acknowledgements

I take this opportunity with much pleasure to thank all the people who have helped me through the course of my journey towards producing this dissertation.

It is my proud privilege to express my sincere gratitude to **Dr. K. R. Justin Thomas** who suggested the field for the present study and has been one of the main sources of encouragement, moral support and valuable guidance from early stage of this research as well as giving me extraordinary experiences throughout the work. Above all and the most needed, he provided me unflinching encouragement and support in various ways. His truly scientist intuition has made him as a constant oasis of ideas and passions in science, which exceptionally inspire and enrich my growth as a student, a researcher and a scientist want to be. I am also thankful to him for encouraging the use of correct grammar and consistent notation in my writings and for carefully reading and commenting on countless revisions of this dissertation. His patience and support helped me overcome many crisis situations and finish this dissertation. Apart from the subject of my research, I learnt a lot from him, which I am sure, will be useful in different stages of my life. I am indebted to him more than he knows.

I would like to thank **Prof. Anil kumar**, Head, Centre of Nanotechnology, IIT-Roorkee for encouraging and allowing us to present the project at our department premises for the partial fulfillment of the requirements leading to the award of M.Tech degree.

I am especially grateful to **Prof. Kamaluddin**, Head of the Department of Chemistry, IIT-Roorkee for providing me all the instrumental and chemical facilities from the department.

This is a great opportunity to express my respect to **Dr. Jayaganathan** (Project coordinator M.Tech.) and **Dr. B. S. S. Daniel** (Subject coordinator) for his encouragement and practical advices. I am pleased to thank **Dr. P. Jeevanandam** and **Dr. K. Gosh** for providing me instrumentation facility whenever I needed.

I am very thankful to my friend Mr. Shaik Firdoz, who has been all ways with me to guide in a correct pathway; I learned lot and still learning from him which is really helping to my life.

One of the most important persons who have been with me in every moment of my dissertation tenure is Mr. Abhishek Bhaeti. I would like to thank him for the many sacrifices he has made to support me.

Special thanks to Mr. B.M.N.K Prasad and Mr. Venkateshwara Rao who have been guided me and supported to finish my dissertation work.

There are a number of people in my everyday circle of colleagues Mr. Abhishek Pathak, Miss. Payal Tayagi, Mr. Dhirendra kumar, Mr. Shushil Rajpoot, Miss. Neha Kapoor, who have supported me a lot.

Very special thanks to all of my class mates for their continuous support and help to complete all my obstacles in my M.Tech program.

I have been fortunate to come across very helpful, decent, noble and funny friends Mr. Ramesh, Mr. Siva Chittrambalam, Mr. A. Naren, Mr. V. Visuventhan, Mr. S. M. Karthik, Mr. S. Raja, Mr. R. Manikandan, Mr. R.M. Shanmuganathan, Mr. V.R. Sreenivasan, Mr. Perumal, Mr. Selvavinayagam, Mr. K.C. Praveen, Mr. C. Rajan, and Mr. C. Ravi Kumar without whom my life would be bleak. They have helped me stay sane through my difficult, thorny, and problematic time. Their support and care helped me overcome setbacks and stay focused on my study. I greatly value their friendship and I deeply appreciate their belief in me. I will forever remember the memories with them.

Finally, this dissertation would not have been possible without the confidence, endurance and support of my family. My family has always been a source of inspiration and encouragement. I wish to thank my parents and uncle, whose love, teachings and support have brought me this far.

U. Rajesh Kumar

Table of Contents

<i>Candidate's declaration</i>	i
<i>Acknowledgements</i>	ii
<i>Table of Contents</i>	iv
<i>List of figures</i>	vi
<i>List of Tables</i>	viii
<i>Abstract</i>	ix
Chapter 1 Aim and Scope	1
1.1 References	4
Chapter 2 Semiconductor nanoparticles/quantum dots and their interaction with organic dyes : A review	7
2.1 Introduction	7
2.2 Characteristics of titanium dioxide	8
2.3 Types of TiO ₂ nanoparticles	9
2.4 Physical characteristics of anatase TiO ₂	10
2.5 Physical characteristics of brookite TiO ₂	11
2.6 Physical characteristics of rutile TiO ₂	13
2.7 Preparation of TiO ₂ nanoparticles	14
2.8 Other forms of TiO ₂	19
2.8.1 Nanotubes and Nanorods	19
2.8.2 Thin films	22
2.9 Doping of TiO ₂ with metal ions	24
2.10 Coating of organic dyes with TiO ₂ nanoparticles	28
2.11 Application in dye sensitized solar cells	30
2.12 Other applications	33
2.12.1 Pigment	33
2.12.2 Photocatalytic applications	34
2.12.3 Waste water remediation using TiO ₂	36
2.13 Cadmium sulfide	38
2.13.1 Physical and chemical properties of CdS	38
2.14 Types of CdS	39
2.15 Physical characteristics of greenockite	40
2.16 Physical characteristics of hawleyite	42
2.17 Preparation of CdS nanoparticles	42
2.18 Other forms of CdS	44
2.18.1 Nanotubes	44
2.18.2 Nanofibres	45
2.19 Coating of organic dyes with CdS nanoparticles	45
2.20 Application in solar cells	46
2.21 Conclusions	48
2.22 References	49
Chapter 3 Semiconductor nanoparticles: Synthetic and analytical procedures	53
3.1 Introduction	53
3.2 Materials	54
3.3 Physical methods	55
3.4 Synthesis of anatase TiO ₂ nanoparticles	55
3.5 Coating of organic dyes on TiO ₂ nanoparticles	56

3.6	Synthesis of cadmium sulfide nanoparticles	56
3.6.1	Method A	56
3.6.2	Method B	56
3.7	Interaction of organic dyes with CdS nanoparticles	57
3.8	Conclusion	57
3.9	References	57
Chapter 4	Characterization: Semiconductor nanoparticles and their interactions with organic dyes	59
4.1	Introduction	59
4.2	Synthesis and characterization of TiO ₂ nanoparticles	61
4.2.1	XRD analysis	61
4.2.2	Solid state electronic spectra	62
4.2.3	FE-SEM analysis	63
4.2.4	Elemental analysis	64
4.3	Coating of organic dyes on TiO ₂ nanoparticles and their characterization	66
4.3.1	Solid state electronic spectra	66
4.3.2	XRD analysis	68
4.3.3	Thermal analysis	71
4.3.4	FE-SEM analysis	73
4.4	Synthesis and characterization of blue emitted colloidal CdS solution	78
4.4.1	Absorption characteristics of the CdS colloids	78
4.4.2	Emission characteristics of the CdS colloids	79
4.4.3	FE-SEM analysis	79
4.5	Interaction of organic dyes with blue emitting CdS particles	80
4.6	Synthesis and characterization of green emitted colloidal CdS solution	83
4.6.1	Absorption characteristics of the green emitting CdS colloids	84
4.6.2	Emission properties	84
4.6.3	FE-SEM analysis	85
4.7	Interaction of organic dyes with green emitting CdS colloids	86
4.8	Synthesis and characterization of CdS/TiO ₂ /D2 nanostructures	89
4.8.1	Absorption spectra	90
4.8.2	Emission properties	90
4.8.3	FE-SEM and EDAX analysis	91
4.9	Conclusions	94
4.10	References	95
Chapter 5	Summary	99

List of Figures

Figure 2.1	Anatase unit cell 3D balls	10
Figure 2.2	Brookite unit cell 3D balls	12
Figure 2.3	Rutile unit cell 3D balls	13
Figure 2.4	SEM images of nanocrystalline TiO ₂ samples calcined at different temperatures	18
Figure 2.5	SEM cross-section view of multi layer TiO ₂ nanorods	20
Figure 2.6	SEM images of different TiO ₂ nanotubes obtained by hydrothermal method.	21
Figure 2.7	TEM images of undoped (a), Al-doped (b), W-doped (c) (Al+W)-doped TiO ₂ powder (d)	26
Figure 2.8	FE-SEM images of (a) TiO ₂ and (b-d) ZnO/TiO ₂ films coated onto FTO glass at different time intervals 5, 30, and 60 min	27
Figure 2.9	Scheme of dye sensitized solar cells	32
Figure 2.10	Different colored paints prepared from TiO ₂	33
Figure 2.11	Role of TiO ₂ as photocatalyst	35
Figure 2.12	Dye waste-water treatment system using TiO ₂ /ITO-oxide electrode	37
Figure 2.13	Greenockite unit cell	40
Figure 2.14	Hawleyite unit cell	42
Figure 2.15	SEM images of CdS nanotubes	44
Figure 2.16	SEM images of CdS nanofibres	45
Figure 2.17	Scheme of quantum dot solar cells	47
Figure 3.1	Structures of the dyes used in this study	54
Figure 4.1	Procedure for the preparation of anatase TiO ₂ nanoparticles	60
Figure 4.2	XRD pattern of heat treated TiO ₂ nanoparticles	62
Figure 4.3	Reflectance and absorbance spectra of heat treated and untreated TiO ₂ nanoparticles	63
Figure 4.4	FE-SEM images of heat treated TiO ₂ nanoparticles at magnification (a) 40,000X & (b) 50,000X	64
Figure 4.5	FE-SEM (a) and EDAX spectrum (b) of the heat treated TiO ₂ nanoparticles	64
Figure 4.6	FE-SEM (a) and EDAX spectrum (b) of TiO ₂ nanoparticles	65
Figure 4.7	Reflectance and absorbance spectra of the dye (D1) coated TiO ₂ nanoparticles	66
Figure 4.8	Reflectance and absorbance spectra of the dye (D2) coated TiO ₂ nanoparticles	67
Figure 4.9	Reflectance and absorbance spectra of the dye (D3) coated TiO ₂ nanoparticles	67
Figure 4.10	Reflectance and absorbance spectra of the dye (D4) coated TiO ₂ nanoparticles	68
Figure 4.11	XRD pattern of the dye (D1) coated TiO ₂ nanoparticles	69
Figure 4.12	XRD pattern of the dye (D2) coated TiO ₂ nanoparticles	69
Figure 4.13	XRD pattern of the dye (D3) coated TiO ₂ nanoparticles	70
Figure 4.14	XRD pattern of the dye (D4) coated TiO ₂ nanoparticles	70
Figure 4.15	TG and DTG curve of the dye (D1) coated TiO ₂	71
Figure 4.16	TG and DTG curve of the dye (D2) coated TiO ₂	71
Figure 4.17	TG and DTG curve of the dye (D3) coated TiO ₂	72
Figure 4.18	TG and DTG curve of the dye (D4) coated TiO ₂	72
Figure 4.19	FE-SEM images of the dye (D1) coated TiO ₂ nanoparticles at magnification (a) 20,000X & (b) 50,000X	73

Figure 4.20	FE-SEM images of the dye (D2) coated TiO ₂ nanoparticles at magnification (a), (b) 20,000X (b) 50,000X &(d) 1,00,000X	74
Figure 4.22	FE-SEM images of the dye (D3) coated TiO ₂ nanoparticles at magnification (a) 50X (b) 10,000X	75
Figure 4.22	FE-SEM images of the dye (D4) coated TiO ₂ nanoparticles	75
Figure 4.23	Absorbance spectrum of the blue emitting CdS quantum dots in DMF	78
Figure 4.24	Emission spectrum of the blue emitting CdS quantum dots in DMF	79
Figure 4.25	FE-SEM images of the blue emitting CdS quantum dots at magnification (a) 20,000X (b) 50,000X &(c) 1,00,000X	80
Figure 4.26	The emission spectra of the blue emitting CdS- D1 system	81
Figure 4.27	The emission spectra of the blue emitting CdS- D2 system	82
Figure 4.28	The emission spectra of the blue emitting CdS- D3 system	82
Figure 4.29	The emission spectra of the blue emitting CdS- D4 system	83
Figure 4.30	Absorbance spectrum of the green emitting CdS quantum dots in DMF	84
Figure 4.31	Emission spectrum of the green emitting CdS quantum dots in DMF	85
Figure 4.32	FE-SEM images of the green emitting CdS quantum dots at magnification (a) 20,000X (b) 50,000X &(c) 1,00,000X	86
Figure 4.33	The fluorescence spectra of the green emitting CdS- D1 system	87
Figure 4.34	The fluorescence spectra of the green emitting CdS- D2 system	87
Figure 4.35	The fluorescence spectra of the green emitting CdS- D3 system	88
Figure 4.36	The fluorescence spectra of the green emitting CdS- D4 system	88
Figure 4.37	Absorption spectra of the CdS/TiO ₂ / D2 composite and D2	89
Figure 4.38	Emission spectra of the CdS/TiO ₂ / D2 composite and D2	90
Figure 4.39	FE-SEM images (a) 10,000X (b) 40,000X (c) 1,00,000X and EDAX spectrum (d) of the CdS/TiO ₂ composites.	92
Figure 4.40	FE-SEM images (a) 50,000X (b) 70,000X (c) 1,00,000X and EDAX spectrum (d) of the CdS/TiO ₂ / D2 composites.	93
Figure 4.41	FE-SEM images (a) 50,000X (b) 70,000X and EDAX spectrum (c) of the CdS/TiO ₂ / D3 composites.	94

List of Tables

Table 2.1	Effect of calcination temperature on physical properties of anatase nanocrystals	19
Table 4.1	Morphology, optical and thermal data observed for the dye coated TiO ₂ nanoparticles	77
Table 4.2	Emission data in DMF solution for blue emitting CdS+ (D1-D4) mixtures	83
Table 4.3	Emission data in DMF solution for green emitting CdS+ (D1-D4) mixtures	89

Abstract

The composites having the compositions TiO₂/Dye, CdS/Dye, and CdS/TiO₂/Dye (where Dye is an organic dye possessing donor-acceptor architecture and carboxylic acid groups) have been synthesized and characterized by different physical methods such as absorption spectroscopy, fluorescence spectroscopy, X-ray diffraction, field emission scanning electron microscopy, and thermogravimetric analysis. The composites derived from (*E*)-2-cyano-3-((4-(diethylamino) phenyl) acrylic acid (**D2**) and TiO₂ exhibited a morphology change from spherical shape of the TiO₂ nanoparticles to the rod shape in the composite. The change in the morphology may be due to the presence of alkyl chain in the dye. The thermal studies revealed an improved stability for each composite when compared to that of the dyes. This establishes the presence of interaction between the anatase TiO₂ nanoparticles and the dye molecules. The interaction of blue and green emitting CdS colloids with the dyes were also investigated by optical and thermal studies. Dyes (*Z*)-2-cyano-3-((4-(dimethylamino) phenyl) acrylic acid (**D1**), (*E*)-2-cyano-3-((4-(diethylamino) phenyl) acrylic acid (**D2**) and (*E*)-2-cyano-3-((4-(diphenylamino) phenyl) acrylic acid (**D4**) effectively accepted the energy from the blue and green emitting CdS colloids in solution. On the contrary no efficient energy transfer occurred between the blue and green emitting CdS particles to the dye (*E*)-2-cyano-3-((4-(methoxy) phenyl) acrylic acid (**D3**). The anomalous behavior is attributed to the comparatively smaller overlap integral observed between the emission of CdS and absorption of the dye (**D3**). Further a slight red-shift observed on increasing the dye concentration may be arising due to the aggregation of the dyes on the CdS surface. The tricomponent composite CdS-TiO₂/**D2** also showed a change in the morphology from homogeneous spherical particles (CdS-TiO₂) to nanofibers (CdS-TiO₂/**D2**).

Chapter 1

Aim and scope

The demand for energy in the world is growing annually. At the moment fossil fuels and nuclear energy are the main sources of energy. These classical energy sources cannot provide us with enough energy for the future any more as these resources are limited and non-replenishable. The stock of carbon-based fuels will be exploited in roughly 50 years from now. Another big problem associated with fossil fuels is that carbon dioxide, the final product of burned fossil fuel, is known to influence the earth climate significantly. Nuclear energy has always been subjected to intensive public discussion due to the security and health risks posed by the nuclear power stations and the disposal problems associated with the radioactive waste. To remedy these problems, concerted efforts have been made to develop new alternate energy sources over the last decades. One of the alternative energy sources is solar energy. The sun is a non-replenishable energy source. It is reliable, clean, and available freely all over the world.

Solar energy is a major energy source due to its harvesting nature of wide spectrum of photons contained in solar radiation and their various applications. Solar cell is a device that converts the energy of sunlight into electricity by a photovoltaic module. The photovoltaic modules are made of semiconductor materials, such as silicon. Photons from the sunlight hit the solar panels and absorbed by the silicon materials, the electrons in the semiconductor materials becomes excited and move to the conduction band of the semiconductor materials, and from there it moves to anode then to cathode through a external circuit which makes the electricity. The common solar power conversion efficiencies achieved with silicon based

solar cells are in the range 15 - 20%. Despite the improvements envisaged over the past decades, silicon based photovoltaic technology has some drawbacks. These include, expensive raw materials, cumbersome fabrication methods, very sensitive to light variations and the lack of environment friendliness. These limitations affect the execution of the solar electricity in a large scale. Therefore, a high efficiency and low cost solar cell technology is the need of the time.

Nanotechnology is currently a flourishing inclination in the science and technology. Development of material engineering in the nanometer scale has produced new photovoltaic materials and systems those could possibly lead to accomplishment of low-cost solar cells in the future. These materials comprise different types of synthetic organic materials and inorganic nanoparticles or nanoparticle systems. The solar cells based on these materials are identified as organic solar cells or molecular solar cells. Three different types of solar cells based on the advances in nanotechnology have emerged: (i) dye sensitized solar cells (DSSC), (ii) hybrid organic solar cells, and (iii) quantum dot solar cells (QDSC). The capture and conversion of light energy in these solar cells is facilitated by modifying a nanostructured semiconductor interface with a dye, conjugate polymer, or semiconductor nanocrystal, respectively. Improving the efficiency of photo-induced charge separation and transport of charge carriers across these nano-assemblies remains a challenge which in turn affects the overall efficiency of the device.

DSSC is one of the most impetus developments occurred in the field of photovoltaics in the last two decades. It was first demonstrated by Grätzel a Swiss scientist, who won the greatest technological innovation of the century award. Excitonic solar cells, such as organic, hybrid organic and inorganic solar cells are promising devices for inexpensive, large-scale solar energy conversion panels. DSSCs are an exciting variant of the

most efficient and stable of the excitonic photovoltaic devices. In these photoelectrochemical cells, a semiconductor nanoparticle such as TiO_2 , ZnO , etc, was used to improve the electron transport in the solar cells. Researchers have designed alternate semiconductor morphologies, such as arrays of nanowires and a combination of nanowires and nanoparticles, to provide a high surface to volume ratio. It allows more adsorption of dyes on semiconductor nanoparticles and the dye modified surface enhances the absorbance in the visible region. Fabricating such a device is an easy process and requires low cost.¹⁻³

Hybrid solar cells combine advantages of both organic and inorganic semiconductors. Hybrid photovoltaics have organic materials such as conjugated polymers those absorb light as the donor and transport holes.⁴ Inorganic materials in hybrid cell are used as the acceptor and electron transporter. The two materials are assembled together in a heterojunction type photoactive layer. By placing one material into contact with each other, the power conversion efficiency can be greater than a single material.⁵ The hybrid photovoltaic device has a significant potential for not only low-cost, but also for scalable solar power conversion. These devices are sometimes referred to as heterojunction solar cells.

Research emphasis in the area of quantum dot solar cells has been aimed at utilizing the unique optical and electronic properties of semiconductor nanocrystals for capture and conversion of light energy.⁶⁻¹⁰ The size-dependent properties of CdSe ,¹¹ CdS ,¹² and other semiconductor nanocrystals make them suitable for tuning the photo response of the solar cells. Quantum dot (QD) solar cells have the potential to increase the maximum attainable thermodynamic conversion efficiency of solar photon conversion up to about 66% by utilizing hot photo-generated carriers to produce higher photo-voltages or higher photocurrents. However, the efficiencies of quantum dot sensitized solar cells have remained rather low (1-2%) when compared to DSSC and organic hybrid cells. The

semiconductor/electrolyte interface plays a crucial role in dictating hole transfer and anodic corrosion of the semiconductor. More focused efforts are necessary to design functionalized or hybrid nanostructures in order to improve the efficiency of these solar cells and minimize the photo corrosion processes.¹³ As the quest for energy solutions continues, we can expect many new exciting discoveries to aid in the capture and conversion of light energy economically and efficiently. Needless to say the study ground and excited state behaviour of the nanoparticles, organic dyes and the nanoparticle-dye conjugates will continue to play an essential role in providing a fundamental understanding of light induced processes and charge transfer events. Also evaluating the interactions of organic dyes (donors) with semiconductor nanoparticles (acceptors) will also enrich our understanding about the electron injection and transfer kinetics at their interface.

In this present work, our main goal is to develop hybrid nanocrystalline semiconductor based organic dye conjugates suitable for application in dye sensitizer solar cells and quantum dot solar cells. So, we focus our attention to synthesize different sizes of anataseTiO₂ and CdS nanoparticles by simple chemical methods and characterize by absorption spectroscopy, spectrofluorimetry, X-ray diffractometer (XRD), and field emission scanning electron microscopy (FE-SEM). It is also our aim to develop organic dye coated nanoparticles and study their absorption and emission properties, thermal and surface morphology.

1.1 References

1. O'Regan, B.; Grätzel, M. *Nature* **1991**, *353*, 737-740.
2. Deb, S. K. *Sol. Energy Mat. Sol. C* **2005**, *88*, 1-10.
3. Kima, K. E.; Song-Rim Janga; Parkb, J.; Vittala, B.; Kang-Jin Kima. *Sol. Energy Mat. Sol. C* **2007**, *97*, 366-370.
4. Milliron, D. J. *MRS Bull.* **2005**, *30*, 41-44.

5. Saunders, B. R.; Turner, M. L. *Adv. Colloid Interface Sci.* **2008**, *138*, 1–23.
6. Mora-Sero, I.; Bisquert, J.; Dittrich, T.; Belaidi, A.; Susha, A. S.; Rogach, A. L. *J. Phys. Chem. C* **2007**, *111*, 14889–14892.
7. Lee, H. J.; Yum, J. H.; Leventis, H. C.; Zakeeruddin, S. M.; Haque, S. A.; Chen, P.; Seok, S. I.; Grätzel, M.; Nazeeruddin, M. K. *J. Phys. Chem. C* **2008**, *112*, 11600–11608.
8. Tachibana, Y.; Umekita, K.; Otsuka, Y.; Kuwabata, S. *J. Phys. Chem. C* **2009**, *113*, 6852–6858.
9. Guijarro, N.; Lana-Villarreal, T.; Mora-Sero, I.; Bisquert, J.; Gomez, R. *J. Phys. Chem. C* **2009**, *113*, 4208–4214.
10. Cui, S. C.; Tachikawa, T.; Fujitsuka, M.; Majima, T. *J. Phys. Chem. C* **2008**, *112*, 19625–19634.
11. Neeleshwar, S.; Chen, C. L.; Tsai, C. B.; Churn, Y. Y. *Phys. Rev. B* **2002**, *71*, 201307-201311.
12. Ma, G.; Tang, S.; Sun, W.; Shen, Z.; Huang, W. *J. Phys. Lett. A* **2002**, *299*, 581-585.
13. Tvrđy, K.; Kamat, P. V. *J. Phys. Chem. A* **2009**, *113*, 3765–3772.

Chapter 2

Semiconductor nanoparticles/quantum dots and their interaction with organic dyes: A

Review

2.1 Introduction

Quantum dots (QDs) are the inorganic semiconductor nanocrystal whose sizes are smaller than the bohr exciton radius and they exhibit size dependent optical properties.¹ The quantum dots exhibit fluorescence properties, *i.e.*, red to blue shift as their size decreases and hence it is tunable and one can obtain a range of colors.² The QDs display narrow size-tunable emission from visible to IR wavelengths, high quantum yields and are resistant to photo bleaching as well as to chemical degradation. The applications of QDs have been explored in various domains of science and technology, *e.g.*, thin film transistors, solar cells, LEDs, lasers and as medical imaging agents.³ Compared to the organic dyes and fluorescent proteins which are conventionally used for bio-imaging, the quantum dots or the nanocrystal fluorophores are significantly better due to their novel optical and electronic properties. By controlling the sizes of the QDs it has not only been possible to achieve *in vivo* imaging of different structures in a cell and in tissues but also to image cellular interactions using

multicolor QDs.⁴ In addition, these materials are finding excellent applications in nanodiagnostics, targeted drug delivery and photodynamic therapy.⁵

Over the decades new methodologies have been developed to prepare semiconductor nanoparticles and quantum dots. Attempts have also been made to evaluate the interaction of organic dyes and natural proteins with nanoparticles. In this chapter, a brief survey of the chemical and physical properties of the titanium dioxide and cadmium sulfide nanoparticles and their uses in various fields is presented.

2.2 Characteristics of titanium dioxide

Titanium dioxide, also known as titanium (IV) oxide or titania, is the naturally occurring oxide of titanium, chemical formula TiO_2 and the most used chemical form of titanium. Titanium dioxide occurs in nature as well-known minerals rutile, anatase and brookite, and additionally as two high pressure forms, a monoclinic baddeleyite-like form and an orthorhombic $\alpha\text{-PbO}_2$ -like form. The most common and stable form is rutile. Anatase and brookite both convert to rutile upon heating. Rutile, anatase and brookite all contain six coordinated titanium.⁶

Titania (TiO_2) powder is one of the most important particulate materials used for many purposes, because of its excellent optical properties of a high refractive index leading to a high hiding power and whiteness, chemical stability, and relatively low production cost.⁷ Out of the yearly use of about 4 million tons in the world, about 60% is used as a pigment for paints, 30% as a filler of plastics and papers, and the remaining 10% for miscellaneous purposes, such as enamels or glazes of ceramics, optical glasses, toners, and cosmetics. Recently, fine particles of titania have attracted a great deal of attention, because of their specific properties as an advanced semiconductor material, such as a solar cell,⁸⁻¹⁰

luminescent material,¹¹⁻¹² and photocatalyst for photolysis of water¹³⁻¹⁶ or organic compounds^{13,14,17-19} and for bacteriocidal action.²⁰⁻²¹

Oxide semiconductors are favored in photo electrochemistry because of their excellent stability against photo-corrosion on optical excitation in the band gap. Moreover, the large band gap (>3 eV) of the oxide semiconductors is needed in DSSC for the transparency of the semiconductor electrode for the large part of the solar spectrum. In addition to TiO₂, semiconductors used in porous nanocrystalline electrodes in dye-sensitized solar cells include for example ZnO, CdSe, CdS, WO₃, Fe₂O₃, SnO₂, Nb₂O₅, and Ta₂O₅. Yet, titanium dioxide has been, and still is, the underpinning semiconductor for dye-sensitized nanostructured electrodes for DSSCs.

2.3 Types of TiO₂ nanoparticles

Two crystalline forms of TiO₂ are common, anatase and rutile. Anatase looks as pyramid-like crystals and is stable at low temperatures, whereas needle-like rutile crystals are dominantly formed at high temperature processes. Single crystals of TiO₂ also have rutile structure. The densities are 3.89 g/cm³ and 4.26 g/cm² for anatase and rutile respectively. Rutile absorbs ca. 4% of the incoming light in the near-UV region, and band gap excitation generates holes that act as strong oxidants that moderate the long-term stability of the dye-sensitized solar cells. The band-gaps of the crystalline forms are 3.2 eV for anatase and 3.0 eV for rutile.

The third crystalline form of TiO₂, brookite, is difficult to produce and is therefore not of practical interest for the dye-sensitized solar cells. Anatase has been the main subject of study in DSSCs. In spite of that recent study revealed that dye-sensitized nanostructured TiO₂ electrodes with pure rutile structure exhibited only 30% smaller short circuit photocurrents than pure anatase films and practically equal open circuit photo voltage.²²

2.4 Physical characteristics of anatase TiO_2

Anatase is a polymorph with two other minerals. The minerals rutile and brookite as well as anatase all have the same chemical composition, TiO_2 , but they have different structures. At higher temperatures, about 915°C , anatase will automatically revert to the rutile structure. Rutile is the more common and the more well known mineral of the three, while anatase is the rarest. Anatase shares many of the same or nearly the same properties as rutile such as luster, hardness and density. However due to structural differences anatase and rutile differ slightly in crystal habit and more distinctly in cleavage.

Anatase and rutile have the same symmetry, tetragonal $4/m\ 2/m\ 2/m$, despite having different structures. In rutile, the structure is based on octahedrons of titanium oxide which share two edges of the octahedron with other octahedrons and form chains (Figure 2.1). It is the chains themselves which are arranged into a four-fold symmetry. In anatase, the octahedrons share four edges hence the four fold axis.

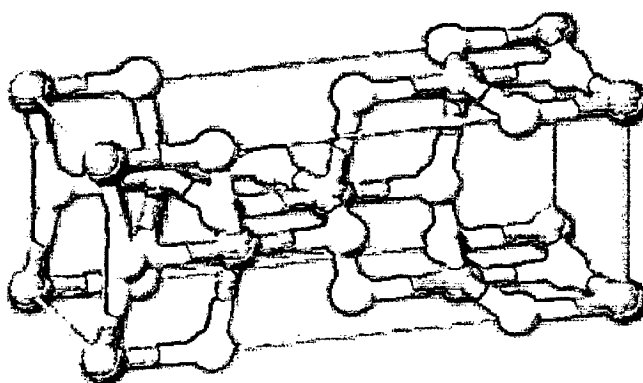


Figure 2.1 Anatase unit cell 3D balls.

Crystals of anatase are very distinctive and are not easily confused with any other mineral. They form the eight faced tetragonal dipyrramids that come to sharp elongated points. The elongation is pronounced enough to distinguish this crystal form from octahedral crystals, but there is a similarity. In fact anatase is wrongly called "octahedrite" in spite of the

difference in forms.

Nice specimens of anatase are associated with quartz and are considered classics in the mineral world. The good cluster well formed crystal shape and interesting character make anatase a popular mineral for collectors.

- Color is brown to black, also yellow and blue.
- Luster is adamantine to sub metallic.
- Transparency crystals are opaque.
- Crystal system is tetragonal; $4/m\ 2/m\ 2/m$.
- Crystal habits include the typical tetragonal dipyramids that come to sharp elongated terminations points. These crystals look like stretched out octahedrons.
- Cleavage is perfect in the basal direction and in four directions, pyramidal.
- Fracture is subconchoidal.
- Streak is white.
- Other characteristics: crystals are easily altered in nature and sometimes pitted.
- Associated minerals include brookite, rutile, quartz, feldspars, apatite, hematite, chlorite, micas, calcite and sphene.
- Notable occurrences include Somerville, Massachusetts and Gunnison Co., Colorado, USA; Tavistock, Devon, England; Austria; Diamantina District, Brazil; in the French Alps and at the Binnatal area of Switzerland.
- Best field indicators are crystal habit, luster, cleavage, density, streak, associations and locality.

2.5 Physical characteristics of brookite TiO_2

Brookite is a polymorph with two other minerals. The minerals rutile and anatase as well as brookite all have the same chemistry, TiO_2 , but they have different structures (Figure 2.2). At higher temperatures, about 750°C brookite will automatically revert to the rutile structure. Rutile is the more common and the more well known mineral of the three. Brookite shares many of the same properties as rutile such as color and luster and some properties are nearly

the same such as hardness and density. However due to structural differences brookite and rutile differ in crystal habit and cleavage.

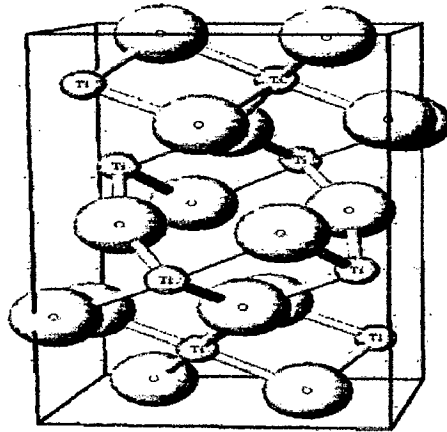


Figure 2.2 Brookite unit cell 3D balls.

- Color is dark brown to greenish black.
- Luster is adamantine to sub metallic.
- Transparency crystals are opaque.
- Crystal system is orthorhombic; $2/m 2/m 2/m$.
- Crystal habits include the typical tabular to platy crystals with a pseudo hexagonal outline. Magnet cove specimens tend to be more equant with complex facets.
- Cleavage is poor prismatically and in the basal direction.
- Fracture is subconchoidal and uneven.
- Streak is light brown to white.
- Associated minerals include anatase, rutile, quartz, feldspars, chalcopyrite, and hematite.
- Notable occurrences include Magnet cove, Arkansas, Butte, Montana, Somerville, Massachusetts and Ellenville, New York, USA; Eicham, Austria; Tremadoc, Wales, England; Ural Mountains, Russia and at St. Gotthard, Switzerland.
- Best field indicators are crystal habit, luster, density, streak, associations and locality.

2.6 Physical characteristics of rutile TiO_2

Rutile is an interesting, varied and important mineral. Rutile is a major ore of titanium, a metal used for high tech alloys because of its light weight, high strength and resistance to corrosion. Rutile is also unwittingly of major importance to the gemstone markets. It also forms its own interesting and beautiful mineral specimens.

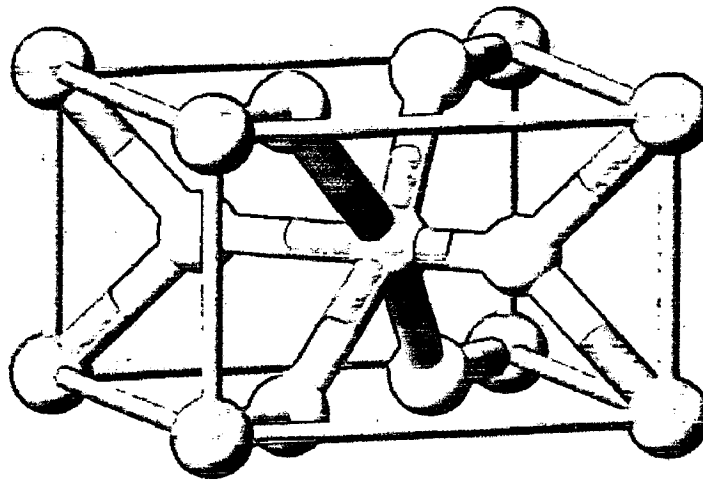


Figure 2.3 Rutile unit cell 3D balls.

Microscopic inclusions of rutile in quartz, tourmaline, ruby, sapphire and other gemstones, produces light effects such as cat's eye and asterisms (stars). A beautiful stone produced by large inclusions of golden rutile needles in clear quartz is called rutilated quartz. Rutilated quartz is sometimes used as a semi-precious stone and/or for carvings. This stone is produced because at high temperatures and pressure, $n(\text{SiO}_2)-n(\text{TiO}_2)$ is in a stable state but as temperatures cool and pressure eases the two separate with rutile crystals trapped inside the quartz crystals.

Twinning is common in rutile crystals, with a cyclic twin forming that is comprised of six or even eight "twins" arranged in a circle (Figure 2.3). A Rutile Star is a formation of crystals

of rutile in a six rayed orientation. The crystals grow off of a hematite crystal and the orientation is caused by its six rhombic faces.

- Color is black or reddish brown in large thick crystals or golden yellow or rusty yellow as inclusions or in thin crystals.
- Luster is adamantine to sub metallic.
- Transparency: crystals are transparent in rather thin crystals otherwise opaque.
- Crystal system is tetragonal; $4/m\ 2/m\ 2/m$.
- Crystal habits include eight sided prisms and blocky crystals terminated by a blunt four sided or complex pyramid. The prisms are composed of two four sided prisms with one of the prisms being dominant. Crystals with some twins forming hexagonal or octahedral circles. A very common habit is thin acicular needles (especially as inclusions in other minerals) or as blades.
- Cleavage is good in two directions forming prisms, poor in a third (basal).
- Fracture is conchoidal to uneven.
- Streak is brown.
- Other Characteristics: striations lengthwise on crystals, high refractive index (2.63) give it a sparkle greater than diamond (2.42).
- Associated minerals are quartz, tourmaline, barite, hematite and other oxides and silicates.
- Notable Occurrences include Minas Geras, Brazil; Swiss Alps; Arkansas, USA and some African localities.
- Best field indicators are crystal habit, streak, hardness, color and high index of refraction (luster).

2.7 Preparation of TiO_2 nanoparticles

Industrially, titania particles are usually manufactured by the treatment of ilmenite ($\text{FeO} \cdot \text{TiO}_2$) with sulfuric acid to produce titanyl sulfate (TiOSO_4), which is then hydrothermally hydrolyzed to anatase or rutile with seed crystals, or alternatively by the chlorination of high-

grade rutile ores with chlorine gas to titanium tetrachloride, which is then evaporated and treated with oxygen to rutile at ca. 1000 °C. In both methods, agglomerated TiO₂ powders are ground and classified into different size grades.²³

In the meantime, a wide variety of methods have been explored and developed for the uniform spherical rutile particles by the forced hydrolysis synthesis of well-defined Titania particles. For example, Matijevi *et al*²⁴ prepared of Ti (IV) ion at 98 °C in highly acidic media in the presence of sulfate ion. The anatase phase was also found to be involved with increasing sulfate concentration. The mean size was on the order of a few micrometers. Bowen^{25, 26} and Oghihara *et al*^{27, 28} prepared uniform amorphous titania spheres on the order of sub micrometers by the hydrolysis of titanium tetraethoxide in ethanol or a mixed solvent of acetonitrile and octanol in sol-gel systems. More recently, with the growing interest in nanotechnology, a number of processes have been applied to the synthesis of nanoparticles of Titania as advanced materials with specific functions. For example, anatase or rutile nanoparticles were prepared in gas phases by hydrolysis of titanium alkoxides^{29, 30} or titanium tetrachloride³¹ at high temperatures. Amorphous nanoparticles were synthesized in reverse micelles in a sol-gel process.^{32, 33} In order to obtain crystalline nanoparticles of titania, titanium hydroxide gel prepared by the sol-gel method was dried and calcined at a high temperature, e.g., below 500 °C for anatase or above 800 °C for rutile, but the phase transition temperature was varied as a function of the preparation conditions of the hydroxide gel.³⁴⁻³⁷ The same purpose can be achieved by hydrolysis of alkoxides in supercritical alcohols^{38, 39} or by hydrothermal hydrolysis at a high temperature such as 150–300 °C.⁴⁰ If the alkoxides used in the hydrothermal reaction to yield anatase particles are replaced by Ti(IV) salts, such as titanium sulfate and titanium tetrachloride, brookite particles are obtained as well as anatase and rutile particles.⁴¹

Bacsa *et al*⁴² prepared rutile and anatase nanoparticles of size 25–55 nm by a hydrothermal process (200–250 °C) of transparent sols, previously prepared by hydrolysis of alkoxides at 20 °C in a sol–gel process with aging at 80 °C for 8 h in 0.074 mol dm⁻³ HNO₃. Here rutile particles were obtained when ethoxide was used as a precursor alkoxide, while isopropoxide and butoxide predominantly yielded anatase. Also, Sugimoto *et al*^{43, 44} found that titanium hydroxide precipitate prepared by the hydrolysis of isopropoxide at room temperature was readily crystallized to anatase even at 100 °C or lower in the neutral and acidic ranges with a maximum transformation rate at pH ~2, as shown in detail in the preceding parts of this series. particularly, in an exceedingly low pH range such as below pH 1, the titanium hydroxide precipitate is slowly crystallized to anatase, rutile, or their mixture even at room temperature.⁴⁵⁻⁴⁸ Cot *et al*⁴⁶ found that while an almost pure anatase phase was observed at 0.25 mol dm⁻³ HNO₃ after the aging of hydroxide precipitate at 60 °C for 24 h, the proportion of rutile phase then gradually increased with increasing concentration of nitric acid up to a maximum of about 60% at 1 mol dm⁻³ HNO₃, and then declined (~40% at 1.25 mol dm⁻³ HNO₃).

Sheng *et al*⁴⁹ developed a useful method in which a two to one mixture of 1-hexadecanamine and titanium but oxide were added to 10 mL absolute ethanol, cooled to 0 °C and, subsequently, 10 mL of water was slowly added to the solution with vigorous stirring. A white viscous precipitate was immediately formed and allowed to age for 24 h at room temperature. After being filtered, the white titanium hydroxide/hexadecane amine complex, Ti(OH)₄/C₁₆H₃₃NH₂, was transferred to a Teflon-lined autoclave and aged at 180 °C for 7 days. The product was then filtered again, washed with water, ethanol and hexane, dried at 60 °C for several hours and calcinated at 500 °C.

Kongsuebchart *et al*⁵⁰ generated nanocrystalline TiO₂ using the solvothermal methods where they used titanium (IV) *n*-butoxide (TNB) as starting material. In general, 15–25 g of TNB was suspended in 100 cm³ of toluene in a test tube, which was then placed in a 300 cm³ autoclave. The gap between the test tube and the autoclave wall was filled with 30 cm³ of the same solvent used in the test tube. The autoclave was purged completely by nitrogen before heating up to 573 K at a rate of 2.5 K/min. Autogeneous pressure during the reaction gradually increased as the temperature was raised. Once the prescribed temperature was reached, the temperature was held constant for 0.5–8 h. After the system was cooled down, the resulting powders were repeatedly washed with methanol and dried in air. The synthesis product was then calcined in a box furnace by heating up to the desired temperature, in the range of 563–583 K, at a rate of 10 K/min and held at that temperature for 1 h in order to remove any impurity that might remain on the samples after washing with methanol.

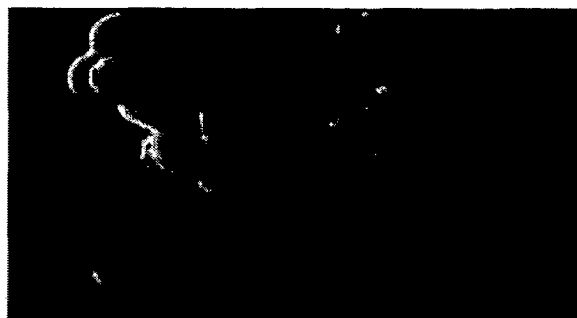
Liau *et al*⁵¹ reported sol–gel method for the constructing TiO₂ nanoparticle in low temperature. The sol–gel TiO₂ was produced by mixing Titanium (IV) isopropoxide (TIP) 3 mL with 30 wt% H₂O₂ 3.17 ml for the mole ratio of 1:12 and together with 99.5% alcohol 94 mL at 75 °C for 6 h. The prepared solution then was spin-coated on the substrate. The coated samples are dried and heated at 75.8 °C for 2 h for fabricating the TiO₂ thin films.

Tayade *et al*⁵² synthesized nanocrystalline TiO₂ by hydrolysis of titanium tetra isopropoxide. A mixture of dry ethanol (100 mL) and titanium tetra isopropoxide (30 mL) was taken in a 250 mL round-bottom flask, continuously stirred for 30 min, and then subjected to ultrasonication for 30 min. Hydrolysis of the titanium tetra isopropoxide solution was carried out by adding distilled water (24 mL) slowly at the rate of 0.5 mL/min with continuous stirring. The solvent from the obtained mixture was removed using a rotavapour apparatus at 343 K under reduced pressure. The powder was then kept in an oven at 393 K

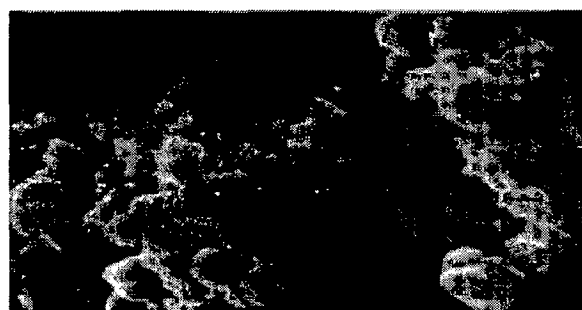
Overnight. The sample thus obtained is identified as NCT-393. The dried sample was calcined at different temperatures (i.e., 583, 673, 753, 833, 913, and 1023 K) under air for 11 h (Figure 2.4).



Calcined at 673K



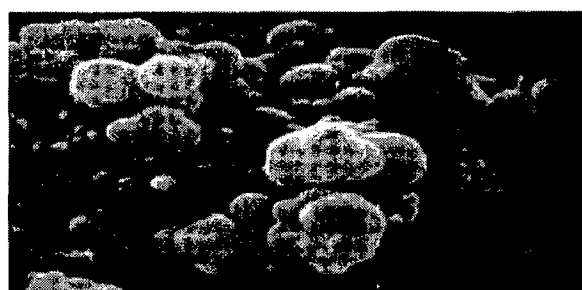
Calcined at 753K



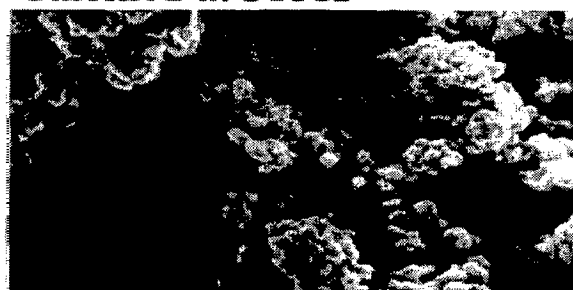
Dried at 393K



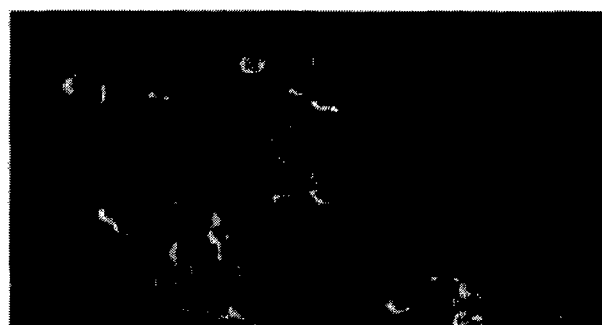
Calcined at 583K



Calcined at 833K



Calcined at 913K



Calcined at 1023K

Figure 2.4 SEM images of nanocrystalline TiO₂ samples calcined at different temperatures.

Table 1.1 Effect of calcination temperature on physical properties of anatase nanocrystals.

Catalyst	BET surface area (m ² g ⁻¹)	Average pore volume (cm ³ g ⁻¹)	Average pore diameter(A)	Anatase crystallite size (nm)	Band edge (nm)	Band gap (eV)
NCT-393	259	0.310	48	08	376.4	3.30
NCT-583	199	0.300	61	09	376.5	3.29
NCT-673	166	0.280	67	12	378.5	3.28
NCT-753	124	0.230	75	14	400.0	3.04
NCT-833	091	0.170	76	19	400.2	3.1
NCT-913	002	0.004	73	29	408.0	3.03
NCT-10233	002	0.005	54	-	411.9	3.01
P-25	061	0.120	82	28	393.7	3.15

From this brief survey of past studies on the synthesis of titania particles, one may notice that the synthesis of uniform crystalline nanoparticles of titania and the systematic control of their size and morphology have never been attained. Thus it seems necessary to study in more detail the underlying mechanism for the formation of titania particles, particularly in the nanosize range, in order to freely control the size and shape of this important particulate material with sufficient uniformity.

2.8 Other forms of TiO₂

2.8.1 Nanotubes and Nanorods

Baek *et al*⁵³ reported the preparation of TiO₂ nanorods. His process basically consists of three steps. Step 1: The stock solution of 3 mol Ti⁴⁺ was diluted with distilled water to obtain 0.5 mol Ti⁴⁺ solution. Step 2: A two liter capacity plastic beaker containing 100 mL of distilled water was taken. Then 0.5 mol Ti⁴⁺ solution and 28% ammonia solution (NH₄OH) were added drop wise (1 drops) simultaneously into 100 mL of distilled water using peristaltic pump. The pH of the resultant solution containing white precipitate was 3.5–4.0. The pH was adjusted to 9.0 with further addition of ammonia solution. The entire contents of the solution were transferred into a glass container and heated to 90 °C for 3 h and filtered.

The precipitate was washed several times to eliminate ions. Step 3: About 8 g (0.02 mole of Ti^{4+}) of the precipitate obtained in step 2 was placed in 500 mL round bottom flask containing 100 mL of distilled water and stirred for 10 min. Then H_2O_2 was added such that the ratio of $\text{Ti}^{4+}/\text{H}_2\text{O}_2$ was 0.0067 with constant stirring. As soon as the addition of H_2O_2 was complete, the color of the precipitate was change from white to turbid yellowish. The transparency of the colloidal solution increased with time and finally light orange colored transparent colloidal solution was formed within 30 min. The pH of the solution was adjusted to 9.00 using 28% NH_4OH solution. The stirring continued for another 3 h. The contents of the solution were divided into two portions. For the first portions of the solutions, the solvent was evaporated at low pressure and the resultant solids were obtained. The second portions of the solution was placed in an oil bath and heated to 100 °C for 3 days with stirring speed of 1000 rpm. At the end, the flask was removed from heating and the solvent was evaporated to dryness to yield white solid nanorods (Figure 2.5).

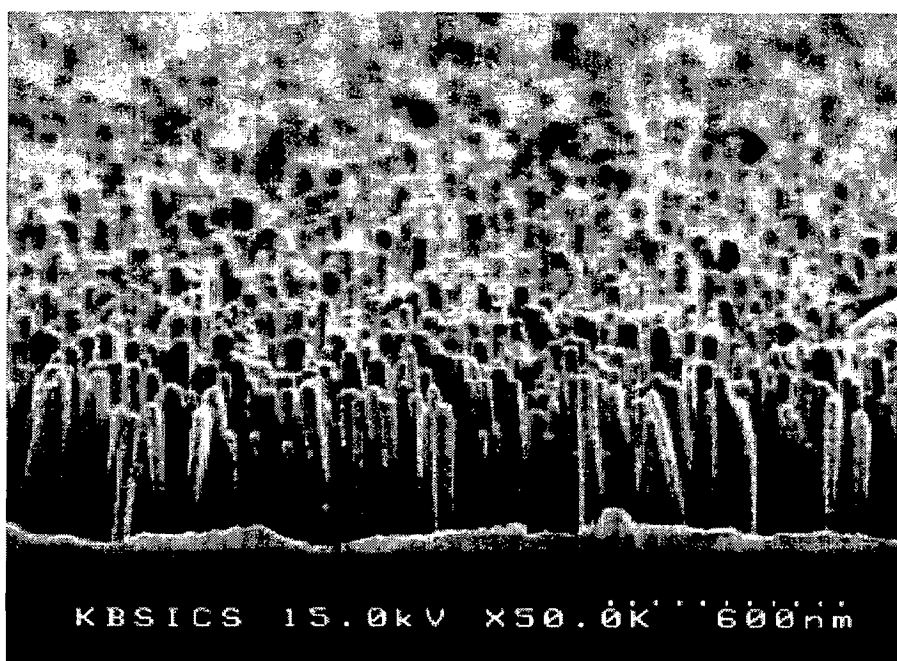


Figure 2.5 SEM cross-section view of multi layer TiO_2 nanorods.

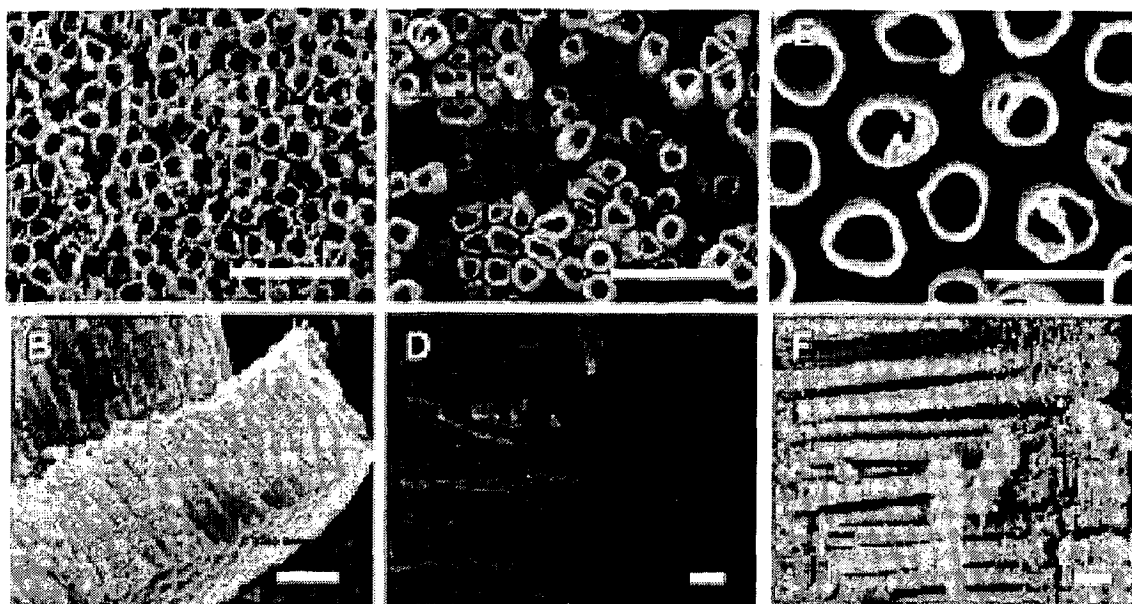
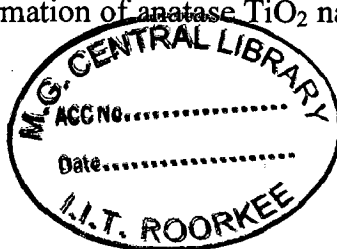


Figure 2.6 SEM images of different TiO₂ nanotubes obtained by hydrothermal method.

Flores *et al*⁵⁴ synthesized TiO₂ nanotube. In this work, anatase TiO₂ nanotubes were prepared. The procedure starts with the addition of 23.5 mL of titanium isopropoxide (Ti (O*i*-C₃H₇)₄) and 4.5 mL of tetraethoxysilane (Si(OEt)₄) in 23 mL of ethanol. The resulting solution was stirred for 15 min at room temperature. In a separate container, 18 g of 4.4 mol HCl in distilled water was added to 23 mL of ethanol. This solution was then slowly added to the mixture of Ti (O*i*-C₃H₇)₄ and Si(OEt)₄ in ethanol. The mixture was allowed to hydrolyze and gel for 3 days at 40 °C and 70% relative humidity. The gel obtained was then heated to 600 °C and held for 2 h, resulting in the precipitation of fine TiO₂ crystals. Amorphous SiO₂-related phases are also present. Part of this gel was treated with a 10 mol NaOH solution for 48 h at 110 °C in an autoclave. Afterwards, the product was washed with distilled water and neutralized with an aqueous 0.1 mol HCl solution. The treated powders were then separated from the mixture by centrifugation and washed with distilled water several times until pH 7. The solid was dried at 90 °C for 3 h followed by calcination at 450 °C for 30 min. This calcination step guarantees the formation of anatase TiO₂ nanotubes, (Figure 2.6) which were evidenced by XRD.



Kim *et al*⁵⁵ synthesized titanate nanotubes by hydrothermal method using commercial Titania (TiO₂) nanoparticles powder as a starting material. A conversion from nanoparticles to nanotubes was achieved by treating the nanoparticle powder with 10 M NaOH at 150 °C, for 48 h, in the autoclave. The precipitates were neutralized thoroughly with distilled water only, then filtered and dried at atmospheric condition (Figure 2.6).

Lee *et al*⁵⁶ for the synthesis and characterization of TiO₂ nanoparticles and nanotubes. Titanium *t*-butoxide (0.03 mol) was dissolved in ethanol (15 mL). Subsequently, 2 mL of acetyl acetone (0.02 mol) was added to the solution and stirred at room temperature for 60 min. This was followed by the addition of 20 mL of 80% acetic acid aqueous solution. The solution was then heated at 80 °C for 5 h with continual stirring. After the solution was cooled to room temperature; the obtained yellow jelly product was washed repetitively with isopropanol and distilled water, followed by drying at 100 °C for 12 h. The dried product was ground into powder using a mortar and pestle. The powder was then calcined at 600 °C for 3 h. As a result, the NTP samples were obtained. NTPs (2 g) were added to the 10 M sodium hydroxide aqueous solution (200 mL). The solution was stirred at 110 °C for three days, and then cooled to room temperature. The resulting products were collected and washed repeatedly in a 0.1 M HCl solution and deionized water until the pH value of the washing solution reached 7. The NTT samples were obtained by drying the products at 110 °C for 24 h.

2.8.2 Thin Films

The preparation of nanocrystalline anatase thin films is of great importance for existing or potential technological applications such as photovoltaic cells, self cleaning windows, electrochemical devices and sensors, coupling membrane separations, and photocatalytic reactions. A key point for some applications is the ability to form anatase layers at low

temperature on substrates exhibiting a low thermal stability such as plastics. Moreover, the accessibility of the chemical species to the titania surface is strongly conditioned by the porous characteristics of the layer: the pore volume, the pore size, the connectivity, and the tortuosity of porous network. An attractive method for tailoring the porosity consists of using the templating effect of mesophases produced by the self-assembly of amphiphilic molecules. Several papers report recent studies on the sol-gel synthesis of mesoporous titania layers using cationic surfactants or diblock or triblock copolymers as structuring agents and titanium chloride, titanium alkoxide or a titanium derivative of triethanolamine as the titania precursor. The as prepared titania layers are mainly amorphous, and thermal nucleation and crystal growth of anatase usually occur for temperatures higher than 350 °C and are often associated with the disappearance of the ordered mesoporosity.

A different procedure was evolved by Zhang *et al*⁵⁷ for the preparation of porous nanocrystalline thick TiO₂ films. In this method pure TiCl₄ was drop wisely added into ice-cold distilled water under vigorous stirring to obtain 1 M stock solution. The solution could be stored for more than one year in a refrigerator without precipitation. 1 M aqueous TiOSO₄·xH₂O solution was prepared by dissolving into distilled water at room temperature. Titanium (IV)-tetra isopropoxide (TTIP) was added into dry ethanol at 1 M. Fresh solutions without precipitates were only used for experiments. Nanocrystalline TiO₂ powder was added to 3.2 g of the 1 M TiCl₄ or TiOSO₄ aqueous solutions, and ground in an agate mortar or about 2 h to get a viscous paste. Since TTIP solution is highly unstable in air, a mixture of 0.8 g P25 and 2.8 g 1 MT TIP solution was prepared in a closed bottle and stirred by a magnetic sifter for one day to get a viscous paste. These pastes were coated on a fluorine-doped SnO₂-coated conductive glass (FTO) or an indium tin oxide (ITO)-coated poly (ethylene terephthalate) (PET) film sheet resistance, ca. 70) by a glass rod and using Scotch tape as spacers. However, the ITO/PET film substrates could not be used for the pastes with TiCl₄

and TiOSO_4 precursors because these acidic pastes damaged the ITO layer, while the paste with TTIP could be used for both substrates. After drying in air at room temperature, the coated substrates were put into a Teflon-lined autoclave. A small amount of distilled water was added at the bottom of the reactor so that the sample is not in direct contact with water but with steam during the reaction. The reactor was placed in an oven at $100\text{ }^\circ\text{C}$ for 12 h. After the hydrothermal treatment, the films were taken out, rinsed with water, and dried in an oven at $100\text{ }^\circ\text{C}$ for 1 h. The resulting film thickness was typically 10 nm, but could be easily controlled by changing the thickness of the spacer.

A film thickness up to 18 nm has been achieved by one coating, without causing any problems in the mechanical stability of the film. In order to confirm the effect of the hydrothermal treatment, a sample without hydrothermal treatment was also prepared. A film was prepared by coating the paste with TTIP precursor and simply drying at $100\text{ }^\circ\text{C}$ in an oven for a control experiment. The hydrothermally-treated film prepared on an FTO glass substrate has also been subjected to a heat treatment at $450\text{ }^\circ\text{C}$ for 30 min to study the effect of post-annealing.

2.9 Doping of TiO_2 with metal ions

Most of the studies were focused on the nanosized TiO_2 with the purpose of improving the light absorption. The high surface-to-volume ratio, inherent in nanoparticles, was useful. Additionally, the small size of TiO_2 crystals can make indirect band electron transition possible and increase the generation rate of electrons and holes. Increase of the generation rate of charge carriers is one way to enhance the photocatalytic activity. On the other hand, electron and hole trapping during their transportation from the interior of the particle to the surface is also very crucial to preventing the recombination of electron and hole pairs. Doping of TiO_2 with transition metal ions offers a way to trap charge carriers and extend the

lifetime of one or both of the charge carriers. Consequently, dopants enhance the efficiency of the photocatalyst. The effect of transition metal dopants on TiO₂ nanoparticles performance is a new area of extensive research.

In photocatalysis, it is the photon-generated electron hole pairs that can facilitate redox reactions on particle surface. The total number of free carriers on the surface determines the efficiency of catalysts. The number and the lifetime of free electron hole are particle size- and dopant-dependent. For large particles, the volume recombination of electrons and holes dominates. This condition largely reduces the number of free charges on the surface and deteriorates the photocatalytic activity. For nanoparticles, the transportation length of e^-/h^+ from crystal interface to the surface is short, which helps to accelerate the migration rate of e^-/h^+ to the surface of the nanoparticle to participate the reaction process. For optimal photocatalysis efficiency there is a critical particle size below which the surface recombination of electron and hole becomes dominant because of the increased surface-to-volume ratio.

TiO₂ semiconductor powders were synthesized by Ko *et al*⁵⁸ using Al and W as photovoltaic property-enhancing impurities (Figure 2.7). Al-doped TiO₂ electrodes increased open-circuit voltage (V_{oc}), but reduced short-circuit current (I_{sc}). In contrast, W-doped TiO₂ had an opposite effect. However, dye-sensitized solar cell efficiency fabricated with doped TiO₂ was remarkably better than that of undoped TiO₂. It seems that these phenomena were related to electrical surface-state modifications induced by metal-ion dopants. These modifications led to significant changes in powder aggregation, charge transfer kinetics, and dye adsorption characteristics. The highest efficiency was found by using aluminum and tungsten doped TiO₂ nanopowders.

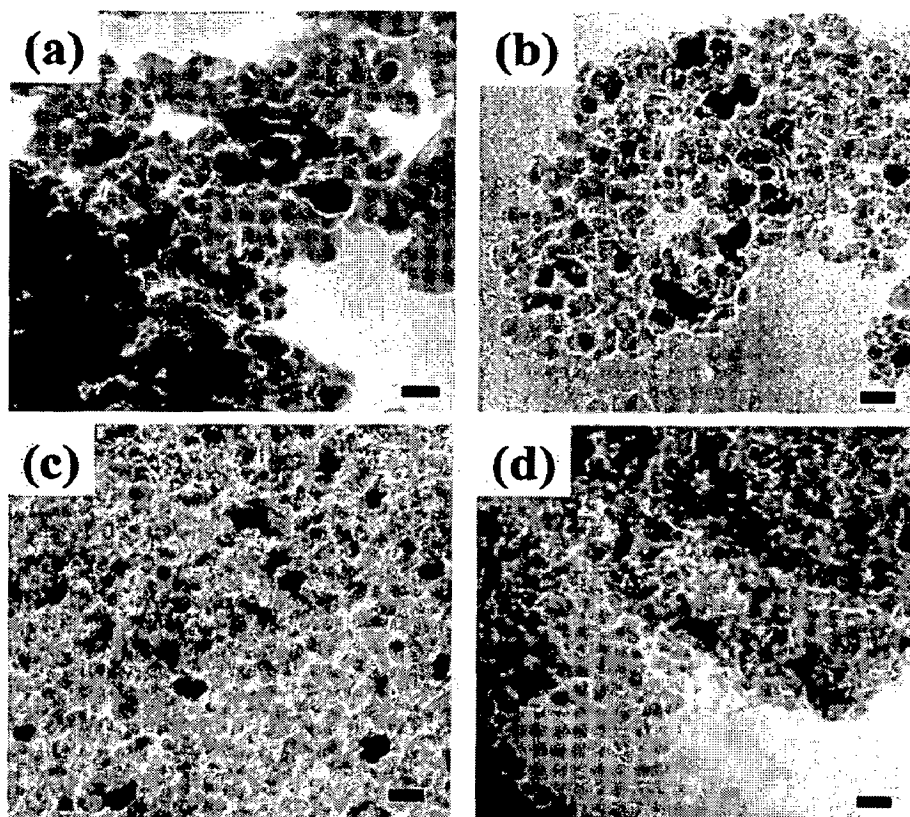


Figure 2.7 TEM images of undoped (a), Al-doped (b), W-doped (c), and (Al +W)-doped TiO_2 powder (d)

The nanostructured mixed metal oxide based on a sol-gel method with surfactant-assisted mechanism, and its application for dye-sensitized solar cell (DSSC) are reported by Kitiyanan *et al.*⁵⁹ The mixed zirconia (ZrO_2) and titania (TiO_2) mesoporous powder possessed larger surface area than the corresponding titania. For the UV action spectra of unsensitized photochemical cell, the mixed zirconia/titania electrode can absorb UV light below 380 nm, corresponding to band gap (E_g) around 3.27 eV, which is higher than that of pure component of titania. Both of these improved properties, i.e., BET surface area and band gap, contributed to the improvement on a short-circuit photocurrent up to 11%, an open-circuit voltage up to 4%, and a solar energy conversion efficiency up to 17%, for the DSSC fabricated by mesoporous zirconia/titania mixed system when compared to the cell that was fabricated only by nanostructured TiO_2 . The cell fabricated by 5 μm thick mixed TiO_2 - ZrO_2 electrode gave the short-circuit photocurrent about 13 mA/cm^2 , open-circuit voltage about 600 mV and the conversion efficiency 5.4%.

Cheng *et al*⁶⁰ prepared nanocrystalline titania films co doped with aluminum and boron by cathodic vacuum arc deposition. In the process, titanium alloy target was used under an O₂/Ar atmosphere, and sensitizations of films were carried out by natural dye-sensitized complex in anhydrous ethanol. The structure, surface morphology and UV-vis spectra of titania films co-doped were measured by X-ray diffraction analysis, scanning electron microscopy and ultraviolet-visible spectrometer. The as-deposited films are found to be amorphous. The films annealed were examined to be of anatase structure with orientation along the (101) planes, the average crystal size is in the range between 41 and 45 nm. SEM results show that there are some pores in the co-doped titania films, the optical properties of the dye-sensitized films were also measured which reveals that the spectral responses of films shift to the visible region. Under simulated sunlight illumination, the overall energy conversion efficiency of dye-sensitized nanocrystalline solar cell is 0.9%.

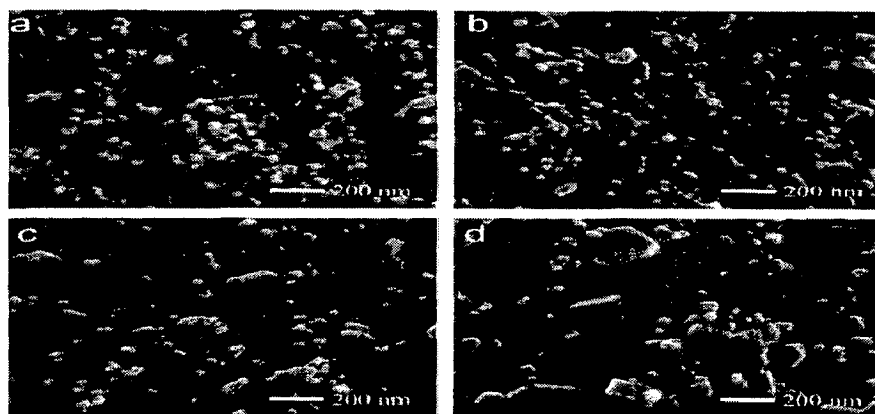


Figure 2.8 FE-SEM images of (a) TiO₂ and (b–d) ZnO/TiO₂ films coated onto FTO glass at different time intervals 5, 30 and 60 min.

For enhancement in the performance of dye-sensitized solar cells containing ZnO-covered TiO₂ electrodes prepared by thermal chemical vapor deposition by Kim *et al*⁶¹ When used in a dye-sensitized solar cell, an enhancement was observed in both short-circuit photocurrent (J_{sc}) and open-circuit voltage (V_{oc}) by 12% and 17%, respectively, relative to those of a cell containing a bare TiO₂ film. The observed J_{sc} enhancement is attributed to the increase in the surface area of the ZnO/TiO₂ film and the V_{oc} enhancement to the formation of a potential

barrier by ZnO at TiO₂/electrolyte interface. The films were characterized by scanning electron microscopy (Figure 2.8), UV-visible spectrophotometer, and x-ray photoelectron spectroscopy. The study results revealed that TiO₂ modification suppresses interfacial recombination which results in increasing efficiency.

Shah *et al*⁶² developed metal organic chemical vapor deposition method was successfully used to synthesize pure TiO₂ and Nd³⁺, Pd²⁺, Pt⁴⁺, and Fe³⁺,doped TiO₂ nanoparticles. Polycrystalline TiO₂ structure was verified with x-ray diffraction, which showed typical characteristic anatase reflections without any separate dopant-related peaks. Transmission electron microscopy observations confirmed the existence of homogeneously distributed 22 nm TiO₂ nanoparticles. The particle size remained the same for the doped samples. The doping level of transition metals was kept at ~1 atomic percent, which was determined by x-ray photoelectron spectra and energy dispersive x-ray spectroscopy. The effects of different types of dopants on the photocatalytic activity were revealed by the degradation of 2-chlorophenols with an UV light source. The photocatalytic efficiency was remarkably enhanced by the introduction of Pd²⁺ and Nd³⁺, Nd³⁺doped TiO₂ showed the largest enhancement. However, Pt⁴⁺changed the 2-chlorophenol degradation rate only slightly, and Fe³⁺ was detrimental to this process. These effects were related to the position of the dopants in the nanoparticles and the difference in their ionic radii with respect to that of Ti⁴⁺.

2.10 Coating of organic dyes with TiO₂ nanoparticles

The conversion of sunlight to electricity using dye-sensitized solar cells (DSSCs) represents one of the most promising methods for future large scale power production from renewable energy sources, due to their easy fabrication techniques as well as low cost method. Briefly DSSCs contain five components: (1) a conductive mechanical support, (2) a wideband gap semiconductor film, (3) a sensitizer, (4) electrolyte or hole conductor, and (5) a

counter electrode. The total efficiency of the dye sensitized solar cells depends on optimization and compatibility of each of its constituent. The sensitizer is a key component harvesting the solar radiation and converting it to electric current by electron injection into the wide band gap semiconductor. As the most successful sensitizer to date is Ru complexes such as the N3/N719 dye^{63, 64} and the black dye⁶⁵ have been intensively investigated, and show record solar energy-to-electricity conversion efficiencies of 11% under AM 1.5 irradiation⁶⁶ but the fabrication cost makes researcher to concentrate other sources. Recently several groups have developed metal free organic sensitizers which show comparable efficiency [10-15].

Wu *et al*⁶⁷ were synthesized and characterized the new organic dyes comprising carbazole, iminodibenzyl, or phenothiazine moieties, respectively, as the electron donors, and cyanoacetic acid or acrylic acid moieties as the electron acceptors/anchoring groups. And made the DSSC assembly by dye adsorbed TiO₂ electrode and Pt-counter electrode were assembled into a sandwich sealed type cell by heating them with hot-melt ionomer film as a spacer, a drop of electrolyte was introduced and sealed. The solar efficiency were achieved 5.53% for the phenothiazine and cyanoacrylic acid substituted dye **D3**, which is higher than the corresponding phenothiazine substituted donor-acceptor dye **D4**, and higher than the corresponding carbazole and iminodibenzyl substituted donor-acceptor dye (**D1** and **D2**, respectively).

Daniel *et al*⁶⁸ synthesized a novel and efficient polyene-diphenylaniline dye by short synthesis route. The diphenylaniline moiety acts as the electron donor and the cyanoacetic moiety acts as the electron acceptor and anchoring groups for attachment on the TiO₂. The dye is readily adsorbed on TiO₂ under a variety of dye-bath conditions. The overall solar-to-

energy conversion efficiency is over 5% in the preliminary tests, in comparison with the conventional N719 dye which gives 6% under the same conditions.

Moon *et al*⁶⁹ reported the dye sensitized solar cells based on the functionalized organic sensitizer, 3-(5-(5-(4-(bis (4-(hexyloxy)-phenyl) amino) phenyl) thiophen-2-yl) thiopen-2-yl)-2-cyanoacrylic acid (D21L6), The TiO₂ electrodes were immersed into a 0.3mM solution of D21L6 in ethanol and kept in room temperature for 15 h. The dye-adsorbed TiO₂ electrode and thermally platinised counter electrode were assembled into a sealed sandwich type. It exhibits a comparable stability to the ruthenium sensitizers under 60 °C heat stresses and AM 1.5 light illuminations where the overall efficiency remained at above 90%.

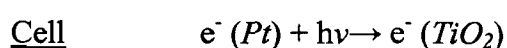
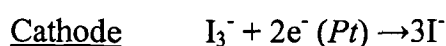
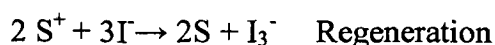
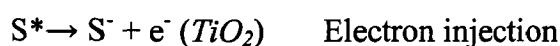
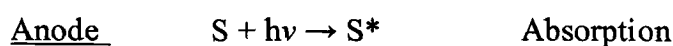
2.11 Application in dye sensitized solar cells

The most promising development is the "titania dye sensitized cells" which use titanium dioxide as the substrate in place of silicon. TDS cells use 2 transparent sheets of glass with conductive coatings and an electrolyte sandwiched between, thus allowing them to be used as a window. They are at present producing electricity commercially at about 10% efficiency and produce about 50 watts per square meter. When used as a window they have the potential of being able to reduce the heat gain into a building and also provide power to it. When considering the surface area of high-rises etc, a lot of power could be collected (bags more than enough for "additional" lighting - and smart building design could overcome any lighting problems anyway)

Part of the attractiveness of this type of cell is its potentially low cost to produce and relatively simple construction. Titanium dioxide is fairly cheap and has been used in antibacterial applications, deodorization, waste water treatment and other decomposition processes of organic compounds and pollutants. (It is an oxidizing agent that is activated by light). It has an anatase crystalline structure, is white to semi-transparent, soluble in water or

alcohol with a pH of 2 ± 0.5 . The use in commercial solar cells requires a higher purity colloidal powder which is more expensive however. The electrodes and the exposure to light are provided by a glass sheet sandwich with conductive coatings of Silicon Dioxide. The titanium dioxide is treated with a synthetic ruthenium bipyridyl based dye on the incoming light surface and works in conjunction with an electrolyte of iodide/triiodide to the other conductive surface to produce a voltage potential. The "back" layer has a catalyst coating upon its SnO_2 layer such as carbon. The photo-excited dye injects an electron through the TiO_2 layer which is passed to the SnO_2 surface and out to the external circuit. The SnO_2 layer is conductive because of the existence of oxygen vacancies which act as donors. Within the iodide electrolyte it (iodide/triiodide) undergoes oxidation at the dye and regeneration at the catalyst coated SnO_2 electrode at the opposite side, thus maintaining an electrolyte balance and completing the circuit. This type of solar cell will eventually have superior performance particularly in lower light levels over the typical PV "semiconductor" types because it doesn't suffer from the electron-hole recombination in the semiconductor material which seriously affects the efficiency of PV cells. (The processes of light absorption and charge separation are differentiated, in PV; absorption of light causes the charge separation).

Since the cell will transmit light through it, it may be possible to use the "amorphous tri-layer" idea and provide several (many) cells sandwiched using thin films and different dyes that are selective to different wavebands of light.



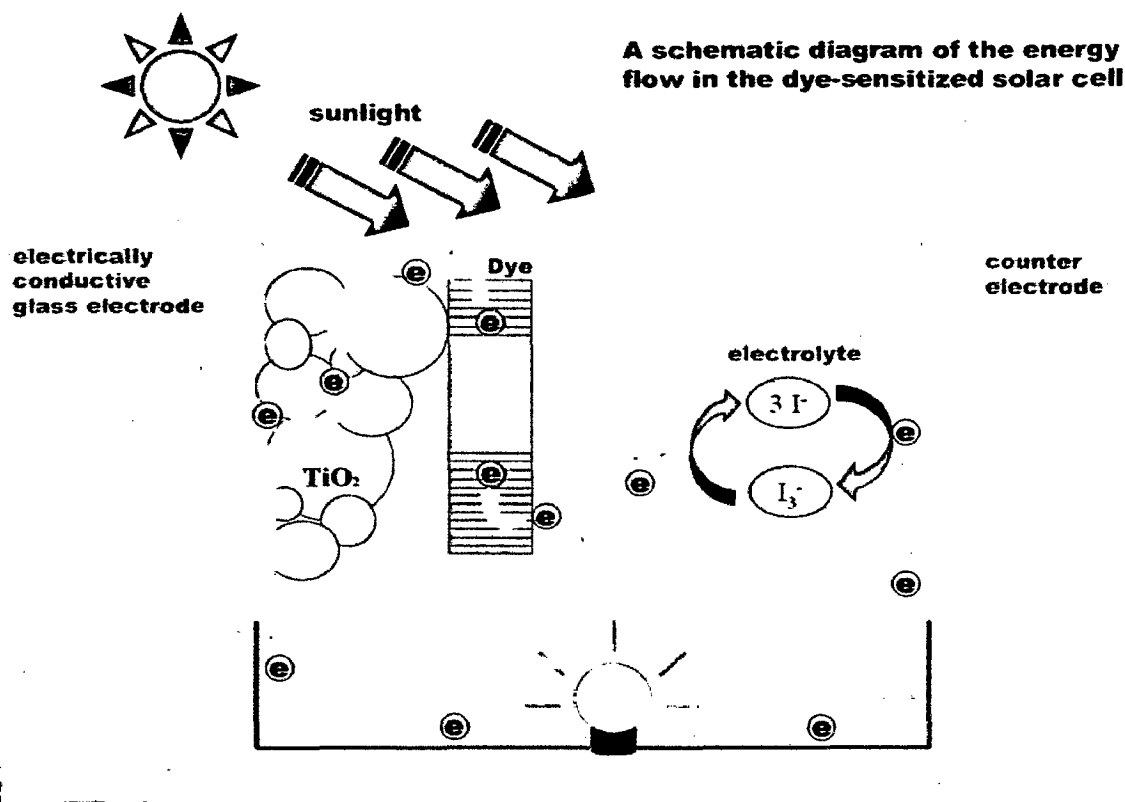


Figure 2.9 Scheme of dye sensitized solar cells.

1. Light passes through the glass plate and SnO_2 coating to stimulate the organic dye (anthocyanins) to produce free electrons.
2. The injected electrons are passed through the TiO_2 layer and collected at the SnO_2 conductive surface and out to an external circuit.
3. The electrolyte gives up electrons to the dye to regenerate it, and in the process is converted to triiodide.
4. The external circuit flows back to the catalyst coated electrode to balance the electrolyte again with electrons. (triiodide back to iodide) (Figure 2.9).

More exciting fact is that these cells can be easily manufactured by a home constructor or in a classroom for a school project. The dye used in the commercial cells is hard to synthesize but can be replaced by naturally occurring juices from "blackberries, raspberries, pomegranate seeds, beets, hibiscus tea leaves, citrus leaves" etc, and are known as flavonoids. Flavonoids have anthocyanins which are present in fruit and plants and are a robust naturally

occurring" dye", the trade off however is performance. This makes this an ideal study project because it uses nature's processes, photosynthesis, oxidation, reduction and catalysts etc, and can be tied and compared to many of the cycles and process on our world, and ties in chemistry, physics, optics etc. Conductive glass plates can be purchased or prepared chemically and are available in any size you want. Care should be taken to minimize contact and handling of the surfaces as this deposit "oils" on the surface which will degrade the cells performance. An ohm-meter will help to determine "which side" has the conductive surface, if you can't see the difference.

2.12 Other applications

2.12.1 Pigment

Titanium dioxide is the most widely used white pigment because of its brightness and very high refractive index ($n = 2.7$), in which it is surpassed only by a few other materials. Approximately 4 million tons of pigmentary TiO_2 are consumed annually worldwide. When deposited as a thin film, its refractive index and color make it an excellent reflective optical coating for dielectric mirrors and some gemstones, for example "mystic fire topaz".

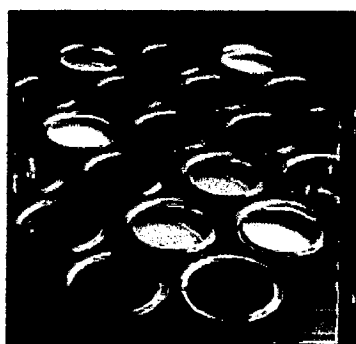


Figure 2.10 Different colored paints prepared from TiO_2 .

TiO_2 is also an effective opacifier in powder form, where it is employed as a pigment to provide whiteness and opacity to products such as paints, coatings, plastics, papers, inks,

foods, medicines (i.e. pills and tablets) as well as most toothpastes (Figure 2.10). Opacity is improved by optimal sizing of the titanium dioxide particles. Used as a white food coloring, it has E number E171. Titanium dioxide is often used to whiten skimmed milk; this has been shown statistically to increase skim milk's palatability. In cosmetic and skin care products, titanium dioxide is used both as a pigment and thickener. It is also used as a tattoo pigment and styptic pencils.

This pigment is used extensively in plastics and other applications for its UV resistant properties where it acts as a UV absorber, efficiently transforming destructive UV light energy into heat. In ceramic glazes titanium dioxide acts as an opacifier and seeds crystal formation. In almost every sunscreen with a physical blocker, titanium dioxide is found because of its high refractive index, its strong UV light absorbing capabilities and its resistance to discoloration under ultraviolet light. This advantage enhances its stability and ability to protect the skin from ultraviolet light. Sunscreens designed for infants or people with sensitive skin are often based on titanium dioxide and/or zinc oxide, as these mineral UV blockers are believed to cause less likely skin irritation than chemical UV absorber ingredients. The titanium dioxide particles used in sunscreens have to be coated with silica or alumina, because titanium dioxide creates radicals in the photo catalytic reaction. These radicals are carcinogenic, and could damage the skin.

2.12.2 Photocatalytic applications

Titanium dioxide, particularly in the anatase form, is a photocatalyst under ultraviolet light. Recently it has been found that titanium dioxide, when spiked with nitrogen ions, or doped with metal oxide like tungsten trioxide, is also a photocatalyst under visible and UV light (Figure 2.11). The strong oxidative potential of the positive holes oxidizes water to create hydroxyl radicals. It can also oxidize oxygen or organic materials directly. Titanium

dioxide is thus added to paints, cements, windows, tiles, or other products for sterilizing, deodorizing and anti-fouling properties and is also used as a hydrolysis catalyst. It is also used in the Grätzel cell, a type of chemical solar cell.

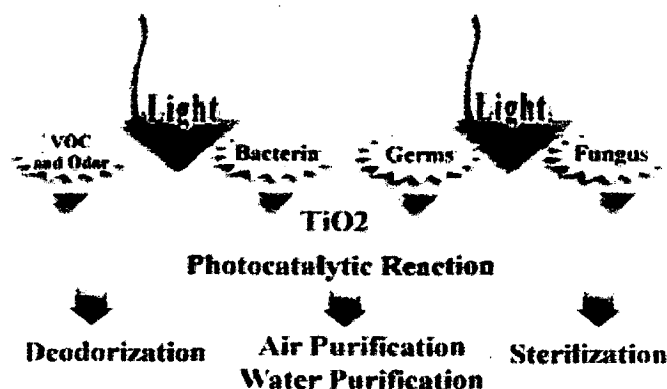


Figure 2.11 Role of TiO₂ as photocatalyst.

The photocatalytic properties of titanium dioxide were discovered by Akira Fujishima in 1972. The process on the surface of the titanium dioxide was called the Honda-Fujishima effect.

Titanium dioxide has potential for use in energy production: as a photocatalyst, as it can

1. Carry out hydrolysis; i.e., break water into hydrogen and oxygen. Were the hydrogen collected, it could be used as a fuel. The efficiency of this process can be greatly improved by doping the oxide with carbon.
2. Produce electricity when in nanoparticle form. Research suggests that by using these nanoparticles to form the pixels of a screen, they generate electricity when transparent and under the influence of light. If subjected to electricity on the other hand, the nanoparticles blacken, forming the basic characteristics of a LCD screen. According to creator Radivojevic, Nokia has already built a functional 200-by-200-pixel monochromatic screen which is energetically self-sufficient.

In 1995 Fujishima and his group at the Research Institute of Toto Ltd. discovered the super hydrophilicity phenomenon for titanium dioxide coated glass exposed to sun light. This resulted in the development of self-cleaning glass and anti-fogging coatings. TiO_2 incorporated into outdoor building materials, such as paving stones in noxer blocks or paints can substantially reduce concentrations of airborne pollutants such as volatile organic compounds and nitrogen oxide.

2.12.3 Waste water remediation using TiO_2

TiO_2 offers great potential as an industrial technology for detoxification or remediation of wastewater due to several factors

1. The process occurs under ambient conditions very slowly, direct UV light exposure increases the rate of reaction.
2. The formation of photocyclized intermediate products, unlike direct photolysis techniques, is avoided.
3. Oxidation of the substrates to CO_2 is complete.
4. The photocatalyst is inexpensive and has a high turnover.
5. TiO_2 can be supported on suitable reactor substrates.

Electrochemical process is an emerging technology for the treatment of waste-water because of its high efficiency and relatively simple system. For this purpose TiO_2 /Indium tin oxide (ITO) electrode for the electrochemical system were developed. Oxide conductor such as ITO has electrical and chemical stability compared to metal conductor. Electrochemical oxidation process using TiO_2 /ITO electrode for the industrial dye wastewater treatment was also investigated. And it was found that the efficiency of electrochemical process using TiO_2 /ITO electrode was sufficiently high for industrial dye waste-water treatment. The electrochemical electrode can be made by spin coating (3000 rpm) of TiO_2 precursor

solution. The precursor solution composed of titanium tetra-isopropoxide, acetyl acetone and ethanol. Substrate is glass substrate which is coated by conducting ITO. After spin coating, the electrode is annealed at 550 °C for 30 min to remove organic components. The effective volume of precursor will crystallize to anatase TiO₂ phase. To perform electrochemical the cell was 1600 cm³ and the effective area of TiO₂/ITO electrode was 294 cm². Working electrode was TiO₂/ITO and counter electrode was Pt. For the experiment, real industrial dye waste-water can be obtained from local textile industry. For comparison, composite dye solution (50 ppm) should be made by mixing different kind of dyes. (Such as reactive red 198, reactive black 5, acid blue 40, acid red 88, basic blue 54 and basic red 46) The degradation efficiency is likely analyzed by UV-Visible spectrophotometer (Figure 2.12).

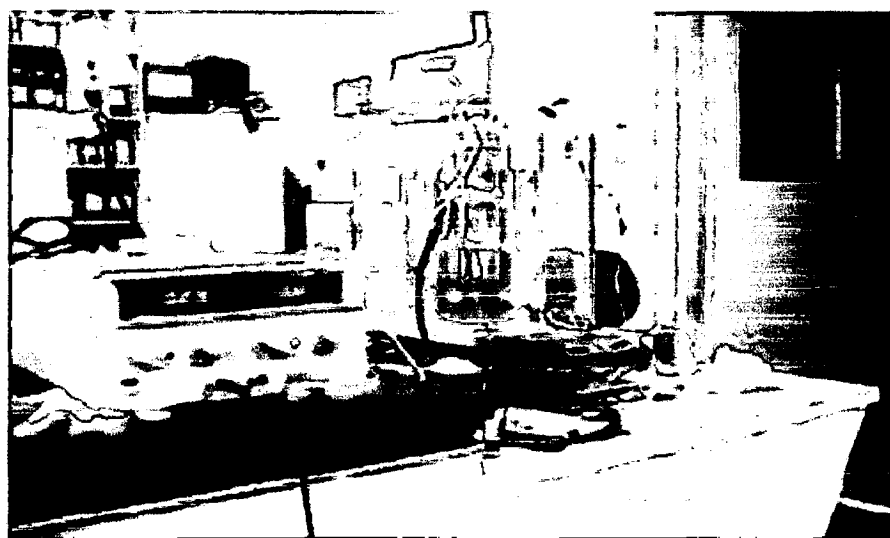


Figure 2.12 Dye waste-water treatment system using TiO₂/ITO oxide electrode.

It is also used in resistance-type lambda probes (a type of oxygen sensor). Titanium dioxide is what allows osseointegration between an artificial medical implant and bone. Titanium dioxide in solution or suspension can be used to cleave protein that contains the amino acid proline at the site where proline is present. This breakthrough in cost-effective protein splitting took place at Arizona State University in 2006.

Titanium dioxide on silica is being developed as a form of odor control in cat litter. The purchased photocatalyst is vastly cheaper than the purchased silica beads, per usage, and prolongs their effective odor-eliminating life substantially. Titanium dioxide is also used as a material in the memristor, a new electronic circuit element. It can be employed for solar energy conversion based on dye, polymer, or quantum dot sensitized nanocrystalline TiO_2 solar cells using conjugated polymers as solid electrolytes.

It has also been recently incorporated as a photocatalyst into dental bleaching products. It allows the use of decreased concentrations of hydrogen peroxide in the bleaching agent, thus claimed to achieve similar bleaching effects with fewer side effects (e.g. transient sensitivity, change in tooth surface topography, etc.) It is also used by film and television companies as a substitute for snow when filming scenes which require a winter setting.

2.13 Cadmium Sulfide

Cadmium sulfide is a chemical compound with the formula CdS . Cadmium sulfide is yellow in color and is a semiconductor.⁷⁰ It exists in nature as two different minerals, hexagonal greenockite⁷⁰ and cubic hawleyite⁷¹ Cadmium sulfide is a direct band gap semiconductor⁷² (gap 2.42 eV) and has many applications for example in light detectors. It forms thermally stable pigments and with the addition of e.g. CdTe , HgS colors ranging from deep red to yellow are formed.⁵

2.13.1 Physical and chemical properties of CdS

- Cadmium sulfide is soluble in acids. This procedure has been investigated as a method of extracting pigment from waste polymers.
- Cadmium sulfide crystals can act as a solid state laser.
- CdS is also known as cadmium yellow and by adding various amounts of selenium and selenide, one can obtain a range of colors, like pigment orange and pigment red.

- These synthetic cadmium pigments are valued for their good thermal stability, light and weather fastness, chemical resistance and high opacity.
- When sulfide solutions that contain cadmium sulfide are irradiated with light, hydrogen gas is generated.
- The conductivity of CdS increases when it is irradiated with light, which is the reason why it is used as a photo resistor.
- When CdS is combined with a p-type semiconductor, it forms the core component of a photovoltaic (solar) cell.
- When fabricated into thin films, it can be used as a transistor.
- Cadmium sulfide is a direct band gap semiconductor, having a band gap of 2.42 eV at 300 K, which is the reason why it appears colored.
- It also has properties of electroluminescence and cathodoluminescence. cathodoluminescence means that when CdS is mixed with copper acting as the activator and aluminum acting as the co activator; it luminesces under electron beam excitation. Thus, it is used as phosphor.
- Polymorph forms of CdS are piezoelectric while the hexagonal types are pyroelectric.
- It is the presence of cadmium that helps to detect forgeries in paintings that are claimed to have been painted before the 19th century.
- Cadmium sulfide is also used as a pigment in plastics.

2.14 Types of CdS

Cadmium sulfide has two crystal forms; the more stable hexagonal wurtzite structure (found in the mineral Greenockite) and the cubic zinc blende structure (found in the mineral Hawleyite). In both of these forms the cadmium and sulfur atoms are four coordinate. There is also a high pressure form with the NaCl rock salt structure.

2.15 Physical characteristics of greenockite

Greenockite is a rare mineral and the only real ore of cadmium. It is a much sought after mineral by collectors both for its rarity and for its nice color and crystal habit. Although it is the most common cadmium mineral, most of the world's supply of cadmium is supplied through the processing of zinc and lead ores where cadmium is a common trace element.

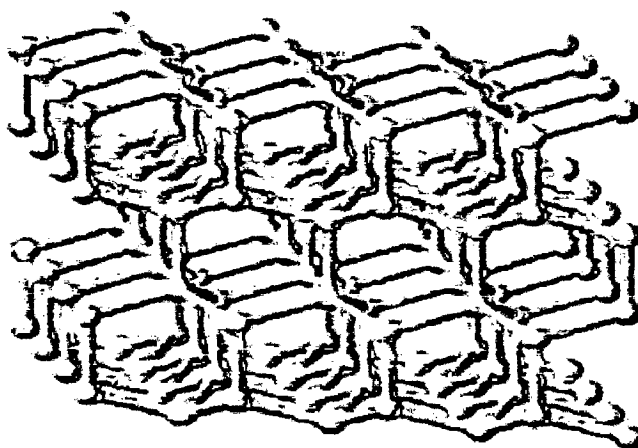


Figure 2.13 Greenockite unit cell

Greenockite has the same structure as the zinc iron sulfide wurtzite. Greenockite's structure is composed of SCd_4 tetrahedrons that are stacked in a layered structure with every other layer exactly the same in an AB AB AB ... hexagonal sequence (Figure 2.13).

The tetrahedrons in greenockite all are oriented in one direction and produce the hexagonal (six fold rotational) symmetry. The symmetry is broken in a perpendicular direction to the major axis and results in a hemimorphic crystal structure. In other words, there is no symmetry element, like a mirror or two fold rotational axis, perpendicular to the major axis and thus crystal faces on top of the crystal are not repeated on the bottom of the crystal. Hemimorphic crystals have different looking tops from their bottoms, as if they never completed the opposite, symmetrical, side; therefore the term hemimorphic or half shape.

Other minerals that have a hemimorphic character are the tourmalines, hemimorphite, wurtzite and zincite among others.

Crystals of greenockite are typically six sided pyramids where the hemimorphic character is easily seen as the top of the crystal is the point and the bottom of the crystal is the pyramid's base. Often the crystals are platy with a hexagonal outline and the hemimorphic character is then not easily distinguished.

- Color is honey, orange, red (or) light to dark brown.
- Luster is adamantine to resinous
- Transparency crystals are transparent to translucent
- Crystal system is hexagonal; 6mm
- Crystal habits include small tapering hemimorphic six sided pyramids and platy hexagonal crystals, also seen as crusts or dustings over crystals of calcite, smithsonite and sphalerite.
- Cleavage is poor in one direction (basal) and good in three other directions (prismatic).
- Fracture is conchoidal.
- Streak is red, orange, or light brown.
- Other characteristics: Striations on pyramidal faces parallel to base, an index of refraction of 2.50 – 2.52 and is soluble in hydrochloric acid giving off hydrogen sulfide gas
- Associated minerals include fluorite, chalcopyrite, quartz, smithsonite, calcite, pyrite, sphalerite, marcasite and prehnite.
- Notable occurrences include greenock (hence the name), Scotland; Llallagua; Bolivia; Paterson, New Jersey; Joplin, Missouri; Arkansas, Illinois and Kentucky, USA.
- Best field indicators are crystal habit, color, streak and cleavage.

2.16 Physical characteristics of hawleyite

Hawleyite is a rare sulfide mineral in the sphalerite group, dimorphous and easily confused with greenockite (Figure 2.14). Chemically, it is a cadmium sulfide, and occurs as a bright yellow coating on sphalerite or siderite in vugs, deposited by meteoric waters. It was discovered in 1955 and named in honor of mineralogist James Edwin Hawley.

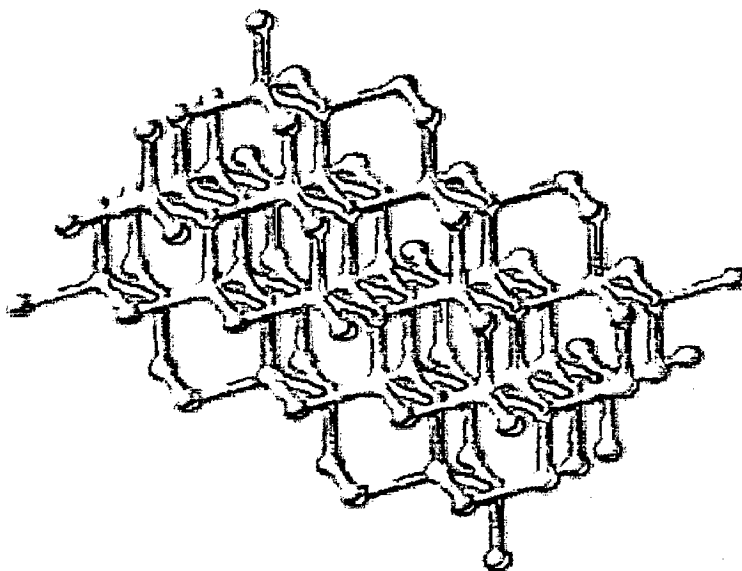


Figure 2.14 Hawleyite unit cell

Cleavage	:	None
Colour	:	Light yellow
Diaphaneity	:	Opaque
Luster	:	Metallic
Streak	:	Light yellow

2.17 Preparation of CdS nanoparticles

Maleki *et al*⁷³ reported the CdS nanoparticles preparation by a chemical reaction route using ethylenediamine as a complexing agent. Cadmium acetate dehydrate ($C_4H_6O_4Cd \cdot 2H_2O$), ethylenediamine ($C_2H_8N_2$) were obtained from Merck. Double distilled water and ethanol was used for washing the particles. A typical procedure for the CdS nanoparticles

synthesis is as follows: appropriate amount of analytically pure Cd $(\text{CH}_3\text{COO})_2 \cdot 2\text{H}_2\text{O}$ was dissolved into a deaerated 35 mol. % aqueous solution of ethylenediamine in a flask at room temperature. Then under vigorous stirring, analytical pure Na_2S was quickly added to this solution, and a milk-white sol was formed soon. Next, the resultant milk-white sol was heated to $100\text{ }^\circ\text{C}$, and kept on stirring at this temperature for about 6 h until the milk white reaction mixture gradually turned to a yellow colour. The final product was then collected and washed with distilled water and ethanol.

Khanna *et al*⁷⁴ generated the fine powder of CdS from direct in-situ reduction of sulphur and cadmium salts in aqueous *N, N*-dimethylformamide Cadmium chloride or cadmium acetate was dissolved in a an appropriate ratio of *N, N*-dimethylformamide and water in a round bottom schlenk flask. Sulphur powder was added to this solution in 1:1 ratio with respect to metal salt. The reaction mixture was then kept under vacuum to remove moisture and oxygen. The reaction mixture was stirred at about $120\text{ }^\circ\text{C}$ for 4–5 h to obtain bright yellow suspension. Filtration followed by washing with water and methanol resulted in formation of fine powder in about 70–80% yield.

Martínez *et al*⁷⁵ Synthesis a CdS nanoparticles by simple method in aqueous media $\text{CdSO}_4 \cdot 2.5\text{H}_2\text{O}$ was dissolved in 1L of deionized water to a concentration of 2 mM. This solution was placed in a 2 L reaction vessel. Under stirring (200 rpm) 18 mmol of 1-thioglycerol were added and the mixture was stirred for an additional five minutes. Ammonium sulfide (30 mmol) was rapidly added under ambient conditions to form cadmium sulfide nanoparticles. This method yields dispersions that are stable even during months.

Zhiyu *et al*⁷⁶ reported a sonochemical method for the synthesis of CdS nanocrystals were prepared by direct precipitation in the presence of sodium hexametaphosphate. 30 mL of 30

mM Na_2S aqueous solution was added drop wise to 30 mL of 30 mM $\text{Cd}(\text{NO}_3)_2$ aqueous solution containing 30 mM sodium hexametaphosphate under ultrasonic irradiation for 2 h. Vigorous stirring was also employed during the irradiation. Then the solvent was removed by evaporation, and the resulting powder was washed with ethanol and deionized water respectively.

2.18 Other forms of CdS

2.18.1 Nanotubes

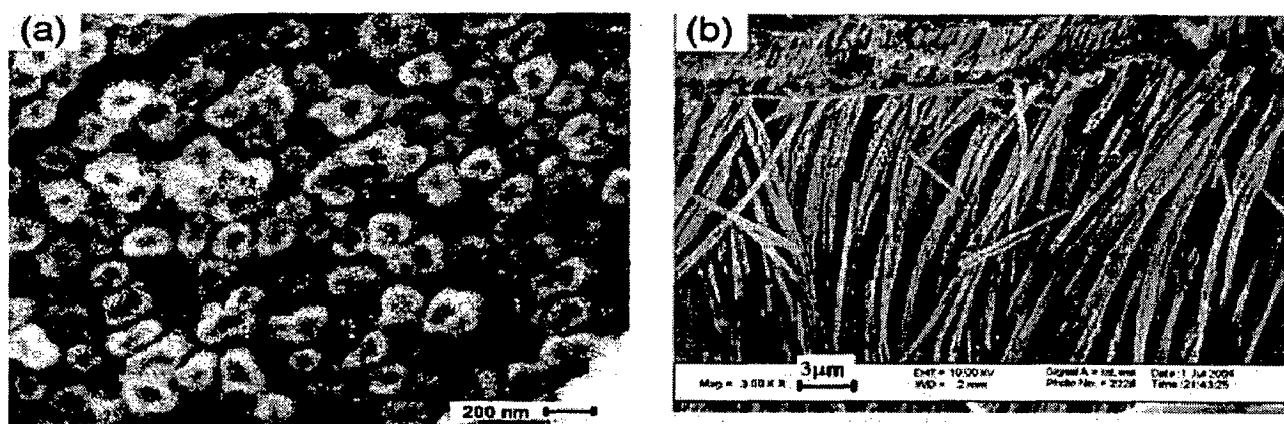


Figure 2.15 SEM images of CdS nanotubes.

Zhang *et al*⁷⁷ reported the synthesis of CdS nanotubes, by the PTFE membrane with pore diameters of 100–300 nm was washed with deionised water to near neutral for use. Cover a PTFE membrane on the mouth of a clean test tube filled with 25 mL of 0.1 mol/ Na_2S solution and seal it up. Vertically mouth-down place the above test tube for 1 h. Then put it into a larger test tube filled with 20 mL of 0.1 mol/l CdCl_2 solutions. After 24 h, the CdS nanotubes are formed. The final products are washed with deionised water and absolute alcohol several times, respectively, and desiccated in vacuum at 60 °C for 1 h (Figure 2.15).

2.18.2 Nanofibres

Guan *et al*⁷⁸ generated CdS nanofibres by Solution – Solid method. In a typical synthesis, 1 mmol of $\text{Ce}_2(\text{CO}_3)_3$ powders were added into 20 mL of $\text{H}_6\text{P}_4\text{O}_{13}$ (0.62 mol/L) aqueous solution under ultrasound stirring; the resulted suspension solution was poured into a Teflon stainless steel autoclave. The autoclave was sealed, and maintained at 100 °C for 12 h, and then allowed to cool to room temperature. Flexible, cellulose paper like material deposited on the bottom of a Teflon cup showed a fibrous morphology for the product. The products were washed with distilled water, and finally dried at 80 °C in air (Figure 2.16).

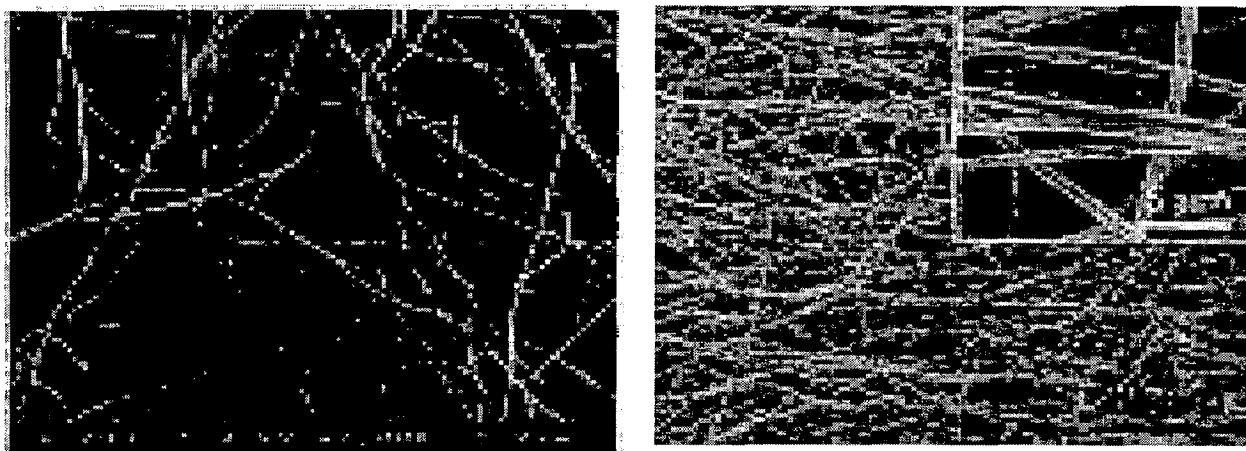


Figure 2.16 SEM images of CdS Nanofibres.

2.19 Coating of organic dyes with CdS nanoparticles

Bulk semiconductor materials have been widely used as photocatalyst for solar energy conversion. An important defect of metal oxide semiconductor is that their photoactivity is limited to the UV region. Therefore the photosensitization of stable, large-band gap semiconductors by visible light using dye is a long term goal.

Jhonsi *et al*⁷⁹ were examined xanthenes derivatives fluorescein, eosin, erythrosine and rose bengal as sensitizers for colloidal CdS nanoparticles. The xanthenes dyes were obtained from Aldrich and used without further purification. Colloidal CdS were prepared by simple

chemical method and get adsorbed with dyes. The interactions were studied by absorption, infra-red, steady state and time resolved fluorescence spectroscopic measurements. Absorption spectrum shows that the surface complex formation through adsorption of dyes on the surface of colloidal CdS. Static nature of quenching has been confirmed by unaltered fluorescence life-time measurements. Based on the energetic calculations the mechanism of electron transfer from excited state dyes to the conduction band of colloidal CdS was suggested.

Jhonsi *et al*⁸⁰ reported the interaction between certain porphyrins and CdS colloids. Porphyrins namely, *meso*-tetrakis(4-methoxyphenyl) porphyrin (TMeOPP), protoporphyrin IX (PPIX) and Zinc (II) *meso*-tetraphenylporphyrin (ZnTPP) were obtained from Sigma-Aldrich. CdS colloids was prepared by chemical methods, the porphyrins was adsorbed on the surface of colloidal CdS and was studied by absorption and fluorescence techniques. This adsorption leads to change in the absorption spectra related to the complex formation. Spectrofluorimetry shows a quenching of fluorescence intensity, due to the transfer of energy from dyes to the colloidal CdS.

Wang *et al*⁸¹ reported the studies on fluorescence resonance energy transfer between CdS nanoparticles and DOCAI dyes. Water-soluble CdS nanoparticles were synthesized in aqueous solution and coated with DOCAI dyes, the UV spectra of CdS-DOCAI indicating that no interaction between the CdS nanoparticles and dye, when the concentration of the nanoparticles was increased. The fluorescence spectra indicate that there was a FRET process between the CdS/DOCAI complex solutions based on their concentrations.

2.20 Application in solar cells

Today, CdS is one of the leading thin film photovoltaic materials due to the optimum band gap of 2.45 eV for the efficient photo conversion, high optical absorption coefficient

and successful development of high efficiency solar cells and modules. Amongst several attractive features, high chemical robustness and a simple phase diagram are the most important ones for large area production of CdS solar modules at industrial scale. The work on CdS thin film solar cell started in 1970s, but the progress in R&D got real impetus in 1980s with the development of various techniques such as electro deposition (ED), screen printing, vacuum evaporation and close spaced sublimation (CSS) and efficiencies exceeding 10% were achieved.

The pioneering work of different groups in the 1990's pushed the efficiency to above 15%, and the present status of the thin film CdS solar cell is more than 16.5% efficiency for devices on TCO coated glass substrates, more than 7% efficiency for devices on flexible metallic substrate and 11% efficiency for devices on flexible polymer substrates. The commercialization of the CdS photovoltaic technology started in 2001 and the CdS photovoltaic modules with output power ranging from 45 to 55 W at a size of 60 cm×120 cm are available in the market. The efficiency of the commercial CdS solar module is about 8% for 55 W modules.

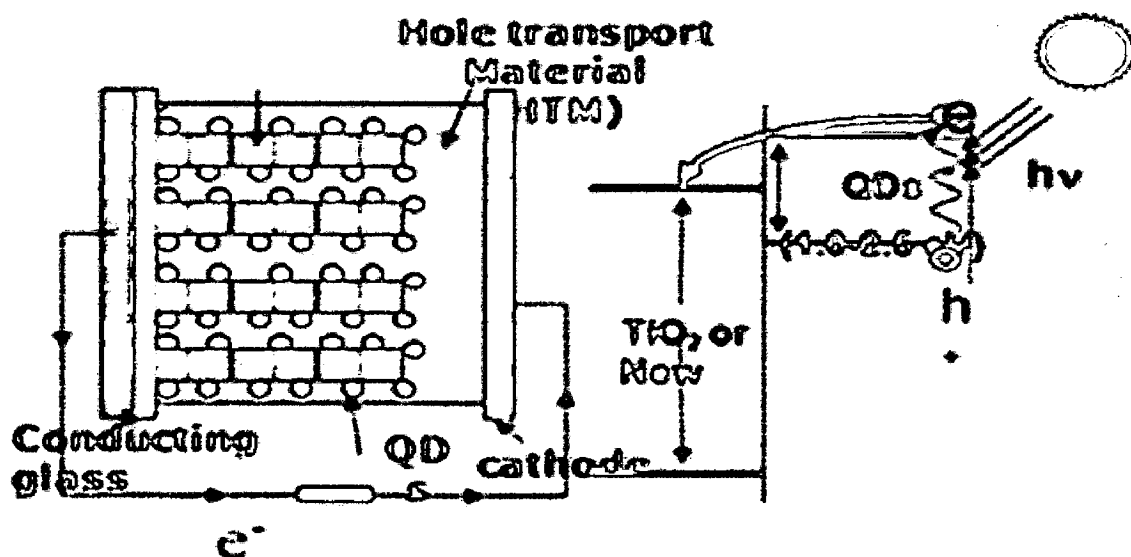


Figure 2.17 Scheme of quantum dot solar cells.

1. Light passes through the glass plate and SnO_2 coating to stimulate the Cadmium sulfide nanoparticles, to produce free electrons.
2. The injected electrons are passed through the TiO_2 layer and collected at the SnO_2 conductive surface and out to an external circuit.
3. The electrolyte gives up electrons to the CdS nanoparticles to regenerate it, and in the process is converted to triiodide.
4. The external circuit flows back to the catalyst coated electrode to balance the electrolyte again with electrons. (triiodide back to iodide) (Figure 2.17).

2.21 Conclusions

The size dependent optical properties of the semiconductor nanoparticles provides alternate pathways for getting efficient light-harvesting ability in different parts of the solar spectrum, fast charge generation and separation and increased conversion efficiency. The efficiency of the solar cells is highly dependent upon the harvesting nature of the material used. A composite of semiconductors material and dyes are considered to be harvesting the visible region of solar spectrum. At present the largest efficiency realized for solar cells is 11% based on inorganic ruthenium complex. As the ruthenium based dyes are costlier efforts are made to obtain new systems derived from cheaper ingredients such as nanocrystalline semiconductor materials and organic dyes. The nature of the interaction of the nanocrystalline semiconductor with the organic dyes is mainly dictated by the anchoring group which is present in the dye molecules but the morphology of the nanocrystals play a crucial role for the adsorption of molecules on its surface. At present several alternate morphologies such as nanowires, nanorods, nanotubes and nanofibres have been developed to

provide a high surface to volume ratio for more suitable adsorption of dyes on semiconductor materials which enhances significantly the light absorption and promotes charge separation.

2.22 References

1. Pradeep, T. *NANO: The essentials, understanding nano science and technology*, Tata Mcgraw-Hill, 2008.
2. Frasco, M. F.; Chaniotakis, N. *Anal. Bioanal. Chem.* **2010**, *396*, 229–240.
3. Jaiswal, J. K.; Simon, S. M. *Trends Cell. Biol.* **2004**, *14*, 9-14.
4. Azzazy, H. M. E. *Clin. Biochem.* **2007**, *40*, 917–927.
5. Norman, G. N.; Earnshaw, A. *Chemistry of the Elements (2nd edition)*, Oxford: Butterworth-Heinemann, 1997.
6. Usami, T.; Yanagida, H.; Taikei, B. K. *Mater. Sci. Eng.* **2002**, *2*, 586-591.
7. O'Regan, B.; Moser, J.; Anderson, M.; Grätzel, M. *J. Phys. Chem. C* **1990**, *94*, 8720-8726.
8. O'Regan, B.; Grätzel, M. *Nature* **1991**, *353*, 737-740.
9. Bahnemann, D.; Bockelmann; Goslich, R. *Sol. Energy Mater. Sol. Cells* **1991**, *24*, 594-607.
10. Sekiya, T.; Kamei, S.; Kurita, S. *J. Lumin.* **2000**, *1140*, 87-89.
11. Zhang, W. F.; Zhang, M. S; Yin, Z. *Phys. Status Solidi (A) Appl. Res.* **2000**, *179*, 319-327.
12. Anpo, S.; Chiba, K.; Tomonari, M.; Hyomen *J. Lumin.* **1991**, *29*, 156-158.
13. Rao, T. N.; Tryk, D. A. *J. Photochem. Photobiol. C* **2000**, *16*, 1-21.
14. Ohno, T.; Tanigawa, F.; Fujihara, K.; Izumi, S.; Matsumura, M. *J. Photochem. Photobiol. A* **1999**, *127*, 107-110.
15. Yoshida, Y.; Matsuoka, M.; Moon, S. C.; Mametsuka, H.; Suzuki, E.; Anpo, M. *Chem. Rev.* **2000**, *26*, 567-574.
16. Neppolian, B.; Sakthivel, S.; Arabindoo, B.; Palanichamy, M.; Murugesan, V *J. Environ. Sci. Health A* **1999**, *34*, 1829-1838.
17. Zhang, T.; Oyama, T.; Aoshima, A.; Hidaka, H.; Zhao, J.; Serpone, N. *J. Photochem. Photobiol. A* **2001**, *140*, 163-172.
18. Grzechulska, J.; Hamerski, M.; Morawski, A.W. *Water Res.* **2000**, *34*, 1638-1644.

19. Maness, P. C.; Smolinski, S.; Blake, D. M.; Huang, Z.; Wolfrum, E. J.; Jacoby, W.A. *Appl. Environ. Microbiol.* **1999**, *65*, 4094-4098.
20. Zheng, H.; Maness, P. C.; Blake, D.M.; Wolfrum, E. J.; Smolinski, S. L.; Jacoby, W.A. *J. Photochem. Photobiol., A* **2000**, *130*, 163-170.
21. Clark, R. J. H. *Thin Solid Films* **1968**, *296*, 267-272.
22. Park, N. G; Lagemaat, J.V.; Frank, A. J. *J. Phys. Chem. B* **2000** *103*, 8989-8994.
23. Matijevi, E.; Budnik, M.; Meites, L. *J. Colloid Interface Sci.* **1977**, *61*, 302-308.
24. Barringer, E. A.; Bowen, H. K. *J. Am. Ceram. Soc.* **1982**, *65*, 199-206.
25. Barringer, E. A.; Bowen, H. K. *Langmuir* **1985**, *124*, 414-420.
26. Ogihara, T.; Ikeda, M.; Kato, M.; Mizutani, N. *J. Am. Ceram. Soc.* **1989**, *72*, 1598-1601.
27. Ogihara, T.; Yanagawa, T.; Ogata, N.; Yoshida. *J. Ceram. Soc. Jpn.* **1993**, *101*, 315-320.
28. Komiyama, H.; Takada, Y.; Yamagiwa, H.; Kera, Y.; Inoue, M.; Inui, T. *J. Mater. Sci. Lett.* **1996**, *15*, 197-202.
29. Schleich, D.M.; Walter, B. *Nanostruct. Mater.* **1997**, *8*, 579-586.
30. Shi, L.; Li, C.; Chen, A.; Zhu, Y.; Fang, D. *Mater. Chem. Phys.* **2000**, *66*, 51-57.
31. Stathatos, E.; Lianos, P.; Monte-Levy, D.; Tsiourvas, D. *Langmuir* **1997**, *13*, 4295-4300.
32. Sakai, H.; Kawahara, H.; Shimazaki, M.; Abe, M. *Langmuir* **1998**, *14*, 2208-2212.
33. Khalil, K. M. S.; Zaki, M. I. *Powder Technol.* **1997**, *92*, 233-239.
34. Khalil, K. M. S.; Baird, T.; Zaki, M. I.; El-Samahy, A. A.; Awad, A. M. *Colloids Surf. A* **1998**, *132*, 31-44.
35. Zhu, Y.; Zhang, L.; Gao, C.; Cao, L. *J. Mater. Sci.* **2000**, *35*, 4049-4054.
36. Suresh, C.; Biju, V.; Mukundan, P.; Warriar, K. G. K. *Polyhedron* **1998**, *17*, 3131-3135.
37. Yin, S.; Sato, T. *Ind. Eng. Chem. Res.* **2000**, *39*, 4526-4530.
38. Masson, O.; Rienx, R.G.; Dauger, A. *Nanostruct. Mater.* **1996**, *7*, 725-733.
39. Kominami, H.; Kohno, M.; Takada, Y.; Inoue, M.; Inui, T.; Kera, Y. *Ind. Eng. Chem. Res.* **1999**, *38*, 3925-3931.
40. Zheng, Y.; Shi, E.; Cui, S.; Li, W.; Hu, X. *J. Am. Ceram. Soc.* **2000**, *83*, 2634-2639.
41. Cassaignon, S.; Koelsch, M.; Jolivet, J. P. *J. Mater. Sci.* **2007**, *42*, 6689-6695.
42. Bacsá, R.R.; Grätzel, M. *J. Am. Ceram. Soc.* **1996**, *79*, 2185-2191.
43. Sugimoto, T.; Zhou, X.; Muramatsu, A. *J. Colloid Interface Sci.* **2002**, *252*, 339-346.
44. Sugimoto, T.; Zhou, X. *J. Colloid Interface Sci.* **2002**, *252*, 347-353.
45. So, W. W.; Park, S. B.; Moon, S. J. *J. Mater. Sci. Lett.* **1998**, *17*, 1219-1224.
46. Cot, F.; Larbot, A.; Nabias, G.; Cot, L. *J. Europ. Ceram. Soc.* **1998**, *18*, 2175-2181.

47. Vorkapic, D.; Matsoukas, T. *J. Am. Ceram. Soc.* **1998**, *81*, 2815-2819.
48. Zhang, R.; Gao, L. *Mater. Res. Bull.* **2001**, *36*, 1957-1962
49. Sheng, Y.; Zhou, B.; Liu, Y.; Zhao, X.; Wang, C.; Pan, Y.; Wang, Z. *C. Mater. Lett.* **2006**, *60*, 1327-1330.
50. Kongsuebchart, W.; Praserttham, P.; Panpranot, J.; Sirisuk, A.; Supphasrirongjaroen, P.; Satayaprasert, P. *J. Cryst. Growth.* **2006**, *297*, 234-238.
51. Liao, L. C.; Chiang, P. *Appl. Surf. Sci.* **2007**, *253*, 3982-3986.
52. Rajesh, J. T.; Ramchandra, V.; Kulkarni, G.; Raksh, V. *Ind. Eng. Chem. Res.* **2006**, *45*, 922-927.
53. Baek, I. C.; Vithal, M.; Chang, A.; Yum, J.; Nazeeruddin, K.; Gratzel, M.; Chung, Y. C.; Seok, S. *Electrochem. Commun.* **2009**, *11*, 909-912.
54. Flores, I. C.; Longo, J. N.; Paoli, M. A.; Winnischofer, H.; Nogueira, A. F. *J. Photoch. Photobio. A* **2007**, *189*, 153-160.
55. Kim, G.; Seo, H. K.; Godble, V. P.; Kim, Y. S.; Yang, O. B.; Shin, H. S. *Electrochem. Commun.* **2006**, *8*, 961-966.
56. Lee, R. H.; Huang, Y. L. *Thin Solid Films* **2009**, *517*, 5903-5908.
57. Zhang, D.; Yoshida, T.; Furuta, K.; Minoura, H. *J. Photoch. Photobio. A* **2004**, *164*, 159-166.
58. Ko, K. H.; Lee, Y. C.; Jung, Y. C. *J. Colloid Interface Sci.* **2005**, *283*, 482-487.
59. Kitiyanan, A.; Ngamsinlapasathia, S.; Yoshikawa, S. P. S. *J. Solid State Chem.* **2005**, *178*, 1044-1048.
60. Cheng, X.; Zen, P.; Kuang, S. H.; Xie, G.; Feng. *Rare Metals* **2006**, *25*, 190-194.
61. Kim, K. E.; Jang, S. R.; Park, J.; Vitta, R.; Kim, K. J. *Sol. Energy Mat. Sol. C* **2007**, *91*, 366-370.
62. Shah, I.; Li, W.; Huang, C. P.; Jung, O. *J.P.N.A.S.* **2002**, *99*, 6482-6486.
63. Kubo, W.; Kambe, S.; Nakade, S.; Kitamura, T.; Wada, Y. *J. Phys. Chem. B* **2003**, *107*, 4374-4381.
64. Wang, P.; Zakeeruddin, S. M.; Moser, J. E.; Gratzel, M. *J. Phys. Chem. B* **2003**, *107*, 13280-13285.
65. Wang, P.; Wenger, B.; Humphry-Baker, R.; Moser, J. E.; Teuscher, J.; Kantelehner, W. *J. Am. Chem. Soc.* **2006**, *127*, 6850-6856.
66. Kuang, D. B.; Wenger, B.; Klein, C.; Moser, J. E.; Humphry-Baker, R. *J. Am. Chem. Soc.* **2006**, *128*, 4146-4154.

67. Wu, T.; Hsiu-sao, M.; Chen, F. L.; Su, G. S.; Chang, W. C.; Wang, P. H.; Lin, C. Y.; Ou-Yang, W. C.; Sun, W. I. *J. Molec. Sci.* **2010**, *11*, 329-353.
68. Daniel, P. H.; Edvinsson, T.; Marinado, T.; Boschloo, G.; Hagfeldt, A.; Sun, L. *Chem. Commun.* **2006**, *66*, 2245-2247.
69. Moon, J. S.; Yum, H. J.; Humphry-Baker, R.; Karlsson, M. K.; Daniel, P. H.; Marinado, T.; Hagfeldt, A.; Sun, L.; Gratzel, M.; Nazeeruddin, K. *J. Phys. Chem. B* **2009**, *113*, 16816-16820.
70. Wiberg, E.; Holleman, A. F. *Inorg. Chem.* **2001**, *56*, 213-218.
71. Traill, R. J.; Boyle, R. W. *Am. Mineral* **1955**, *40*, 555-559.
72. Kittel, C. *Introduction to Solid State Physics (7th Edition)*, Wiley, **1995**.
73. Maleki, M.; Ghamsari, S. M.; Mirdamadi, S.; Ghasemzadeh, R. *Quantum Opt.* **2007**, *10*, 30-32.
74. Khanna, P. K.; Subbarao, V. V. V. *S Mater. Lett.* **2004**, *58*, 2801-2804.
75. Martinez-Castanon, M. A.; Sanchez-Loredo, J. R.; Ruiz, F. *J. Mater.* **2005**, *1*, 2-7.
76. Zhiyu, W.; Zhongping, Y.; Bo, L.; Bo, Y.; Guodong, Q.; Xianping, F. *J. Wuhan Univ. Technol.* **2009**, *24*, 698-701.
77. Zhang, Z. L.; Wu, Q. S.; Ding, Y. P. *Inorg. Chem. Commun.* **2003**, *6*, 1393-1394.
78. Guany, M.; Sun, J.; Shang, T.; Zhou, Q.; Han, J.; Aiqin, J. *J. Mater. Sci. Technol.* **2010**, *26*, 45-48.
79. Jhonsi, A. M.; Kathiravan, A.; Renganathan, R. *J. Mol. Struct.* **2009**, *921*, 279-284.
80. Jhonsi, A. M.; Kathiravan, A.; Renganathan, R. *Spectrochim. Acta A* **2008**, *71*, 1507-1511.
81. Wang, L.; Liu, Y.; Qi Chen, H.; Ni Liang, A.; Gong Xu, F. *Chinese Chem. Lett.* **2007**, *18*, 369-372.

Chapter 3

Semiconductor nanoparticles: Synthetic and analytical procedures

3.1 Introduction

Nanometer-Sized semiconductor materials are an intensive research area during the past two decades due to their exciting novel applications in photovoltaic, electro-optical, micromechanical and sensor devices.¹⁻⁴ The color tunability of semiconductor nanoparticles as a function of size is one of their most attractive characteristics. The control and improvement of the luminescence properties of quantum dots have been a major goal in synthetic procedures of nanoparticles. II-VI semiconductor nanoparticles are currently of great interest for their practical applications such as zero-dimensional quantum confined materials, and in optoelectronics and photonics. Numerous reports are available in the literature on synthetic techniques as well as potential applications of nano-sized semiconductor particles.⁵⁻⁹ Colloidal methods provide effective routes to preparing semiconductor nanoparticles that are soluble in organic solvents and which have a narrow size distribution. Our main focus is on solar cells based on these semiconductor nanostructured due to their low cost energy conversion in a large scale. Semiconductor materials such as TiO₂, CdS, CdSe, CdTe, are more favour for the solar cells because of the greater band gap (>2 eV), which makes harvesting of wide solar spectrum, commercially

available materials and their stability against photo corrosion.¹⁰⁻¹² In the present work we are mainly focused to synthesis anatase TiO₂ nanoparticles and cadmium sulfide nanoparticles by simple chemical reaction method and also to make coating with different organic dyes to study the interactions.

3.2 Materials

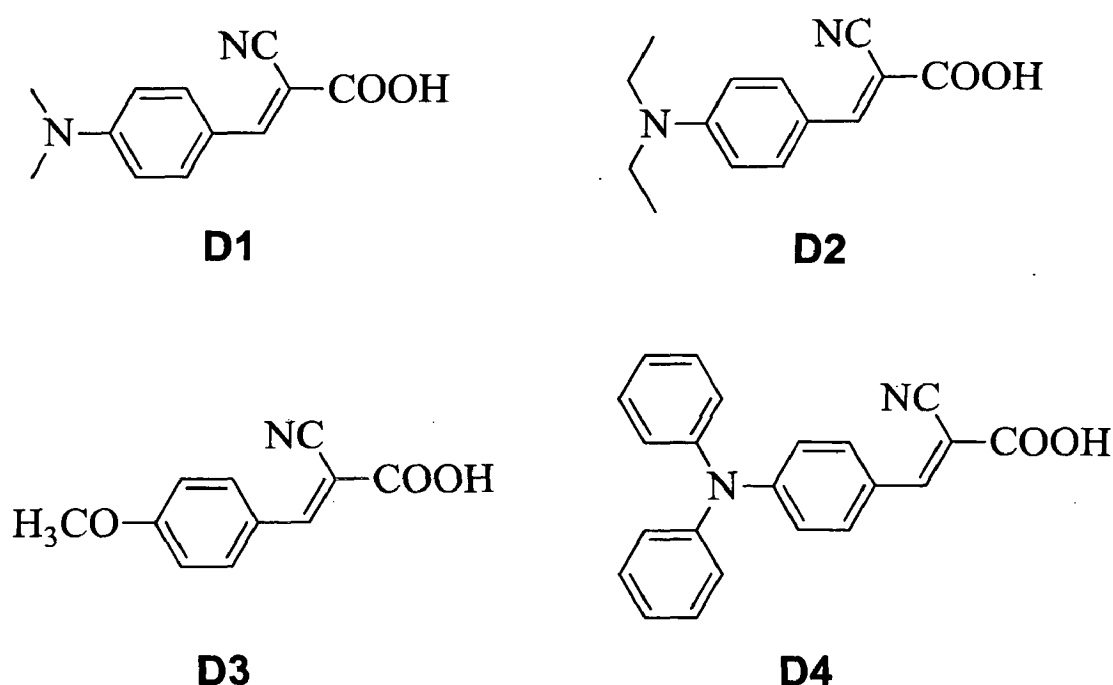


Figure 3.1 Structures of the dyes used in this study.

Titanium tetraisopropoxide, cadmium chloride (CdCl₂), cadmium acetate and sulphur powder was purchased from commercial sources and was used as received. Solvents such as ethanol and *N,N*-dimethylformamide (DMF) were freshly distilled from suitable drying agent prior to use. The donor groups in the dyes are varied to study the effect of ligand basicity on the adsorption behavior. The dyes (Figure 3.1) (*Z*)-2-cyano-3-((4-(dimethylamino)phenyl) acrylic acid (D1), (*E*)-2-cyano-3-((4-(diethylamino) phenyl) acrylic acid (D2), (*E*)-2-cyano-3-

((4-(methoxy) phenyl) acrylic acid (**D3**) and (*E*)-2-cyano-3-((4-(diphenylamino) phenyl) acrylic acid (**D4**) were synthesized by following the reported procedures.¹³⁻¹⁸

3.3 Physical Methods

The crystal structure and the phase of the samples were determined by X-ray diffraction (XRD) using Bruker X-ray diffractometer and using $\text{CuK}\alpha$ radiation ($\lambda = 0.154178$ nm). A scan rate of $2^\circ/\text{m}$ was applied to record the powder patterns in the 2θ range of $0-90$ degree and the average particle size were calculated by Scherrer Formula ($t = 0.94 \times \lambda / \beta \cos\theta$), where t is the average thickness of the particle, λ is the X-ray wavelength, β is the line broadening at half the maximum intensity in radians, and θ is the Bragg angle. The UV-visible spectrum of the nanoparticles was recorded using UV-1800 Shimadzu spectrophotometer in the wavelength range of 200-750 nm. Particle morphology, size and elemental analysis were estimated from field emission scanning electron microscope (FE-SEM) using FEI-Quanta 200F scanning electron microscope. Fluorescence measurements were carried on a RF-5301 PC Shimadzu spectrofluorophotometer and the thermal studies were performed on a Perkin-Elmer (Pyris Diamond) thermal analyzer under nitrogen atmosphere with a heating rate of 10°C per minute.

3.4 Synthesis of anatase TiO_2 nanoparticles

Nanocrystalline anatase TiO_2 was synthesized by hydrolysis of titanium tetra isopropoxide¹⁹ A mixture of dry ethanol (100 mL) and titanium tetra isopropoxide (30 mL) was taken in a 250 mL round-bottom flask, Continuously stirred for 30 min, and then subjected to ultrasonication for 30 min. Hydrolysis of the titanium tetraisopropoxide solution was carried out by adding distilled water (24 mL) slowly at the rate of 0.5 mL/min with

continuous stirring. The solvent from the obtained mixture was removed using a rotary evaporator at 70 °C under reduced pressure. The powder was then kept in vacuum desiccators for drying. Finally the dried sample was calcined at 127 °C for 11 h.

3.5 Coating of organic dyes on TiO₂ nanoparticles

In a round bottom flask anatase TiO₂ nanoparticles (100 mg, 1.25 mmol) and 1.1 equivalents of organic dyes (**D1**, **D2**, **D3**, & **D4**) were mixed in 15 mL ethanol. This mixture was stirred overnight. The reaction mixture was filtered and the solid obtained was dried under vacuum. To identify the presence of photocatalytic activity, the coating was performed both in the presence and absence of light.²⁰

3.6 Synthesis of Cadmium sulfide nanoparticles

3.6.1 Method A

Cadmium chloride (0.75 g) was dissolved in 1:1 mixture of *N,N*-dimethylformamide (75 mL) and water (75 mL) in a round bottom Schlenk flask. Sulphur powder (0.12 g) was added to this solution in 1:1 ratio with respect to metal salt and stirred for 30 min. Nitrogen was passed under the reaction mixture for 30 min to remove moisture and oxygen. Then the reaction mixture was stirred at about 120 °C for 5 hours to obtain bright green fluorescent suspension.²¹

3.6.2 Method B

Cadmium acetate (0.86 g) was dissolved in 1:1 mixture of *N,N*-dimethylformamide (75 mL) and water (75 mL) in a round bottom Schlenk flask. Sulphur powder (0.12 g) was added

to this solution in 1:1 ratio with respect to metal salt and stirred for 30 min. Nitrogen was purged through the reaction mixture for 1 h to remove moisture and oxygen. Then the reaction mixture was stirred at about 130 °C for 8 h to obtain bright blue fluorescent suspension.²¹

3.7 Interaction of organic dyes with CdS nanoparticles

A 0.05 M of blue or green emitting CdS dispersed in dimethylformamide was mixed with the corresponding organic dyes (D1, D2, D3, & D4) in different ratios in such a way the final concentration of the organic dyes were 1%, 2% or 5% relative to CdS concentration. The interaction of the dye with CdS was studied by the fluorescence spectroscopy.²²

3.8 Conclusions

Nanoparticles of anatase TiO₂ and CdS have been successfully synthesized in different sizes by simple chemical method. The average particle sizes were calculated by Scherrer formula from X-Ray diffraction data. Morphology, size and elemental analyses were performed by field emission-scanning electron microscopy (FE-SEM). The nanoparticles were successfully coated with the organic dyes. The conjugates obtained were thoroughly characterized by absorption, emission and thermal studies. The interaction of the CdS nanoparticles with the selected dyes was monitored by absorption and emission spectroscopy. Efficient energy transfer from blue and green emitting CdS colloids to the organic dyes indicates the possibility of using these nanocomposites as light harvesting components in solar cells.

3.9 References

1. Brus, L. *J. Phys. Chem. B* **1986**, *90*, 2555-2560.

2. Henglein, A. *Chem. Rev.* **1989**, *89*, 1861-1873.
3. Weller, H. *Adv. Mater.* **1993**, *5*, 88-94.
4. Alivisatos, A. P. *Science* **1996**, *271*, 933-937.
5. Tamborra, M.; Striccoli, M.; Comparelli, R.; Curri, M. L.; Petrella, A.; Agostiano, A. *Nanotechnology* **2004**, *15*, 5240-5246.
6. Tessler, N.; Medvedev, V.; Kazes, M.; Kan, S.; Banin, U. *Science* **2002**, *295*, 1506-1058.
7. Klimov, V. L.; Mikhailowsky, A. A.; Xu, S.; Malko, A.; Hallingsworth, J. A.; Leatherdole, C. A. *Science* **2000**, *290*, 340-346.
8. Battaglia, D.; Peng, X. *Nano. Lett.* **2002**, *2*, 1027-1030.
9. Abdulkhadar, M.; Thomas, B. *Nanostruct. Mater.* **1995**, *5*, 289-295.
10. Whitesides, G. M.; Grzybowski, B. *Science* **2002**, *295*, 2418-2421.
11. Duan, X.; Niu, C.; Chen, V. S. J.; Parce, J. W.; Empedocles, S.; Goldman, J. *Nature* **2003**, *425*, 274-278.
12. McAlpine, M. C.; Friedman, R. S.; Jin, S.; Lin, K.; Wang, W.; Lieber, C. M. *Nano Lett.* **2003**, *3*, 1531-1535.
13. Katz, H. E.; Schilling, M. L. *J. Am. Chem. Soc.* **1989**, *111*, 7554-7557.
14. Das, S.; Jana, A.; Ramanathan, V.; Chakraborty, T.; Ghosh, S.; Das, P. K.; Bharadwaj, P. K. *J. Organomet. Chem.* **2006**, *691*, 2512-2516.
15. Aviv, G.; Pnina, Y.; Chaim, G.; Alexander, L. *J. Med. Chem.* **1989**, *32*, 2344-52.
16. Sharma, S.; Bhatia, M. S. *J. Indian Chem. Soc.* **1991**, *68*, 612-614.
17. Xu, W.; Peng, B.; Chen, J.; Liang, M.; Cai, F. *J. Phys. Chem. C* **2008**, *112*, 874-880.
18. Hagberg, D. P.; Marinado, T.; Karlsson, K. M.; Qin, K. N. P.; Boschloo, G.; Brinck, T.; Hagfeldt, A.; Sun, L. *J. Org. Chem.* **2007**, *72*, 9550-9556.
19. Rajesh J. T.; Ramchandra, V.; Kulkarni, G.; Raksh, V. J. *Ind. Eng. Chem. Res.* **2006**, *45*, 922-927.
20. Moon, J. S.; Yum, H. J.; Humphry-Baker, R.; Karlsson, M. K.; Daniel, P. H.; Marinado, T.; Hegfeldt, A.; Sun, L.; Gratzel, M.; Nazeeruddin, K. *J. Phys. Chem. B* **2009**, *113*, 16816-16820.
21. Khanna, P. K.; Subbarao, V. V. V. S. *Mater. Lett.* **2004**, *58*, 2801-2804.
22. Jhonsi, A. M.; Kathiravan, A.; Renganathan, R. *Spectrochim. Acta A* **2008**, *71*, 1507-1511.

Chapter 4

Characterization: Semiconductor nanoparticles and their interactions with organic dyes

4.1 Introduction

Quantum dots (QDs) have attracted significant attention in recent years for the development of next generation solar cells due to their unique features.¹ The substitution of dyes with QDs can provide several benefits: greater photo stability, larger absorption coefficients, and ability to modulate photo response by size quantization.² Extensive research work is going on the semiconductor nanoparticles to alter the spectral properties by the incorporation of dye molecules. Now it is an established fact that systematic manipulation of atoms, molecules and cluster on the surface of nanoparticles are quite feasible and could lead to the desired luminescence properties.³⁻⁷ Incorporation of dye molecules on the surface of nanoparticles are carried out by techniques like physical adsorption, covalent binding, electrostatic binding, etc.⁸⁻¹¹ There are various dye molecules, whose interaction with nanoparticles yield surface modified nanoparticles, which results in the changing their optical properties due to transfer of energy or electron from the excited state level to the conduction band of semiconductor nanoparticles. Most of the previous work in synthesis of ruthenium complexes and doped with nanoparticles has focused due to their good efficiency

towards the large scale, but the cost effective and difficult fabrication, consider a new variety of dyes based on organic molecules with suitable anchoring group. In the present work we have used different types of aromatic/hetero-aromatic and varying length of aromatic conjugations with suitable anchoring groups are used to coat on the synthesized semiconductor nanoparticles under room temperature and also study their effect by absorption, fluorescence, FT-IR, spectroscopy, thermal analysis, XRD, FE-SEM, EDAX and analysis.

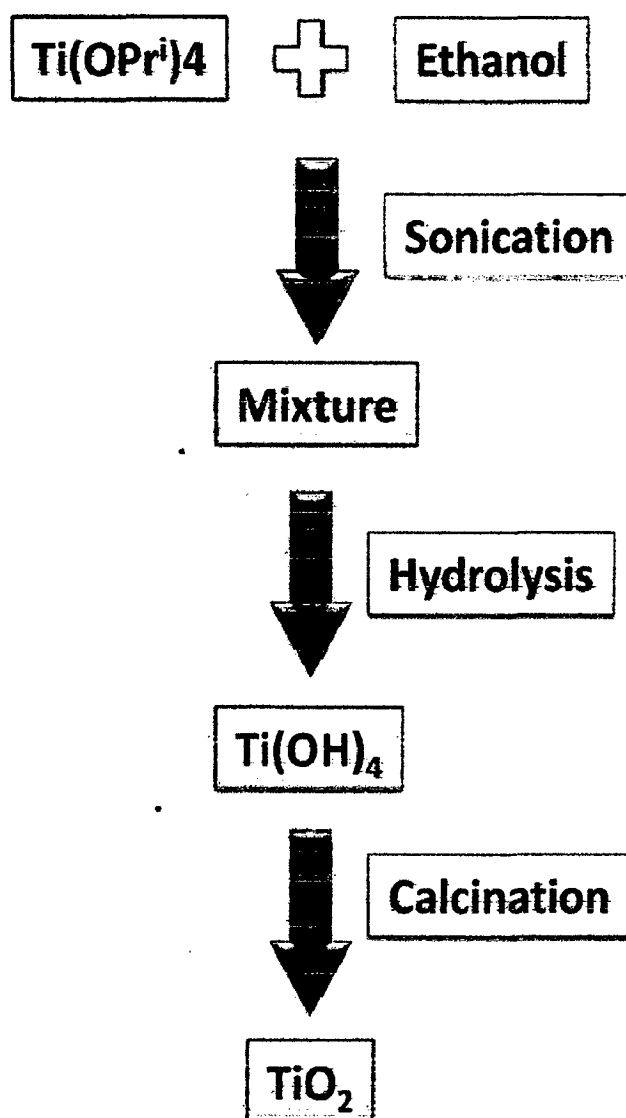


Figure 4.1 Procedure for the preparation of anatase TiO₂ nanoparticles

4.2 Synthesis and characterization TiO₂ nanoparticles

Synthetic procedure for the anatase TiO₂ nanoparticles is illustrated in Figure 4.1. Titanium tetraisopropoxide (30 mL) and dry ethanol (100 mL) were taken in a 250 mL round-bottom flask, and stirred thoroughly for 30 min and subjected to then sonication for 30 min. Hydrolysis was performed by adding distilled water (24 mL) slowly at the rate of 0.5 mL/min with vigorous stirring. The solvent from the obtained mixture was removed using a rotary evaporator at 70 °C under reduced pressure. The powder was then stored in vacuum desiccator for drying. Finally, the dried sample was calcined at 127 °C for 11 h to obtain anatase TiO₂ nanoparticles.¹² As there is growing interest for microwave assisted synthesis of materials, we have also studied the effect of microwave heating on the nanoparticles. Typically the nanoparticles placed in a crucible were subjected to microwave for 1 min in high power mode. The color of the particles changed to tan color.

4.2.1 XRD analysis

The XRD pattern observed for the nanoparticles is shown in Figure 4.2. Characteristic diffraction peaks due to the anatase phase are present in the XRD pattern. The broadened peaks are indicating that the sizes of the particles are in nanoranges.¹² In order to achieve more confirmative information, the Debye-Scherrer formula was used to calculate the size of the nanoparticles.

Debye-Scherrer formula

$$(t = 0.94 \times \lambda / \beta \text{ Cos } \theta)$$

where t is the average thickness of the particle, λ is the X-ray wavelength, β is the line broadening at half the maximum intensity in radians, and θ is the Bragg angle.

The average grain size is estimated from the major XRD peak for the anatase phase around $2\theta = 25.39^\circ$, which is 16 nm. The reported size was 8 nm for the TiO_2 particles obtained in a similar methodology.¹²

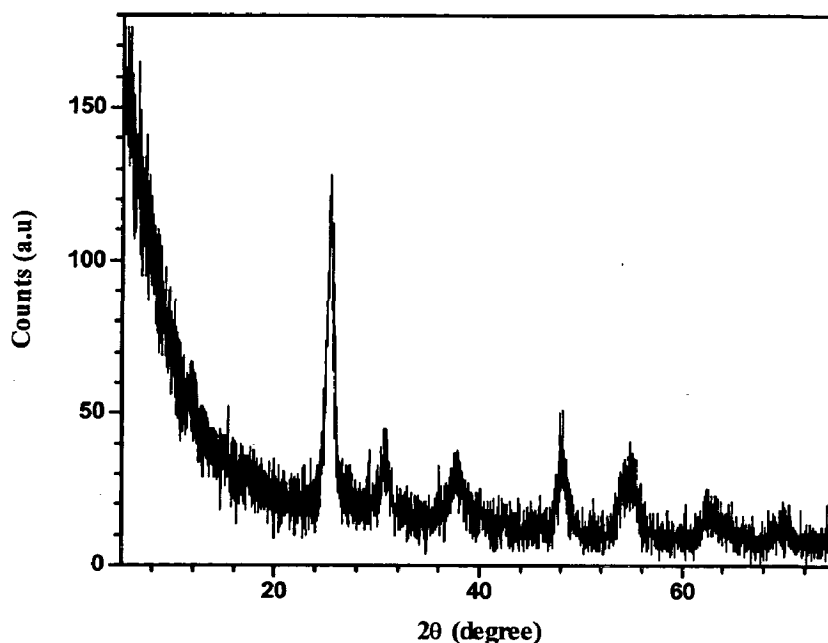


Figure 4.2 XRD pattern of heat treated TiO_2 nanoparticles

4.2.2 Solid state electronic spectra

The as synthesized TiO_2 particles and the heat treated samples were characterized by solid state electronic spectroscopy in reflectance mode. Figure 4.3 shows the reflectance and absorbance spectra (calculated from the reflectance data by Kubelka Munk transformation)¹³ of the heat treated (microwave & 123°C) and as prepared samples. The samples absorbed around 320 nm and illustrates that the optical absorption edge of the heat treated samples shifted to the lower wavelength region when compared to the untreated sample. These result confirms that there is a change of size on heating. We have also calculated the band gap of the samples from the optical edge. They are 3.08 and 3.17 eV respectively for the untreated and heat (127°C) treated samples. The observed absorption and band gap values are in

keeping with those reported in the literature. Literature methods produced TiO_2 nanoparticles with the band gap ranging from 3 to 3.2 eV and the absorbance around 325 nm.¹⁴

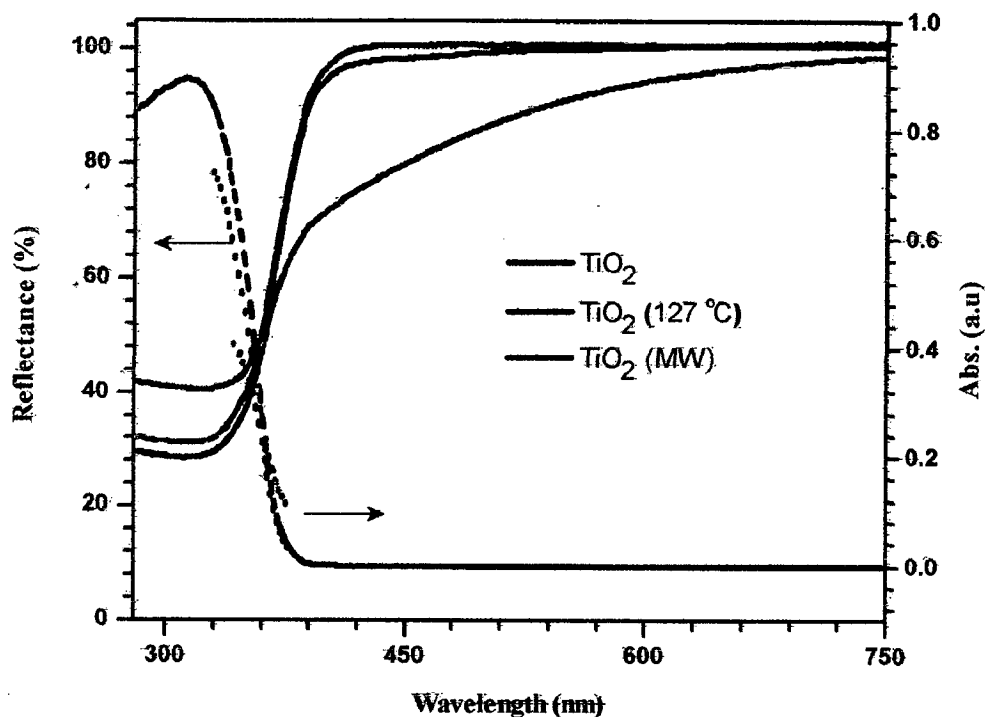


Figure 4.3 Reflectance and absorbance spectra of treated and untreated TiO_2 nanoparticles.

4.2.3 FE-SEM analysis

The FE-SEM images of the heat treated (127°C) TiO_2 nanoparticles are shown in Figure 4.4. It can be seen that the particles are spherical in nature and high resolution FE-SEM image (Figure 4.4 (b)) clearly indicates particle sizes ranging from 80-120 nm. Formation of large size particles is due to ageing, small dimensions and high surface to volume ratio of the particles. Under these conditions it is easy for them to agglomerate with each others to form large spherical particles. We can also find from these images that the morphology of the particles is almost homogeneous in nature.¹² Formation of homogenous nanoparticles is a subject of recently investigations as they are expected to exhibit unique optical properties.

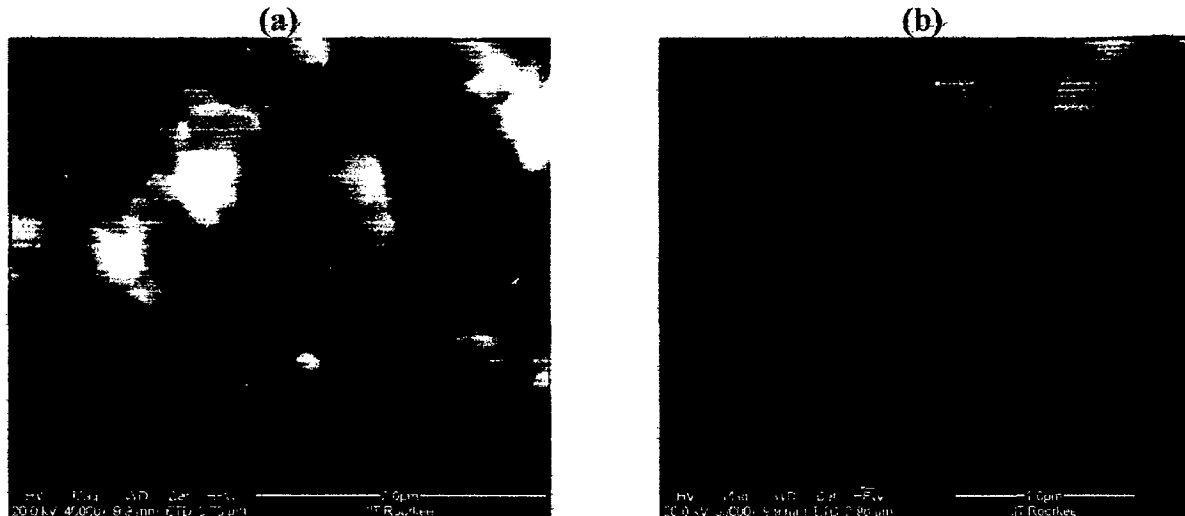


Figure 4.4 FE-SEM images of heat treated TiO_2 nanoparticles at magnification: (a) 40000X & (b) 50000X.

4.2.4 Elemental analysis

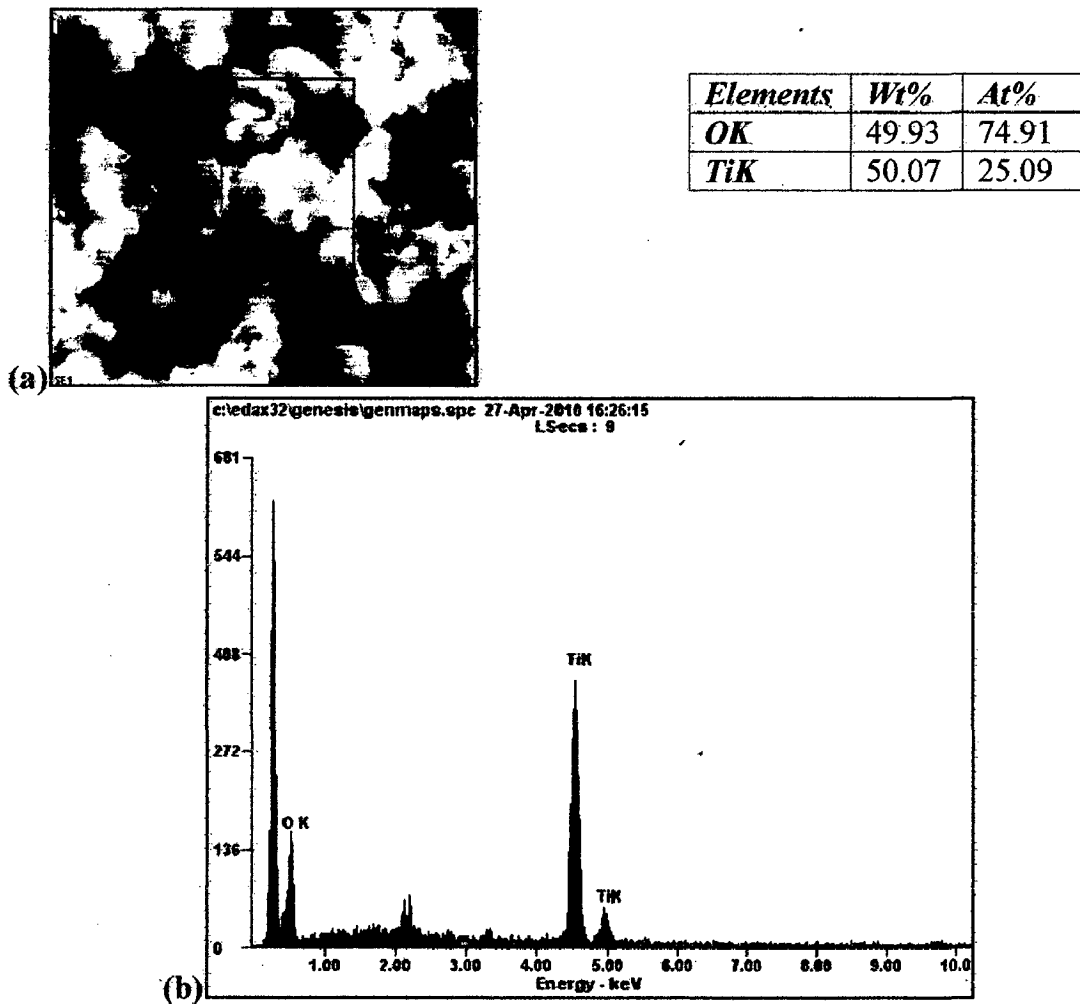


Figure 4.5 FE-SEM (a) and EDAX spectrum (b) of the heat treated TiO_2 nanoparticles.

4.2 Synthesis and characterization TiO₂ nanoparticles

Synthetic procedure for the anatase TiO₂ nanoparticles is illustrated in Figure 4.1. Titanium tetraisopropoxide (30 mL) and dry ethanol (100 mL) were taken in a 250 mL round-bottom flask, and stirred thoroughly for 30 min and subjected to then sonication for 30 min. Hydrolysis was performed by adding distilled water (24 mL) slowly at the rate of 0.5 mL/min with vigorous stirring. The solvent from the obtained mixture was removed using a rotary evaporator at 70 °C under reduced pressure. The powder was then stored in vacuum desiccator for drying. Finally, the dried sample was calcined at 127 °C for 11 h to obtain anatase TiO₂ nanoparticles.¹² As there is growing interest for microwave assisted synthesis of materials, we have also studied the effect of microwave heating on the nanoparticles. Typically the nanoparticles placed in a crucible were subjected to microwave for 1 min in high power mode. The color of the particles changed to tan color.

4.2.1 XRD analysis

The XRD pattern observed for the nanoparticles is shown in Figure 4.2. Characteristic diffraction peaks due to the anatase phase are present in the XRD pattern. The broadened peaks are indicating that the sizes of the particles are in nanoranges.¹² In order to achieve more confirmative information, the Debye-Scherrer formula was used to calculate the size of the nanoparticles.

Debye-Scherrer formula

$$(t = 0.94 \times \lambda / \beta \text{ Cos } \theta)$$

where t is the average thickness of the particle, λ is the X-ray wavelength, β is the line broadening at half the maximum intensity in radians, and θ is the Bragg angle.

The average grain size is estimated from the major XRD peak for the anatase phase around $2\theta = 25.39^\circ$, which is 16 nm. The reported size was 8 nm for the TiO_2 particles obtained in a similar methodology.¹²

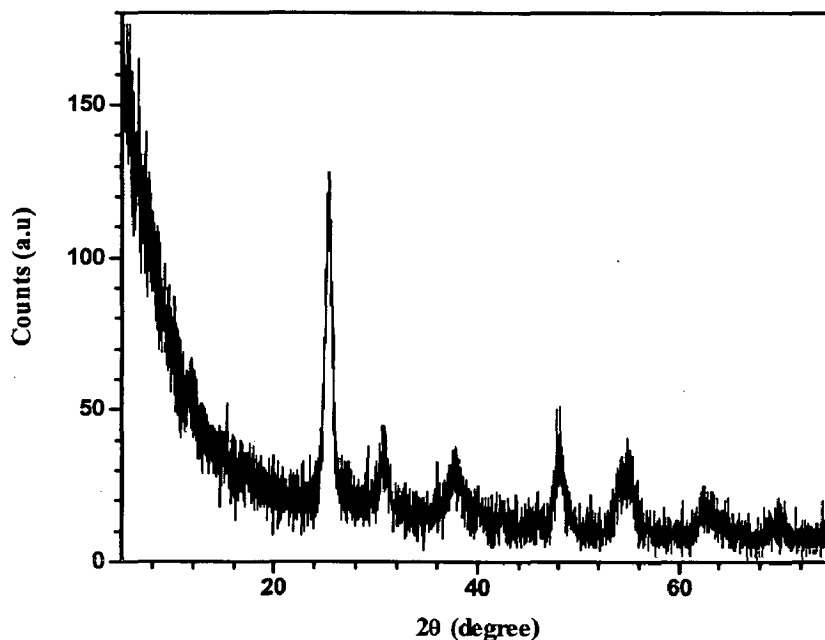


Figure 4.2 XRD pattern of heat treated TiO_2 nanoparticles

4.2.2 Solid state electronic spectra

The as synthesized TiO_2 particles and the heat treated samples were characterized by solid state electronic spectroscopy in reflectance mode. Figure 4.3 shows the reflectance and absorbance spectra (calculated from the reflectance data by Kubelka Munk transformation)¹³ of the heat treated (microwave & 123°C) and as prepared samples. The samples absorbed around 320 nm and illustrates that the optical absorption edge of the heat treated samples shifted to the lower wavelength region when compared to the untreated sample. These result confirms that there is a change of size on heating. We have also calculated the band gap of the samples from the optical edge. They are 3.08 and 3.17 eV respectively for the untreated and heat (127°C) treated samples. The observed absorption and band gap values are in

keeping with those reported in the literature. Literature methods produced TiO_2 nanoparticles with the band gap ranging from 3 to 3.2 eV and the absorbance around 325 nm.¹⁴

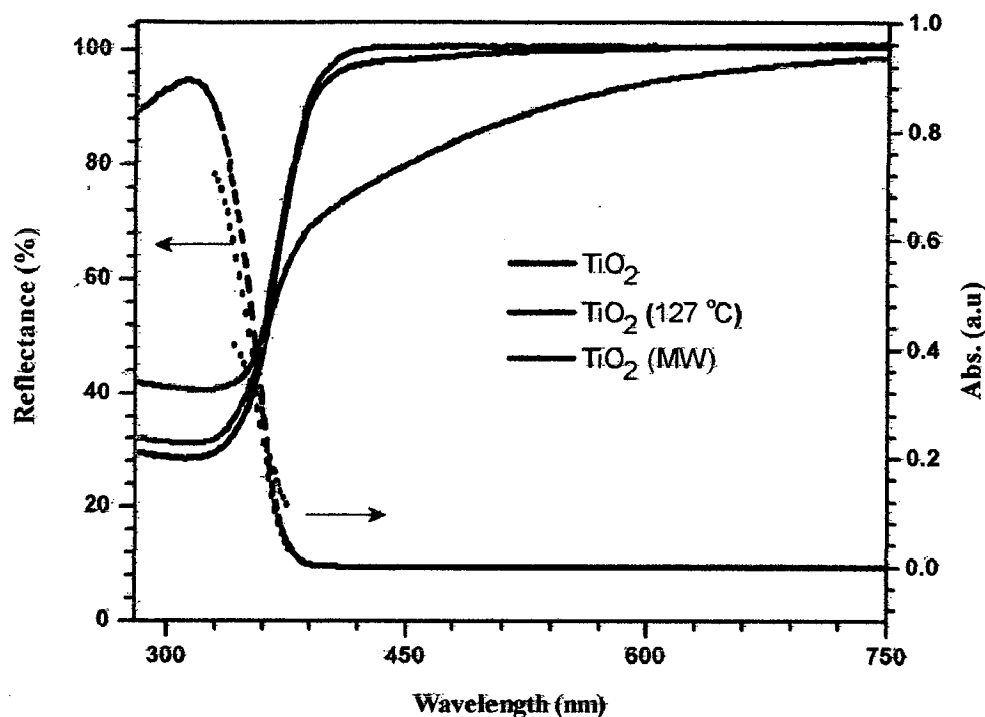


Figure 4.3 Reflectance and absorbance spectra of treated and untreated TiO_2 nanoparticles.

4.2.3 FE-SEM analysis

The FE-SEM images of the heat treated (127 °C) TiO_2 nanoparticles are shown in Figure 4.4. It can be seen that the particles are spherical in nature and high resolution FE-SEM image (Figure 4.4 (b)) clearly indicates particle sizes ranging from 80-120 nm. Formation of large size particles is due to ageing, small dimensions and high surface to volume ratio of the particles. Under these conditions it is easy for them to agglomerate with each others to form large spherical particles. We can also find from these images that the morphology of the particles is almost homogeneous in nature.¹² Formation of homogenous nanoparticles is a subject of recently investigations as they are expected to exhibit unique optical properties.



Figure 4.4 FE-SEM images of heat treated TiO_2 nanoparticles at magnification (a) 40000X & (b) 50000X.

4.2.4 Elemental analysis

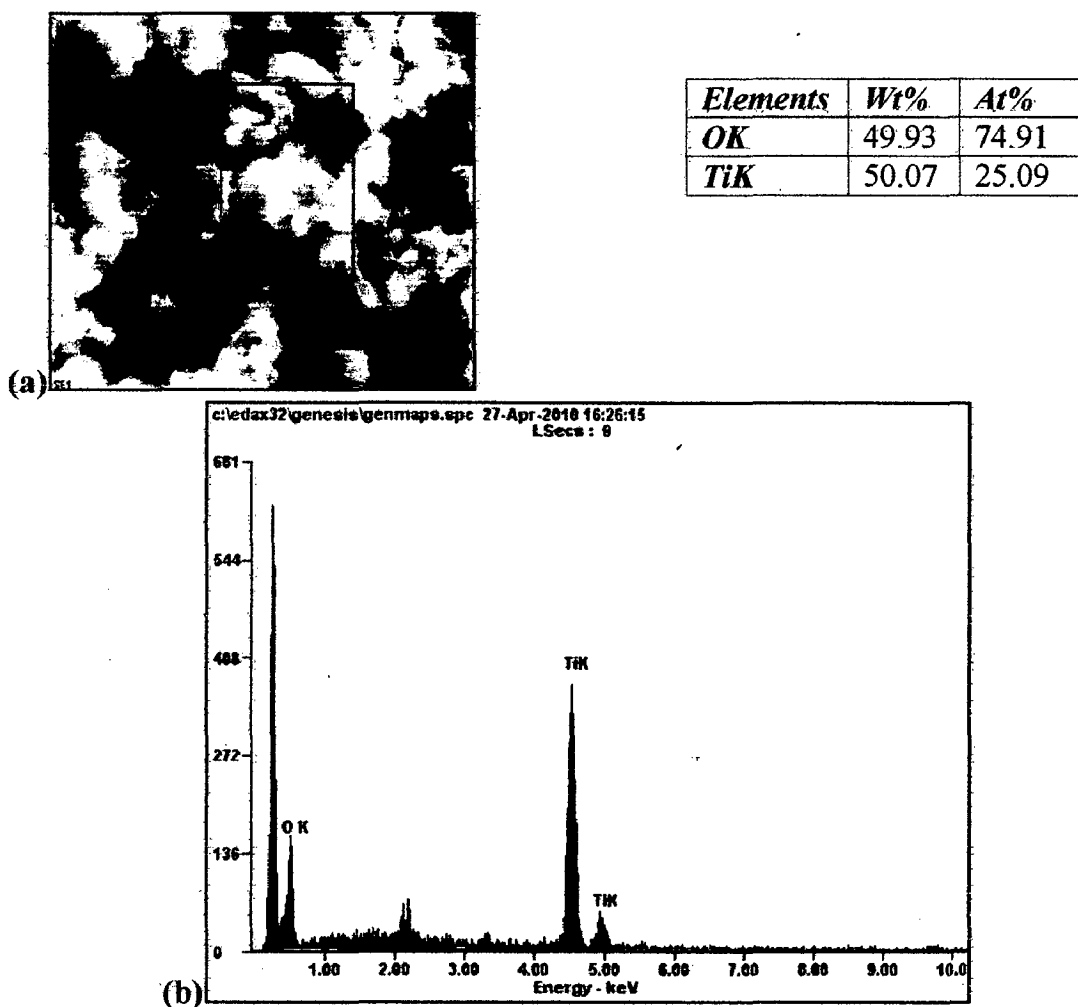


Figure 4.5 FE-SEM (a) and EDAX spectrum (b) of the heat treated TiO_2 nanoparticles.

The EDAX technique is used to study the elemental composition of the samples using energy dispersive X-ray analysis. The EDAX analysis system works as an integrated feature of scanning electron microscopy (SEM). We scanned the middle area of the image to find out the composition of particles as shown in Figure 4.5 (a) and observed the predominant elements of titanium and oxygen with a weight ratio of 50:50%. It confirms the presence of titanium dioxide without impurities (Figure 4.5 (b)). And we have also evaluated the analysis for a single particle as shown in Figure 4.6 (a) and 4.6 (b). The composition remained same and corroborated the exclusive formation of TiO_2 .¹⁵

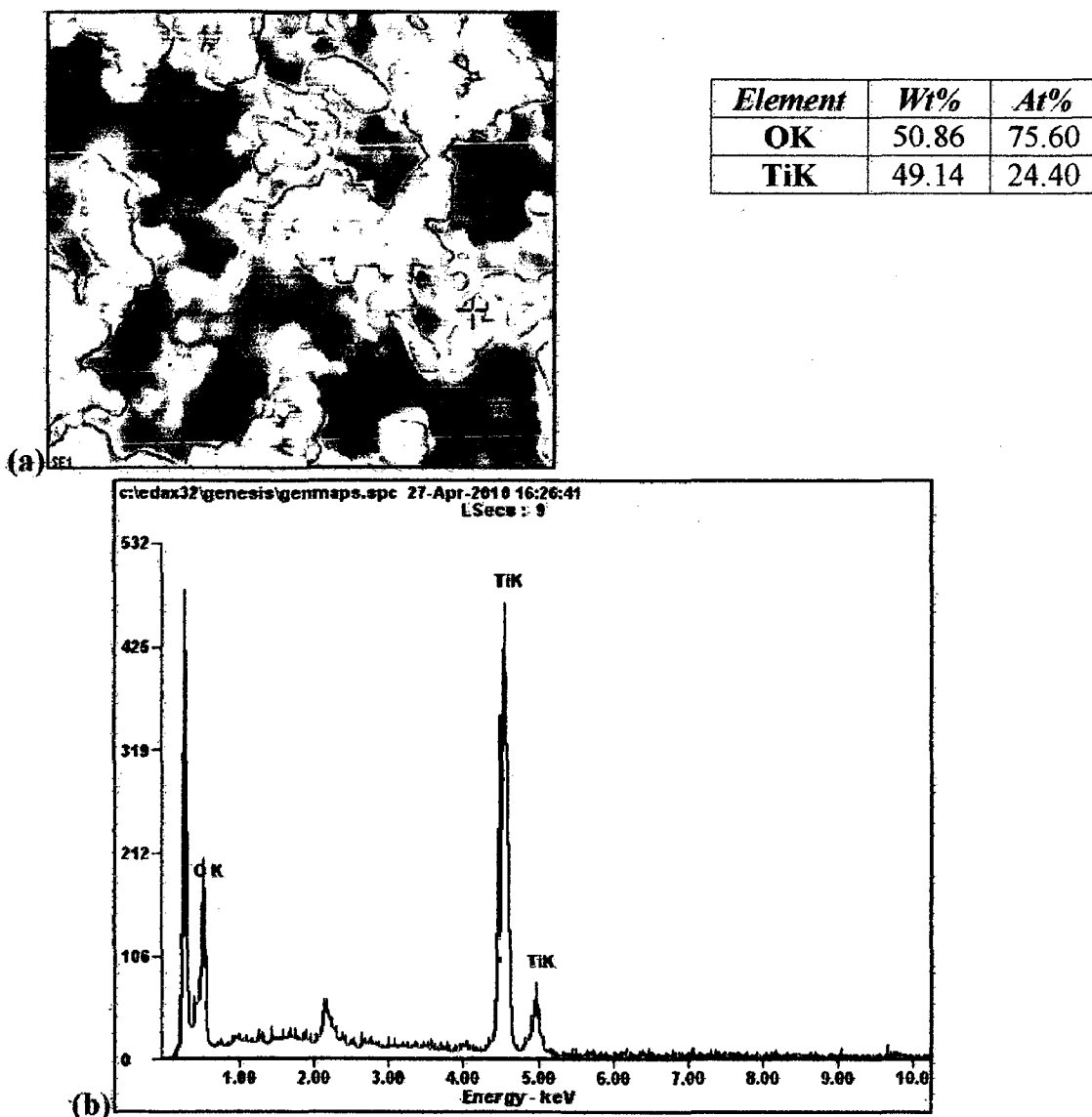


Figure 4.6 FE-SEM (a) and EDAX spectrum (b) of TiO_2 nanoparticles.

4.3 Coating of organic dyes on TiO₂ nanoparticles and their characterization

In a round bottom flask anatase TiO₂ nanoparticles (100 mg, 1.25 mmol) and 1.1 equivalents of organic dyes (**D1**, **D2**, **D3**, & **D4**) were taken and mixed with 15 mL ethanol. This mixture was kept stirring for overnight. The reaction mixture was filtered and the solid was dried under vacuum for further characterization. To evaluate the photocatalytic activity the coating was performed in the presence and absence of light separately.¹⁶⁻¹⁸

4.3.1 Solid state electronic spectra

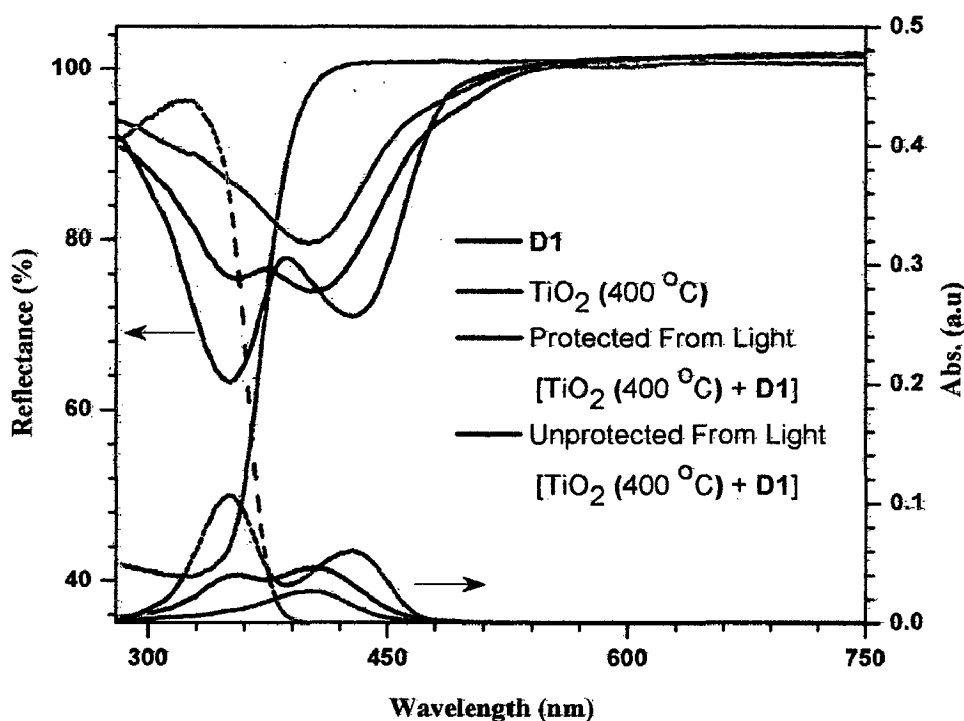


Figure 4.7 Reflectance and absorbance spectra of the dye (**D1**) coated TiO₂ nanoparticles.

The samples obtained from the both protected and light exposed procedures were characterized by a solid state electronic spectra. From the Figure 4.7 it is evident that the dye is coated on the TiO₂ nanoparticles and characteristic peaks due to the dye are appearing at around 350 nm and 427 nm for the protected sample while the unprotected sample gives a

single peak at 400 nm. The disappearance of peak at 350 nm in the unprotected samples indicates that there may be photocatalytic reactions which degraded the dye (D1) molecules partially in the presence of TiO_2 nanoparticles.¹⁹ A slight blue shift observed for the higher wavelength peak strongly supports the interaction of the dyes *via* the carboxylic anchoring unit with the TiO_2 nanoparticles.²⁰

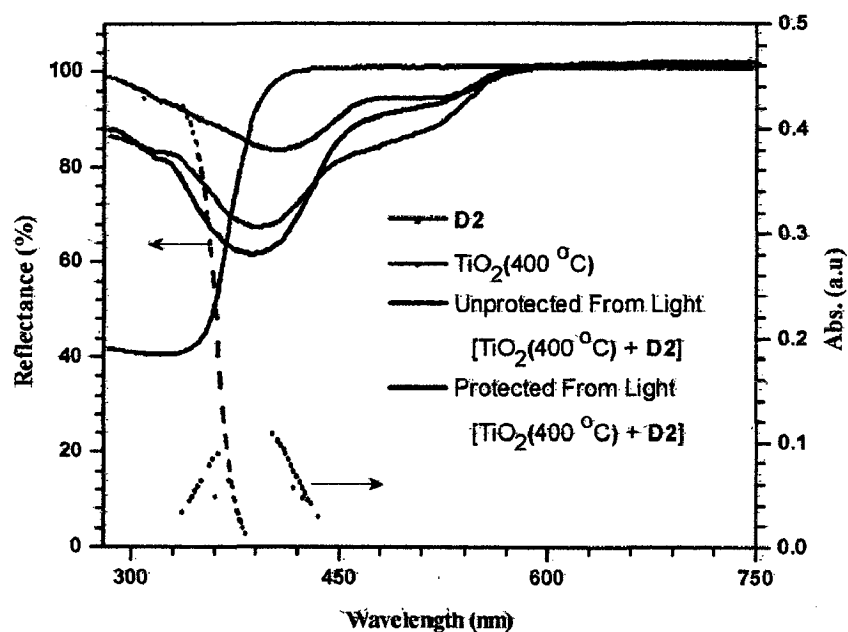


Figure 4.8 Reflectance and absorbance spectra of the dye (D2) coated TiO_2 nanoparticles.

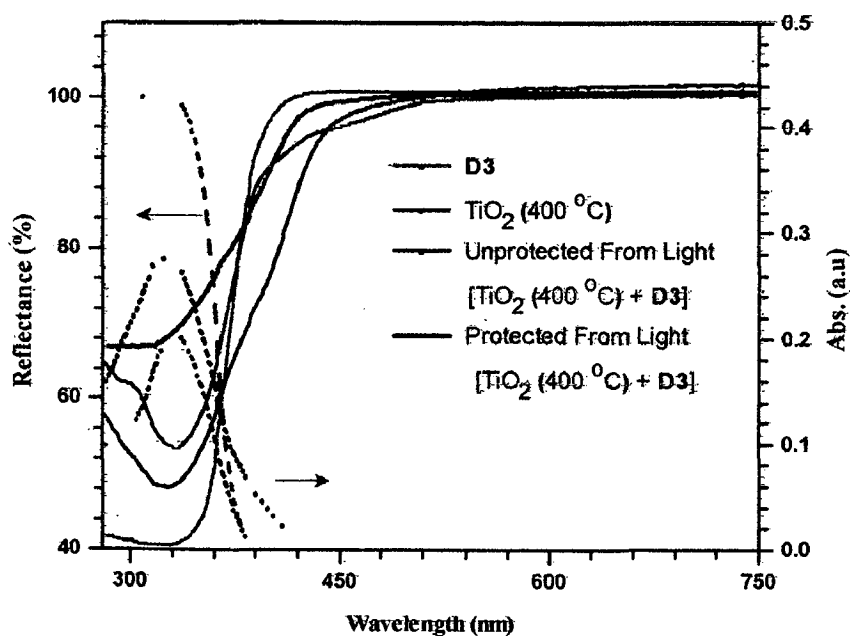


Figure 4.9 Reflectance and absorbance spectra of the dye (D3) coated TiO_2 nanoparticles.

Figures 4.8, 4.9 and 4.10 illustrates the optical absorbance recorded for the composites. The patterns clearly shows that the dyes are interacting with the TiO_2 nanoparticles via the carboxylic anchoring groups. The band gap calculated for the composites from the optical edge is listed in Table 4.1 and ranges from 2.33 – 3.17 eV. The reduction of the band gap on inclusion of the organic dye indicates that the optical properties of the composites are mainly decided by the low band gap organic dyes.

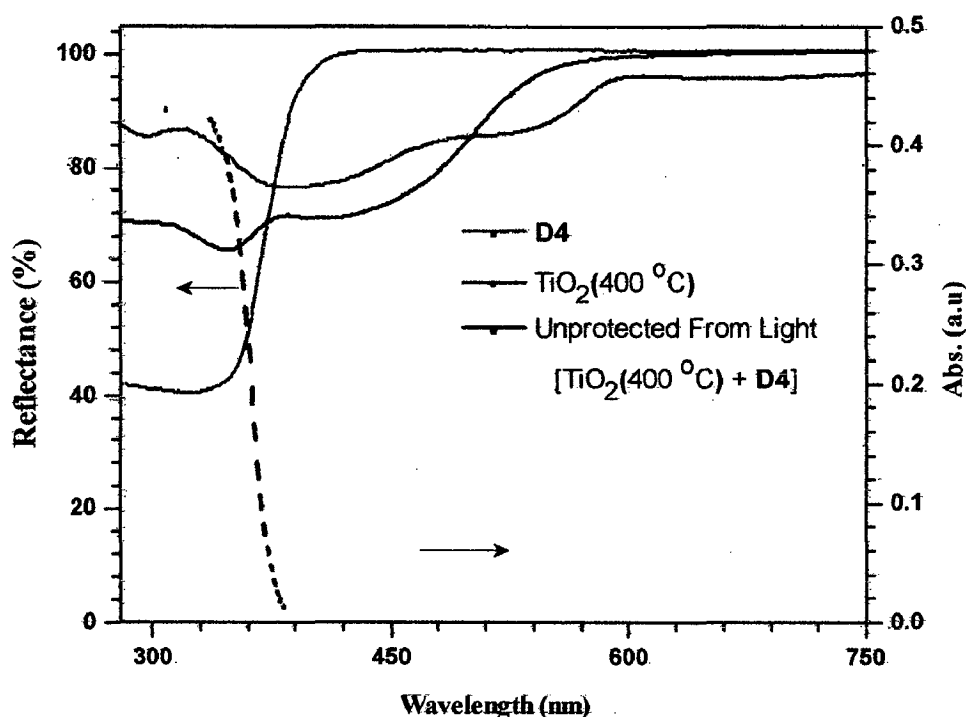


Figure 4.10 Reflectance and absorbance spectra of the dye (D4) coated TiO_2 nanoparticles.

4.3.2 XRD analysis

To determine the crystalline nature of the composites and their average thickness, the XRD measurements were carried out at room temperature over the diffraction angle $0-90^\circ$. The typical XRD patterns observed for the composites are shown in Figures 4.11, 4.12, 4.13 and 4.14. The average particle sizes of the composites were estimated by the Scherrer equation from the half width of the broadened plane and are listed in Table 4.1.²¹

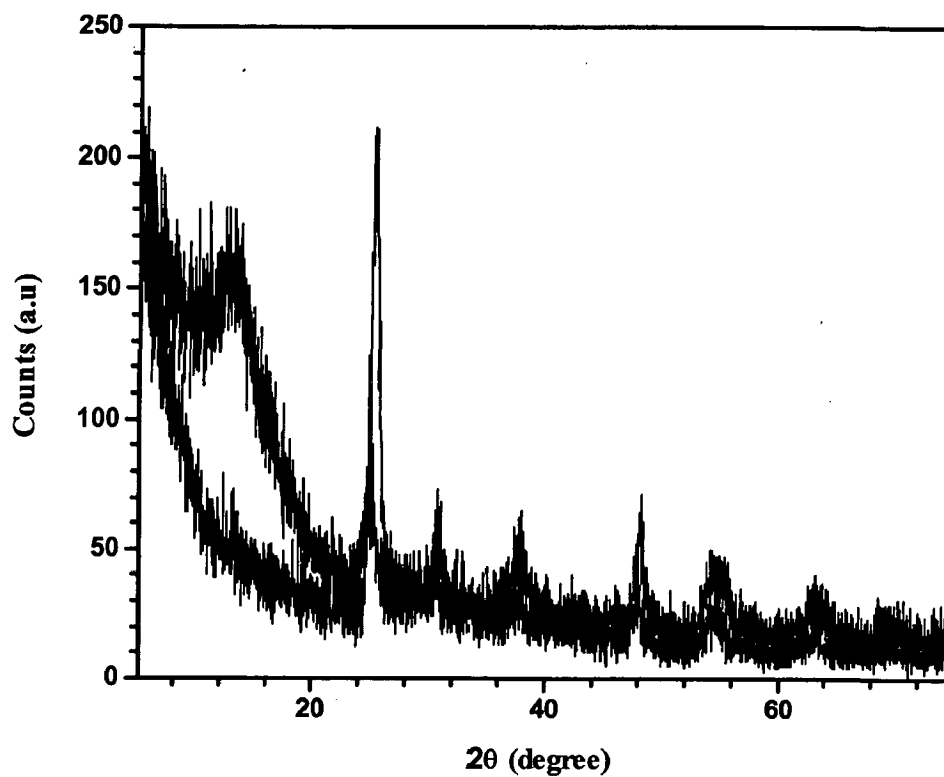


Figure 4.11 XRD pattern of the dye (D1) coated TiO_2 nanoparticles.

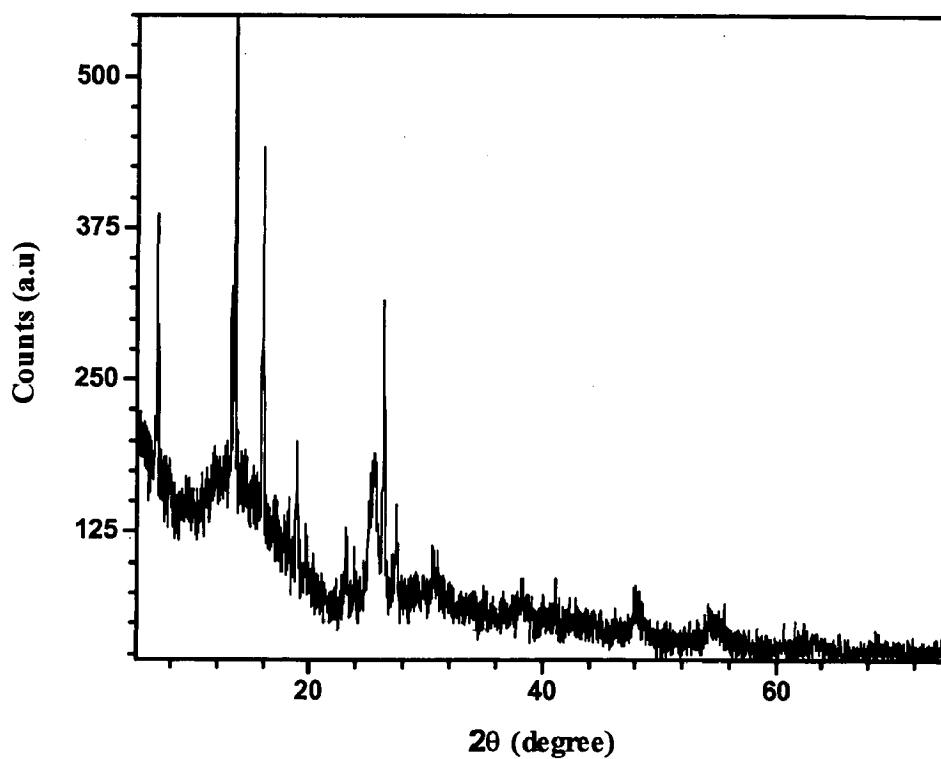


Figure 4.12 XRD pattern of the dye (D1) coated TiO_2 nanoparticles.

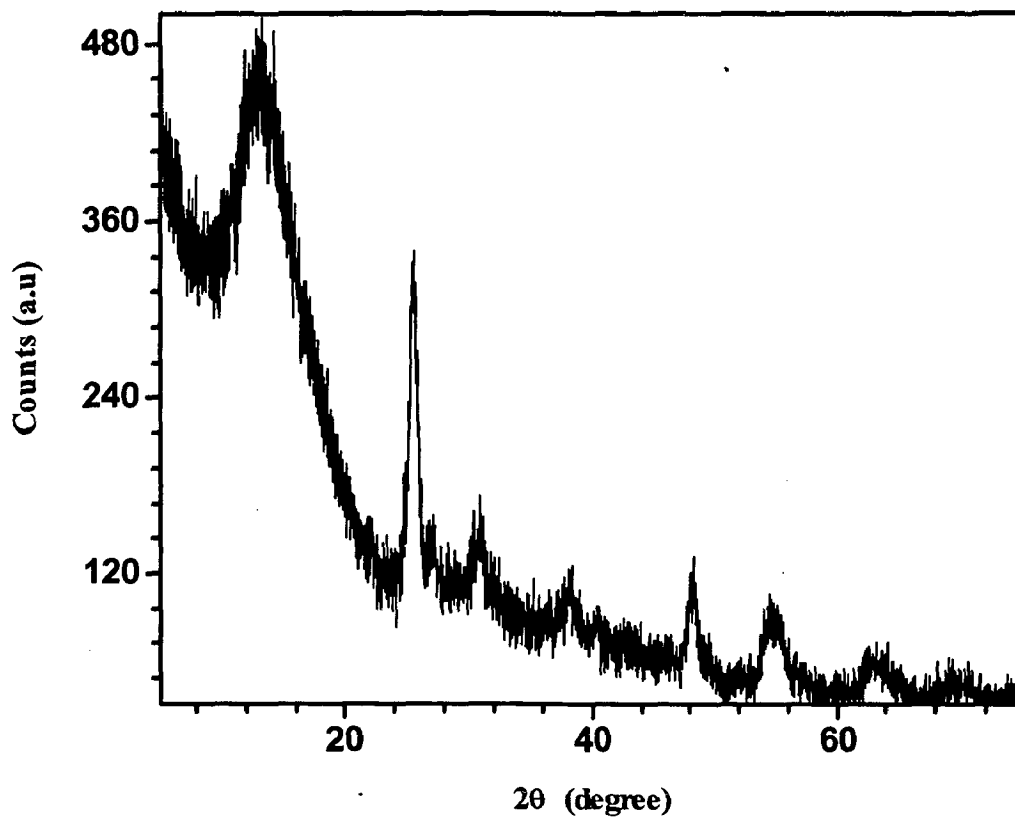


Figure 4.13 XRD pattern of the dye (D3) coated TiO_2 nanoparticles.

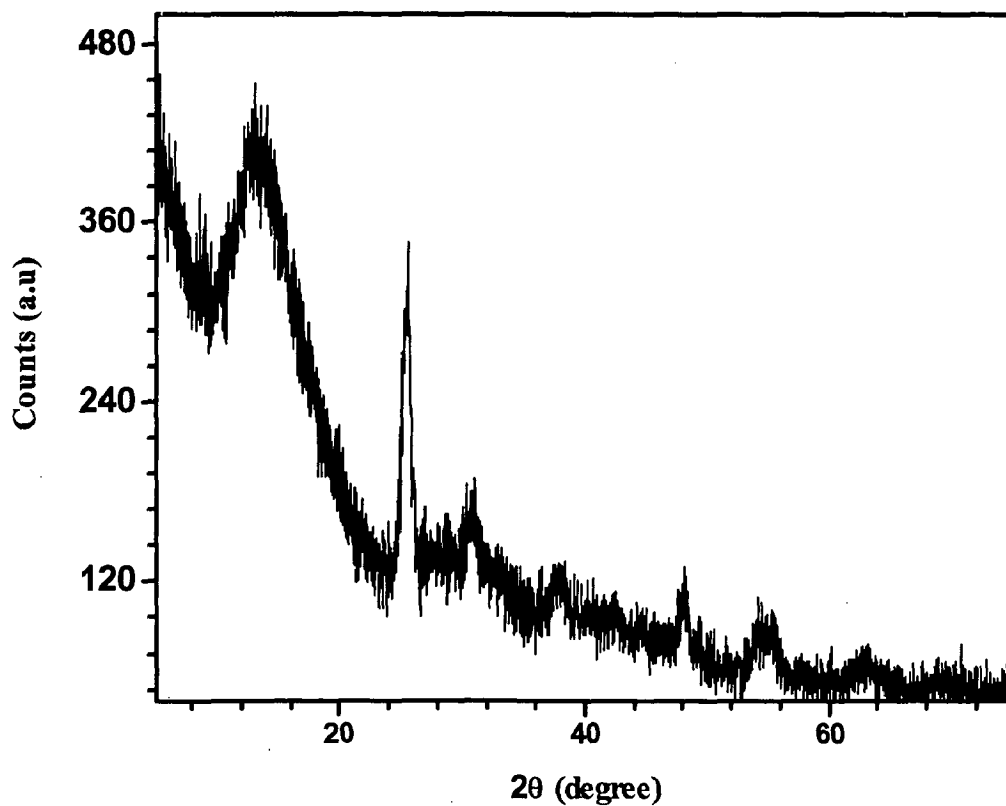


Figure 4.14 XRD pattern of the dye (D4) coated TiO_2 nanoparticles.

4.3.3 Thermal analysis

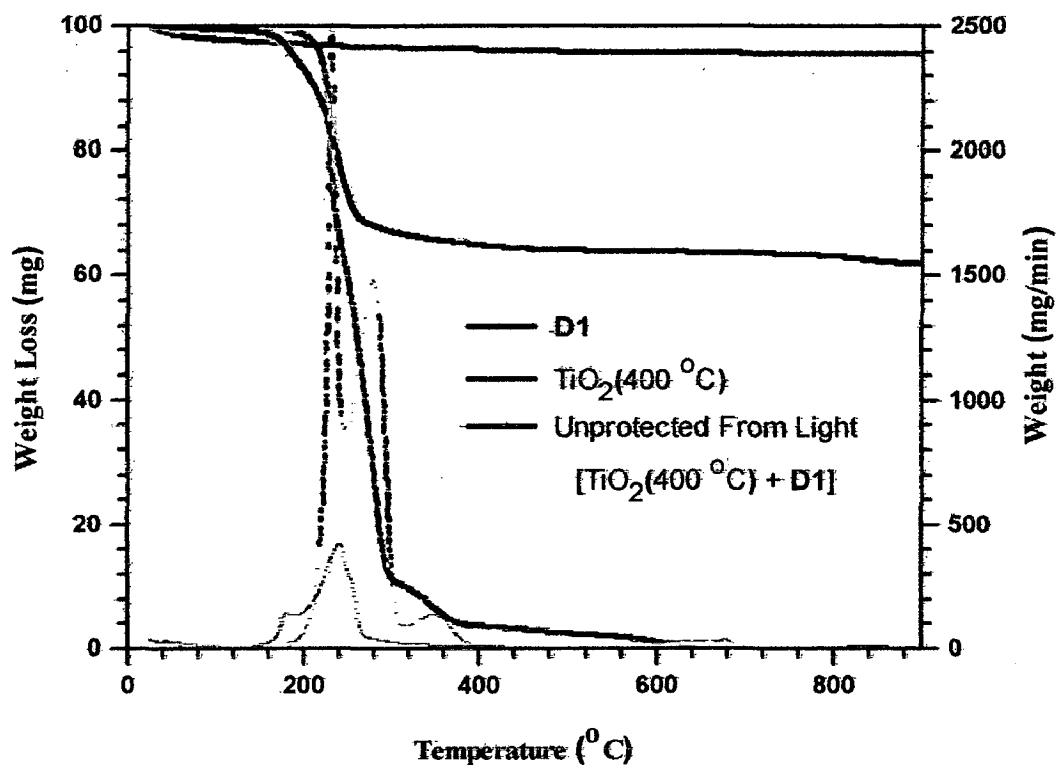


Figure 4.15 TG and DTG curve of the dye (D1) coated TiO_2 nanoparticles.

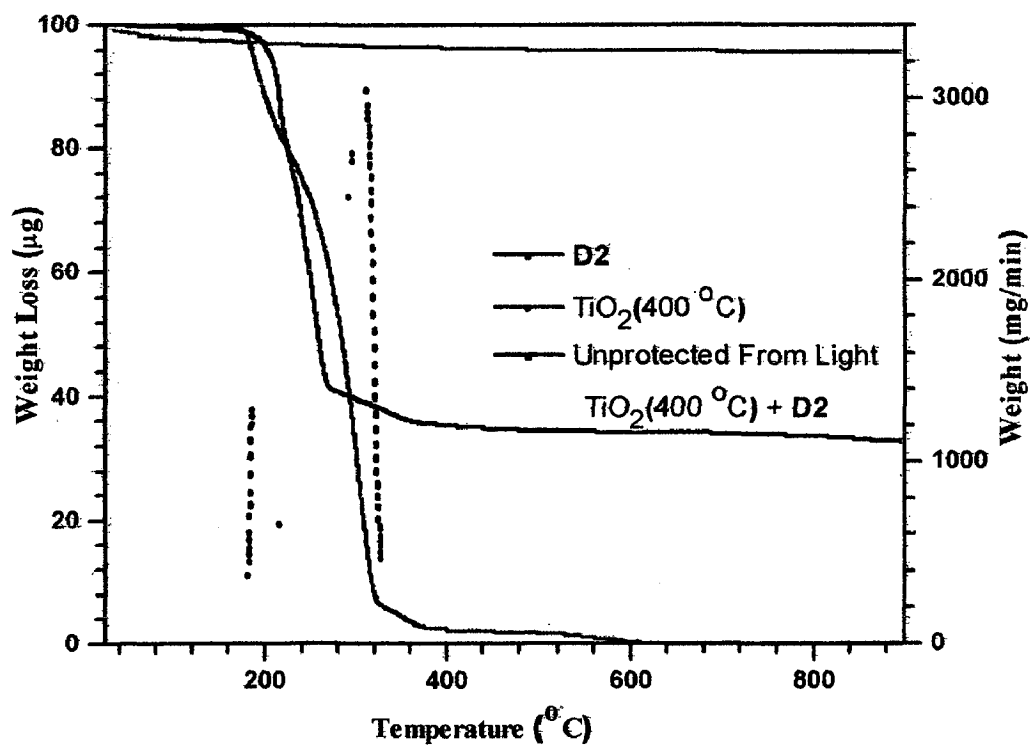


Figure 4.16 TG and DTG curve of the dye (D2) coated TiO_2 nanoparticles.

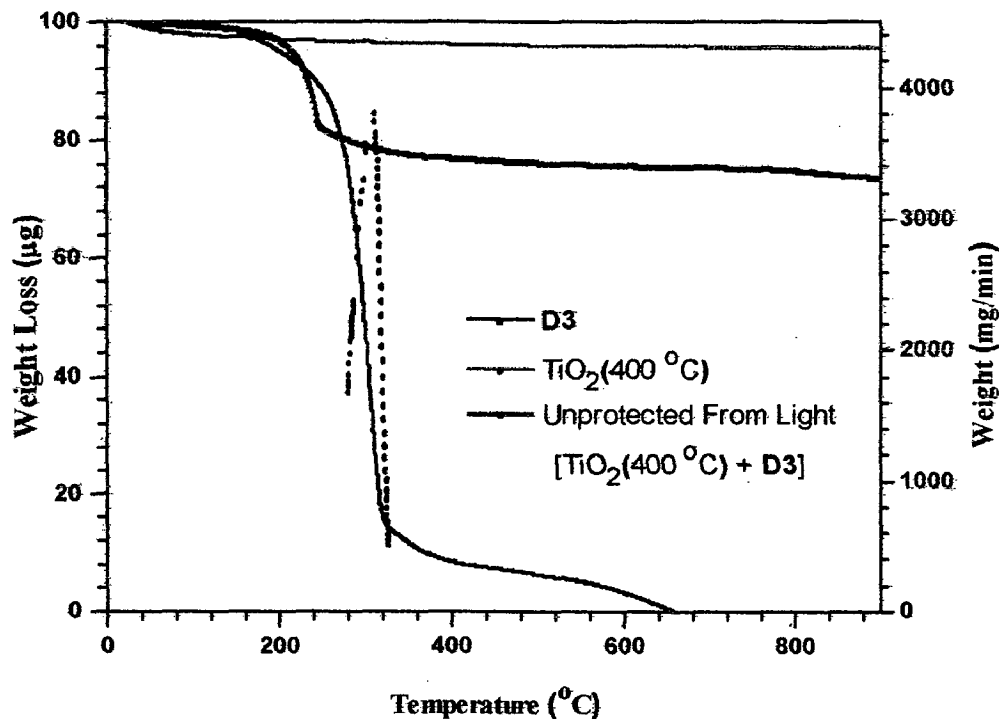


Figure 4.17 TG and DTG curve of the dye (D3) coated TiO₂ nanoparticles.

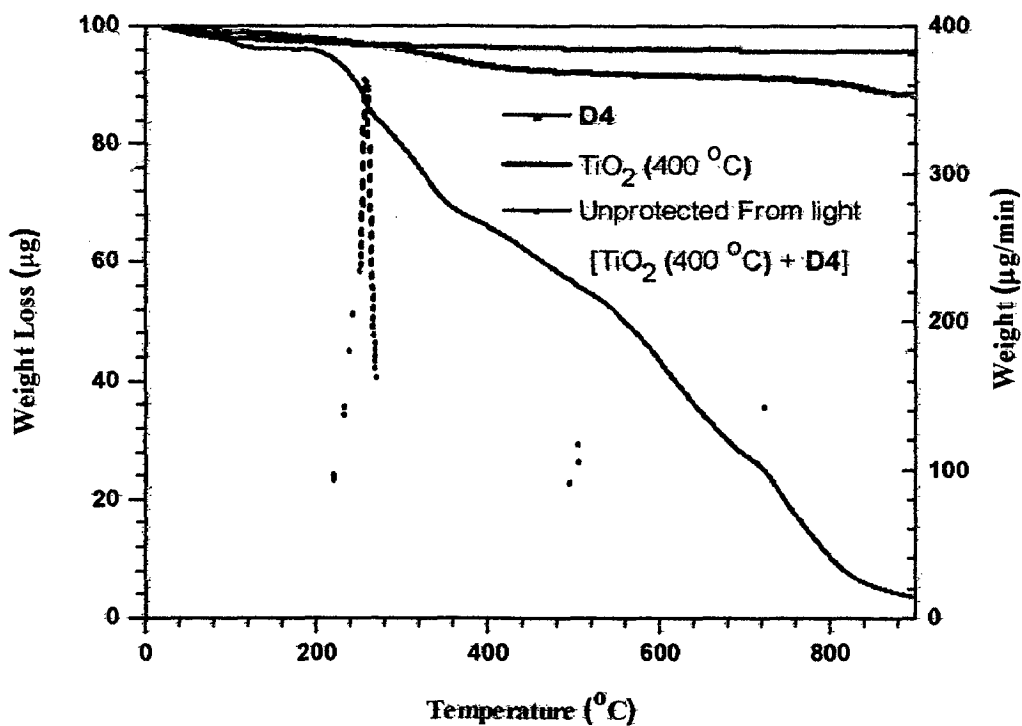


Figure 4.18 TG and DTG curve of the dye (D4) coated TiO₂ nanoparticles.

The thermal properties of the TiO₂ nanoparticles and the dye composites were studied by thermogravimetric analysis. The thermograms recorded for the four different dye coated

samples along with the parent TiO_2 nanoparticles are displayed in Figures 4.15, 4.16, 4.17 and 4.18. TiO_2 nanoparticles resist thermal degradation over a wide range (up to $900\text{ }^\circ\text{C}$).^{22, 23} The composites exhibited decomposition at the temperature in which the pure dyes started degrading. The onset temperature of the composites is listed in Table 4.1. From the TGA analysis the dye content in each of the unprotected composites from light are estimated as 34%, 43% and 17% for the dyes **D1**, **D2** and **D3** respectively. For **D4** a reasonable estimate could not be made as it exhibited enhanced thermal stability similar to nanocrystalline TiO_2 .

4.3.4 FE-SEM analysis

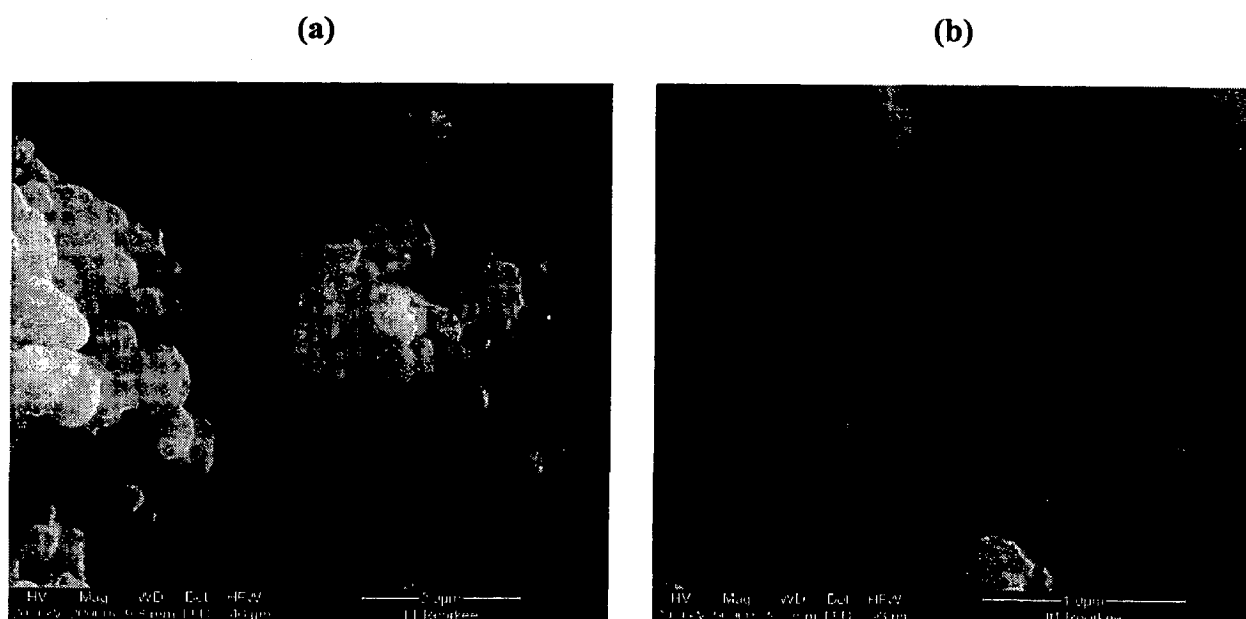


Figure 4.19 FE-SEM images of the dye (**D1**) coated TiO_2 nanoparticles at magnification (a) 20,000X & (b) 50,000X

The FE-SEM was used to observe the microstructure of the prepared composites. Figure 4.19 (a) shows that the particles are spherical in nature with different size ranging from 200-300 nm in agglomerated form.²⁴⁻²⁶ At high resolution, we observe that the dye (**D1**) is adsorbed on TiO_2 as shown in Figure 4.19 (b).

Figure 4.20 shows the FE-SEM picture of the **D2** composites at different magnification levels. The image clearly shows that the spherical particles are arranged in a linear form to produce a rod shaped structure. These changes from spherical to rod shape due to the interaction of **D2** molecules on the TiO_2 surfaces is attributed to the presence of lengthy ethyl chain which directs the agglomeration in a single direction.²⁶

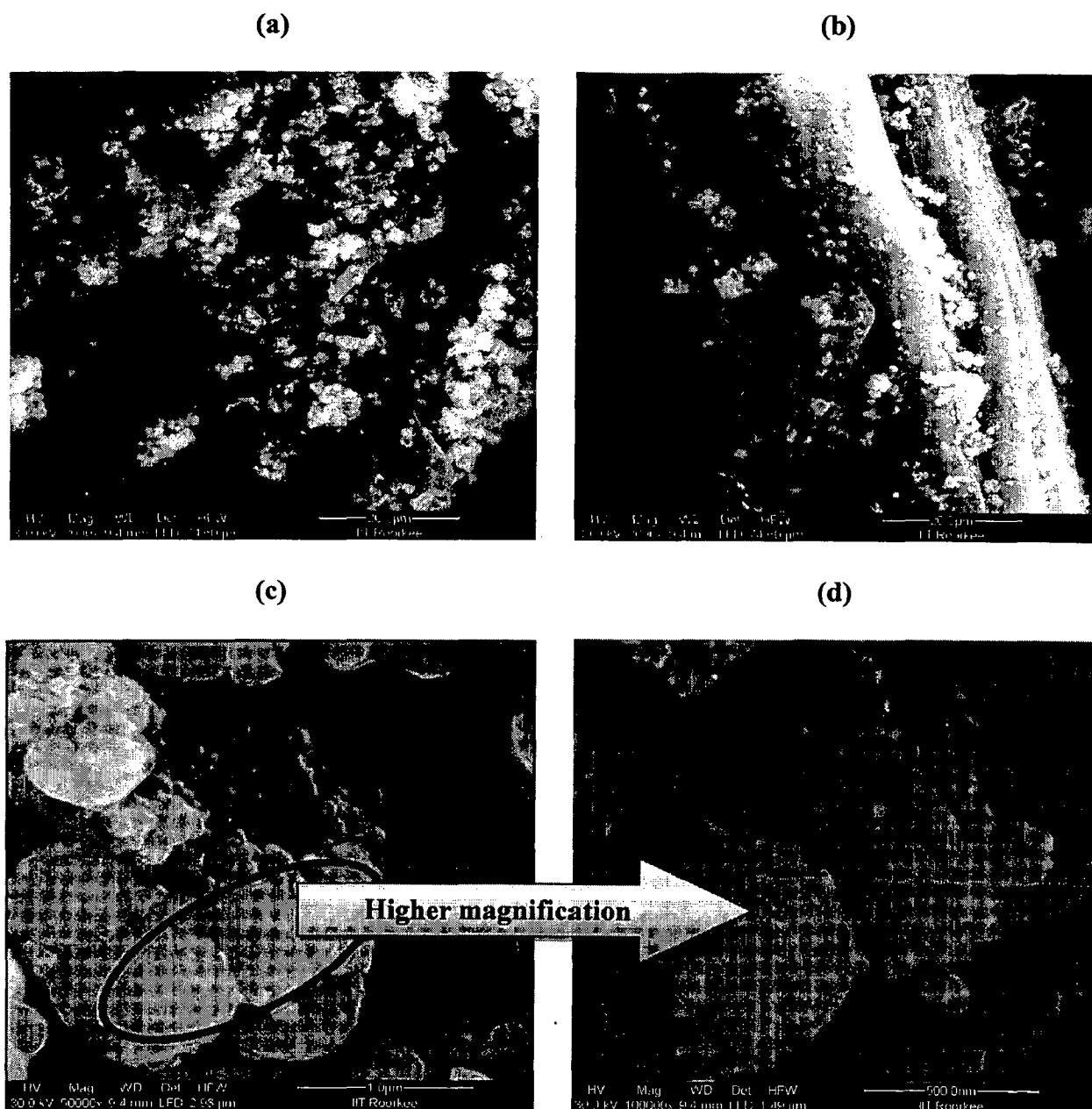


Figure 4.20 FE-SEM images of the dye (**D2**) coated TiO_2 nanoparticles at magnification (a), (b) 20,000X (c) 50,000X & (d) 1,00,000X.

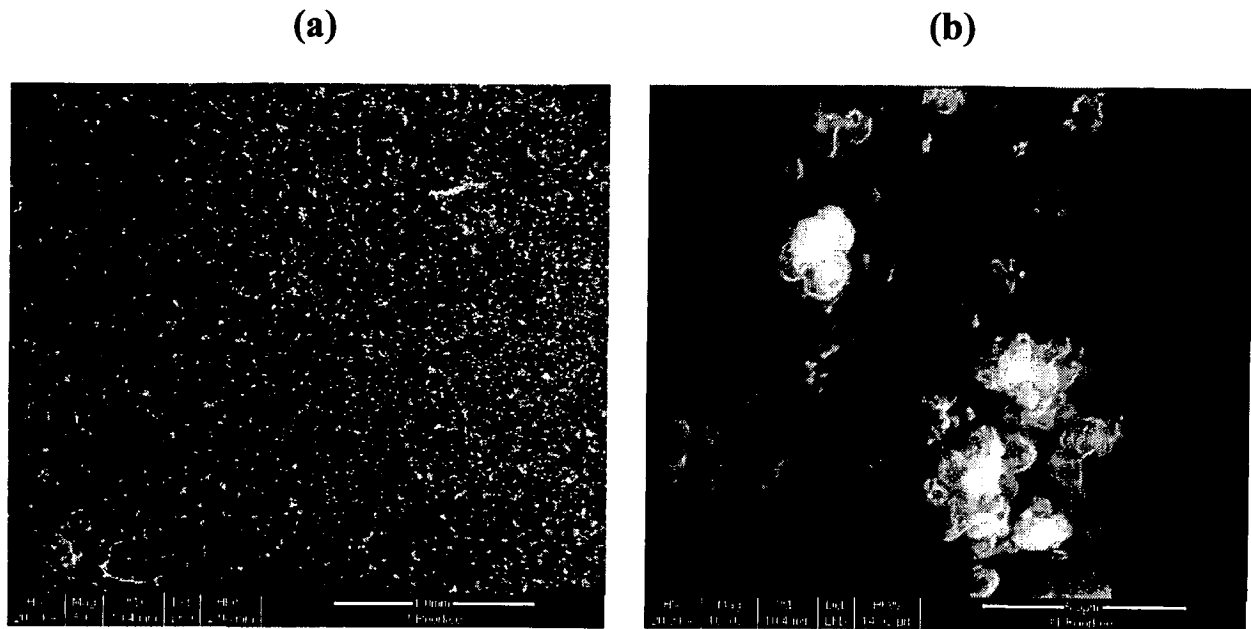


Figure 4.21 FE-SEM images of dye (D3) coated TiO₂ nanoparticles at magnification (a) 50X & (b) 10,000X

Figure 4.21 presents the FE-SEM images of the D3 containing composites at different magnifications; the images clearly show that the composite assumes spherical shapes in range of sizes due to the agglomeration.

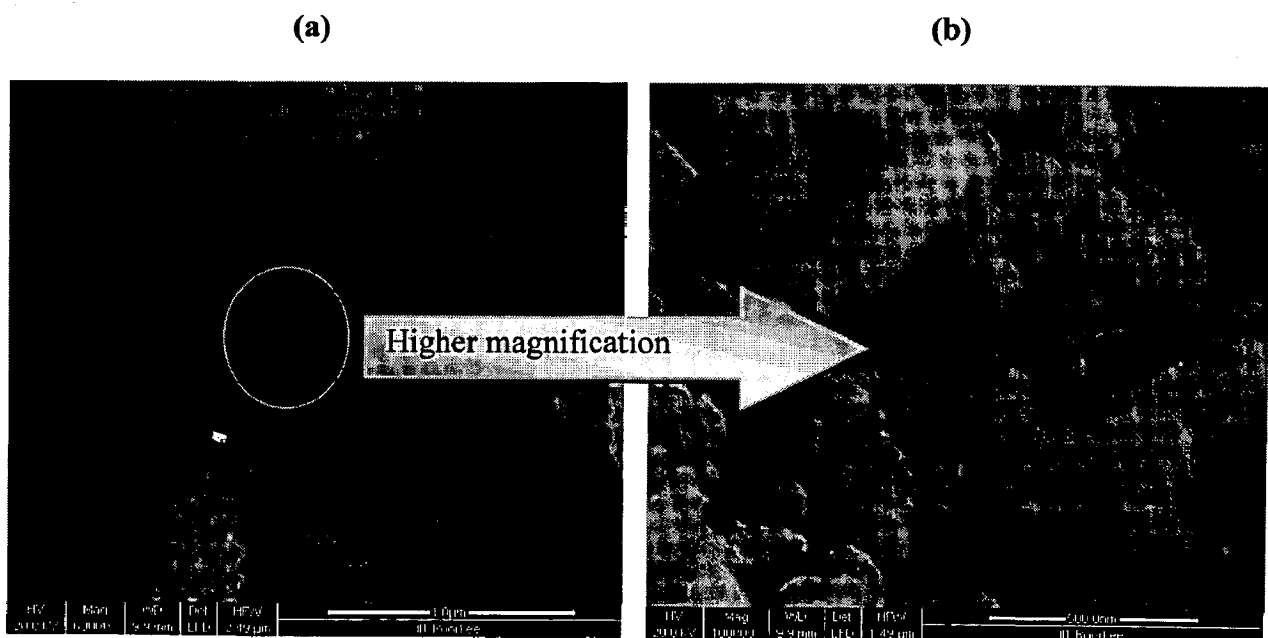


Figure 4.22 FE-SEM images of the D4 dye coated TiO₂ nanoparticles.

Figure 4.22 shows the FE-SEM picture of the composites derived from the dye **D4**. The images clearly establish the spherical nature of the particles however non-uniform size distribution realized is attributed to the agglomeration. As the TiO_2 nanoparticles are largely monodispersed, the size distribution observed for the dye coated TiO_2 particles indicate the role of dyes in nucleation. In all the cases particles are agglomerate form with non-homogeneous in nature, this may be due to ageing factor, small dimensions and high surface to volume ratio of particles, it is easy for them to agglomerate with each others.

Table 4.1 Morphology, optical and thermal data observed for the dye coated TiO₂ nanoparticles

Compounds	Optical Edge (nm) ^a	Band gap (eV)	Size (nm) ^b	Onset Temperature, °C ^c	Shape ^d
TiO ₂	378	3.08	-	-	Spherical
TiO ₂ (Microwave)	396	3.13	-	-	Spherical
TiO ₂ (400 °C)	390	3.17	15.99	904	Spherical
TiO ₂ (400 °C) + D1	491	2.53	200	188	Spherical
TiO ₂ (400 °C) + D2	476	2.605	250	206	Rod & Spherical
TiO ₂ (400 °C) + D3	433	2.862	130.56	215	Spherical
TiO ₂ (400 °C) + D 4	531	2.333	119.57	334	Spherical

^a from optical spectra, ^b from XRD using formula, ^c temperature corresponding to 5% weight loss, ^d as shown in FE-SEM.

4.4 Synthesis and characterization of blue emitted colloidal CdS solution

Cadmium acetate (0.86 g) and sulphur powder (0.12 g) were taken in a round bottom flask. *N, N*-dimethylformamide (75 mL) and water (75 mL) were added and stirred for 30 min. Nitrogen gas was passed through the reaction mixture for 1 h with vigorous stirring to remove oxygen. The inert mixture was heated at 130 °C for 8 h to obtain blue emitting colloidal solution.²⁷

4.4.1 Absorption characteristics of the CdS colloids

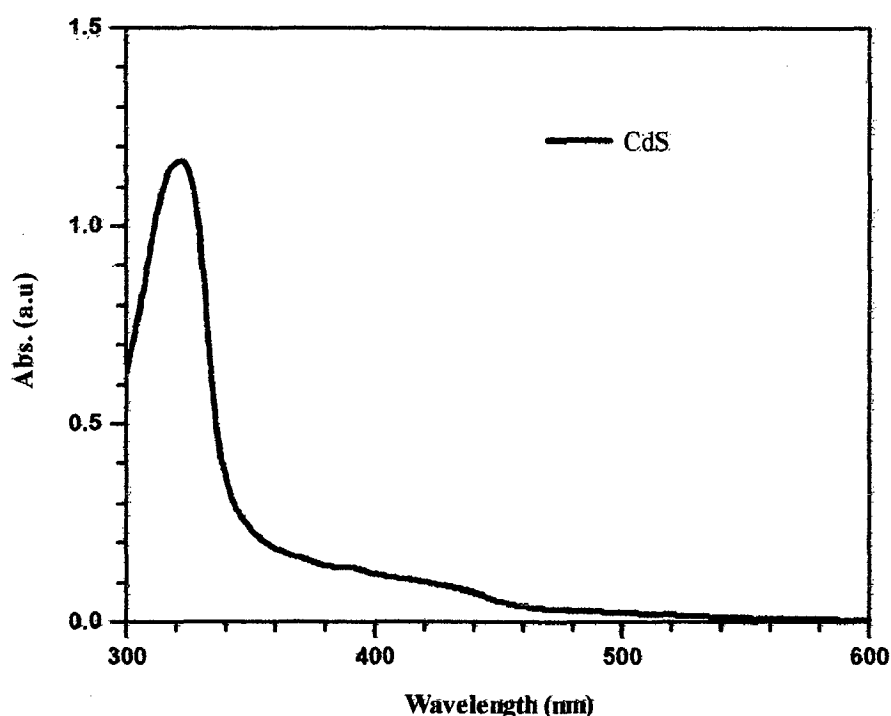


Figure 4.23 Absorbance spectrum of the blue emitting CdS quantum dots in DMF

Figure 4.23 shows the optical absorbance of the blue emitting colloidal CdS particles. We have measured the absorbance spectra of the dispersion in the range between 300-600 nm using *N, N*-dimethylformamide (DMF) as medium and observed an absorption peak at 320

nm.²⁶ It shows a blue shift when compared to that of the bulk CdS which absorbs at 512 nm.²⁸ Since there is a large blue shift in comparable to the bulk, it is considered to be due to the reduction of the particle size.²⁷ This clearly indicates the presence of quantum confinements in the reactions due to the proper controlling of nucleation growth.

4.4.2 Emission characteristics of the CdS colloids

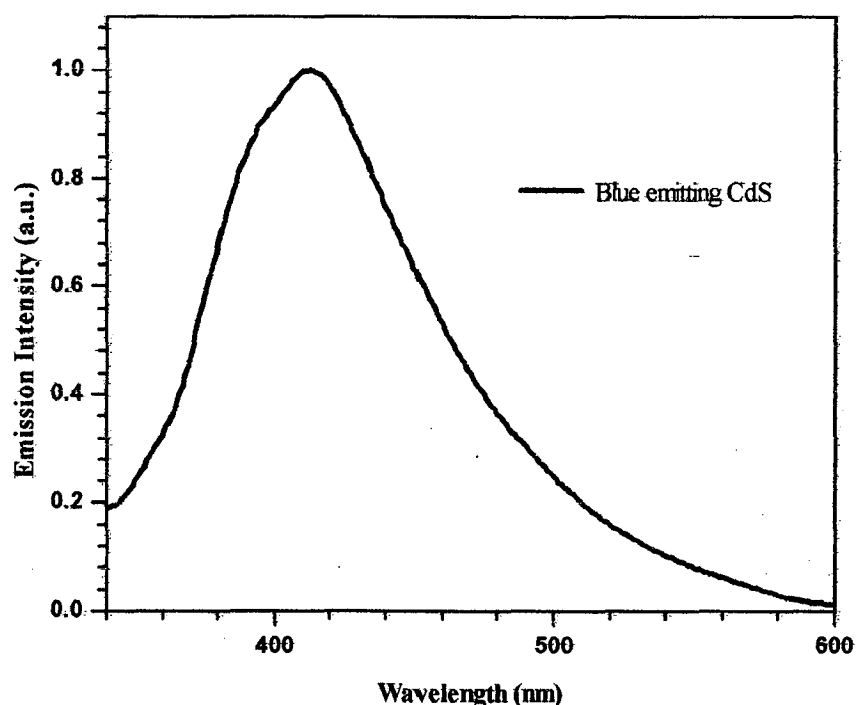


Figure 4.24 Emission spectrum of the blue emitting CdS quantum dots in DMF

The emission spectrum of the CdS colloids was measured in the range of 330-600 nm by exciting at 320 nm. Figure 4.24 shows the corresponding emission profile. The emission peak was observed at 412 nm with a considerable tailing in the lower energy side.²⁹ The emission color may be best described as blue.

4.4.3 FE-SEM analysis

FE-SEM was used to observe the morphology of the prepared colloidal CdS solution at different magnifications. Figure 4.25 shows that the particles are spherical in nature with the

size range of 50-200 nm and agglomerate each other due to aging factor.²⁷

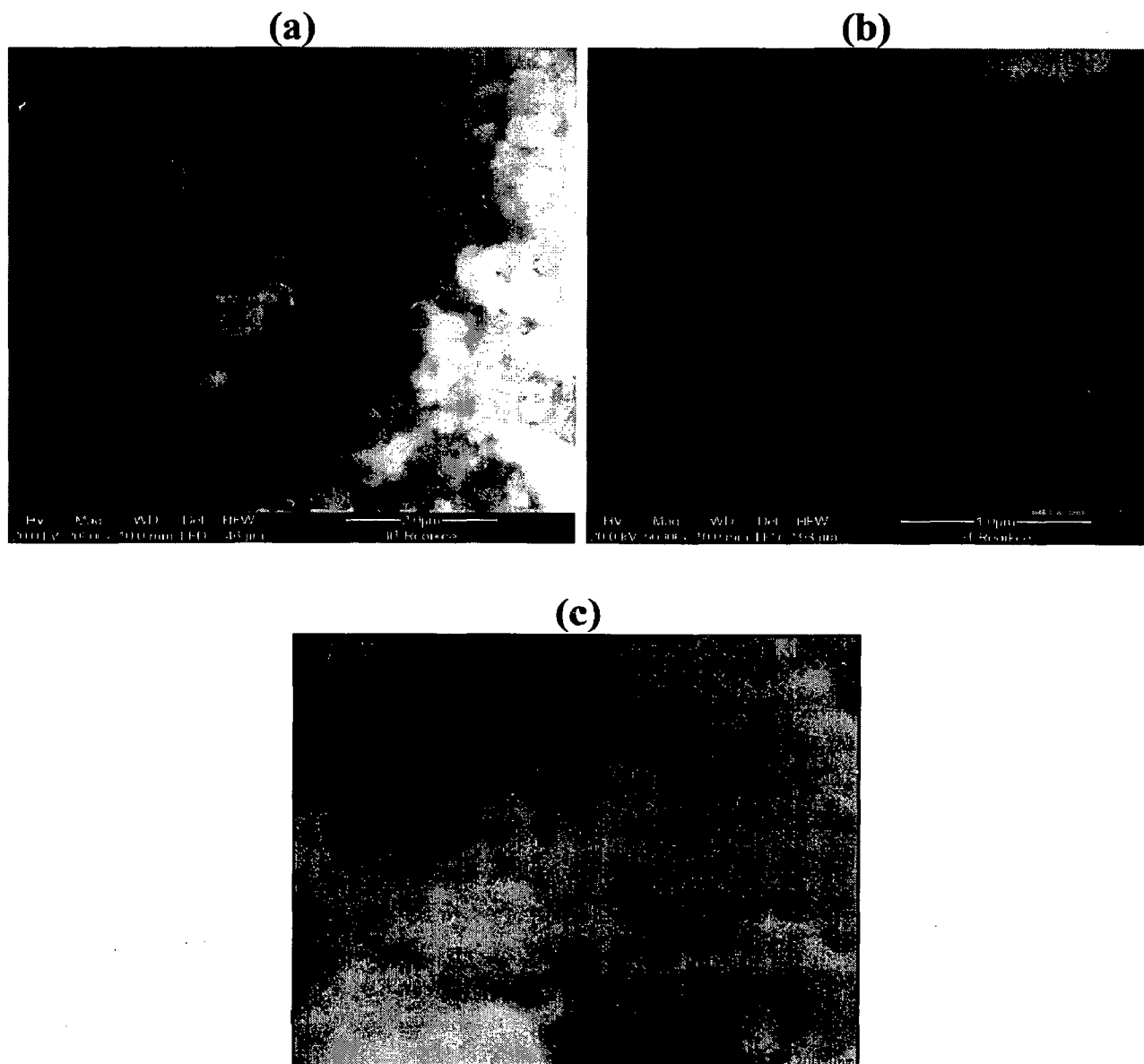


Figure 4.25 FE-SEM images of the blue emitting CdS quantum dots at magnification (a) 20,000X (b) 50,000X (c) 1,00,000X

4.5 Interaction of organic dyes with blue emitting CdS particles

Approximately 0.05 M of blue emitting CdS dispersions were interacted with 1%, 2% and 5% organic dyes (D1, D2, D3, and D4) in dimethylformamide and the changes in the emission spectra were monitored by fluorescence spectroscopy.³⁰ Addition of dye to the colloids completely quenches the emission of the colloidal particles. The emission from the

dye appears in the red-shifted region when compared to the bare dye. The extinction of emission due to colloidal CdS and appearance of the intense emission from the organic dyes indicate an efficient energy transfer from colloidal CdS to organic dyes. Also on increasing the concentration of the dye a gradual red shift in emission is observed (see Figures 4.26, 4.27 and 4.29). In the case of dye **D3**, the emission due to CdS colloids and the organic dye were observed (Figure 4.28). Peak at 412 nm is due to CdS and at 512 nm originates from the organic dye. This clearly indicates an inefficient energy transfer from the CdS to the organic dye. Energy transfer efficiency is largely dependent on the overlap of emission spectra of the donor with the absorption spectra of the acceptor. The absorption maximum observed for the dye **D3** is 340 nm which is significantly blue-shifted from the emission spectra of the CdS colloids and results in smaller overlap integral and less efficient energy transfer.

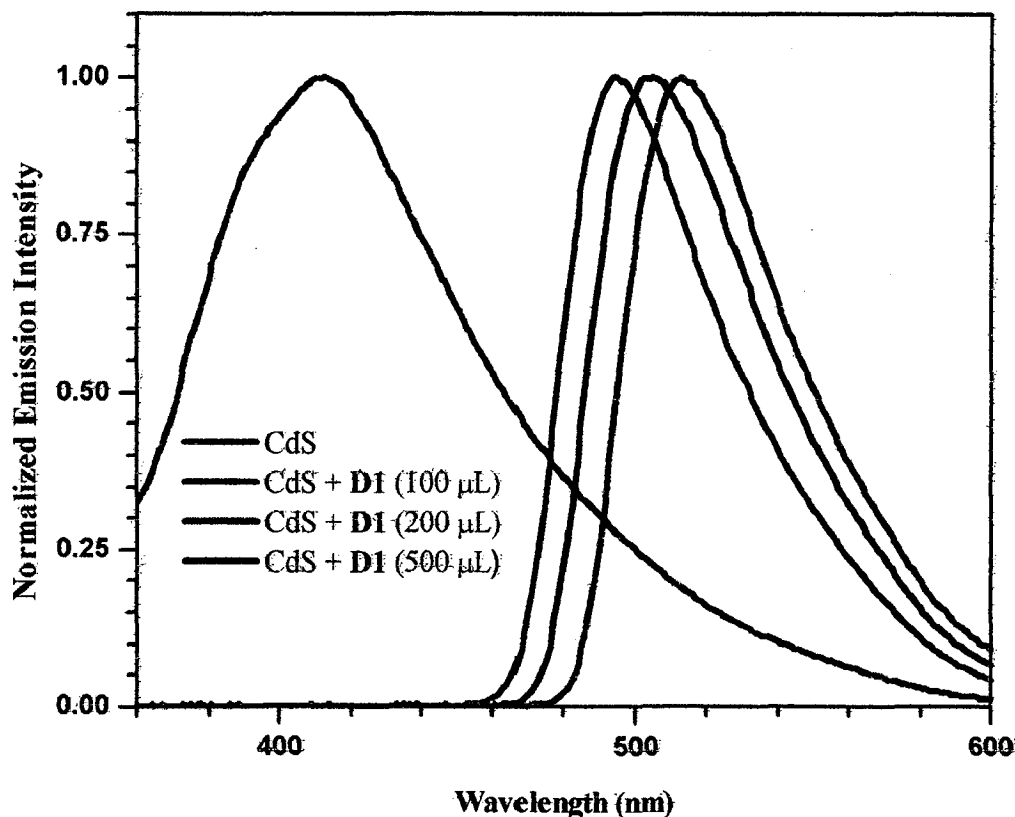


Figure 4.26 The emission spectra of the blue emitting CdS-D1 system.

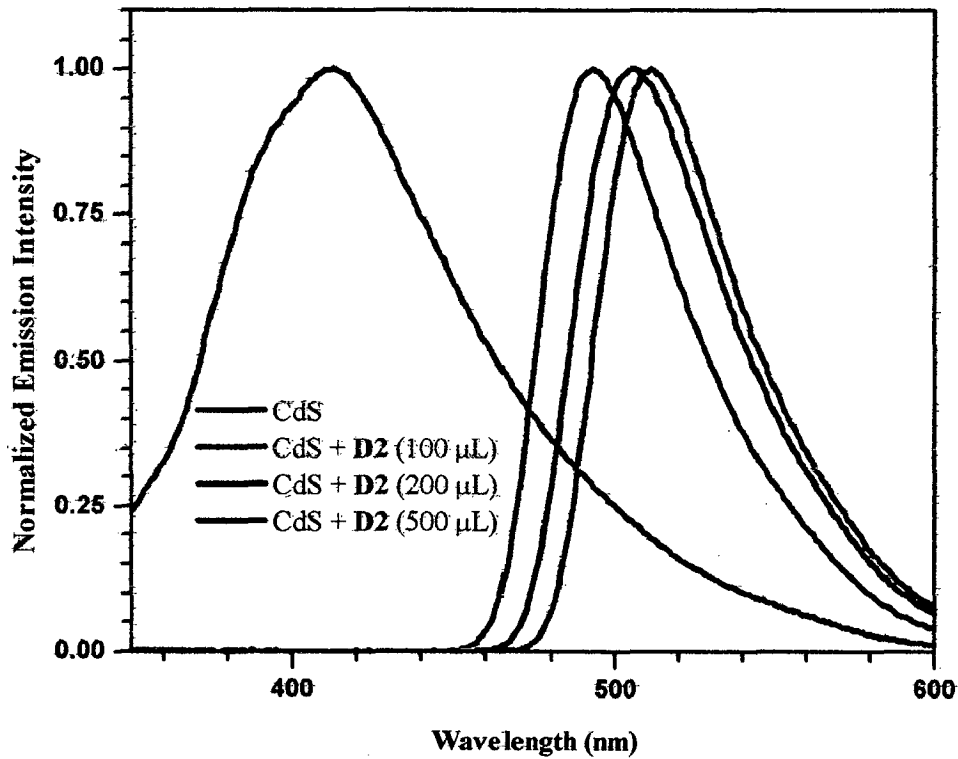


Figure 4.27 The emission spectra of the blue emitting CdS-D2 system.

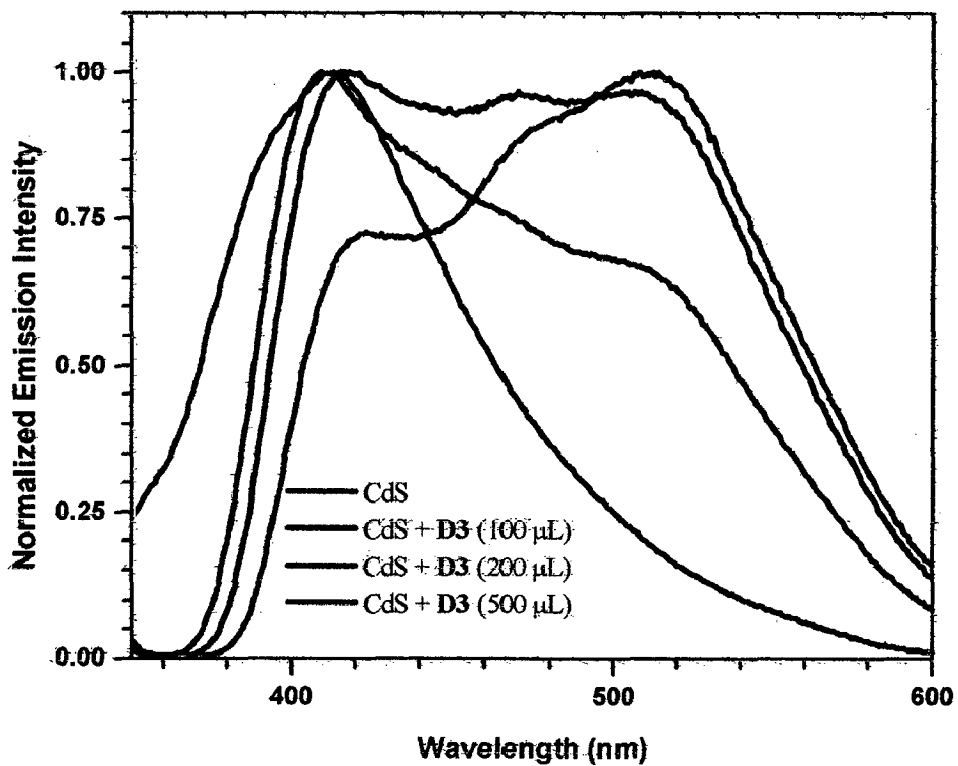


Figure 4.28 The emission spectra of the blue emitting CdS-D3 system.

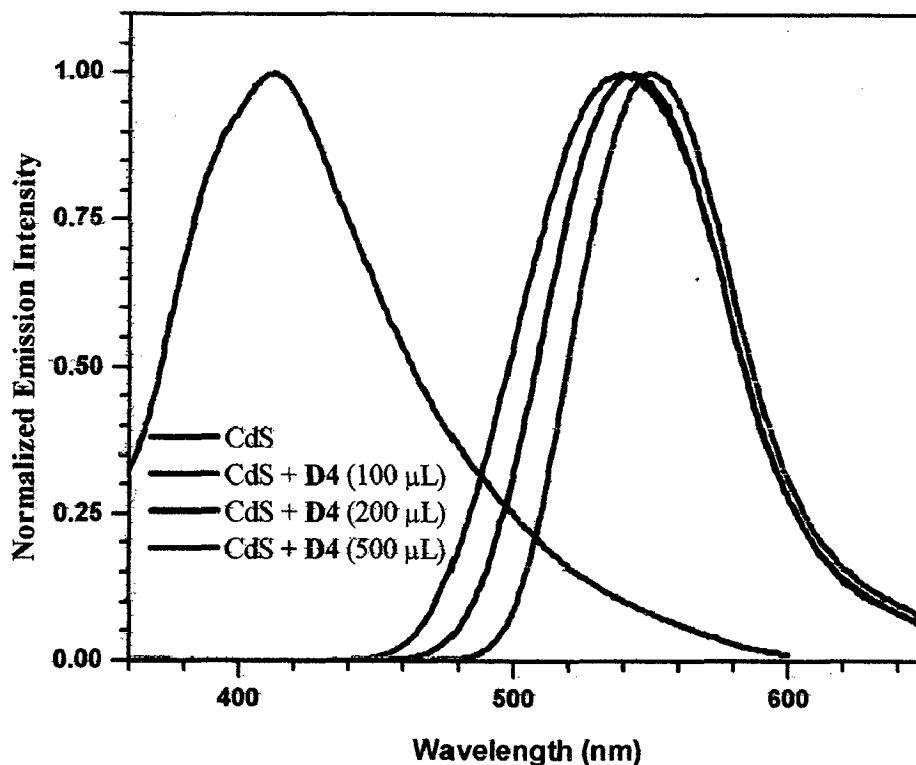


Figure 4.29 The emission spectra of the blue emitting CdS-D4 system.

Table 4.2 Emission data in DMF solution for blue emitting CdS + (D1-D4) mixtures.

Dye Conc.	1 %	2 %	5 %
System	λ_{\max} , nm	λ_{\max} , nm	λ_{\max} , nm
CdS-D1	494	503	513
CdS-D2	492	506	511
CdS-D3	410	416	422
CdS-D4	537	543	550

4.6 Synthesis and characterization of green emitting colloidal CdS

Cadmium chloride (0.75 g) and sulphur powder (0.12 g) were mixed in a round bottom flask with *N, N*-dimethylformamide (75 mL) and water (75 mL) and stirred for 30 min. The mixture was brought under nitrogen atmosphere by purging N_2 gas through it for 30 min. Under N_2 the mixture was heated at 120 °C for 6 h to obtain a green emitting colloidal solution.²⁷ The colloidal solution was used as such in the subsequent analysis.

4.6.1 Absorption characteristics of the green emitting CdS colloids

Figure 4.30 shows the optical spectra of the green emitting colloidal dispersion recorded in dimethylformamide. We measured the absorbance spectra in the range between 280-420 nm and observed a prominent peak at around 360 nm.²⁷ It shows a blue shift from that bulk CdS 530 nm,²⁸ however, a red shift when compared to that of the blue-emitting CdS colloids (*vide supra*). Since there is a large blue shift in comparison to the bulk, it is speculated to possess smaller particle size but higher than that of blue-emitting ones.

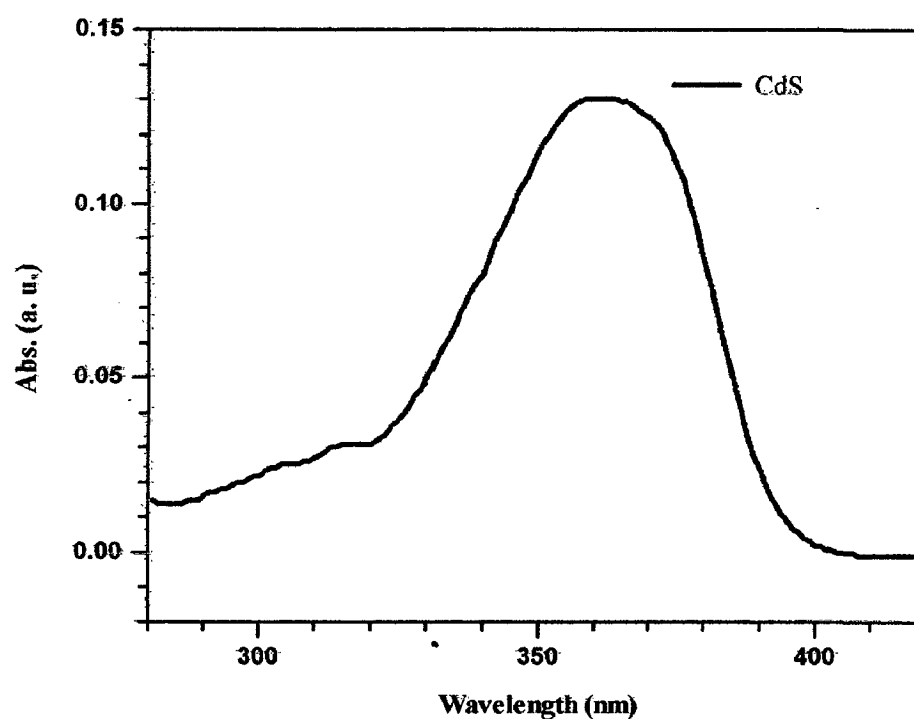


Figure 4.30 Absorbance spectra of green emitting CdS quantum dots in DMF.

4.6.2 Emission properties

The fluorescence spectrum of the CdS colloids was examined in the range of 370-600 nm. by exciting at 360 nm (Figure 4.31). The emission peak was observed at 442 nm with a

considerable broadening in the green region.³¹ The emission profile is 30 nm red-shifted when compared to the blue-emitting CdS colloids.

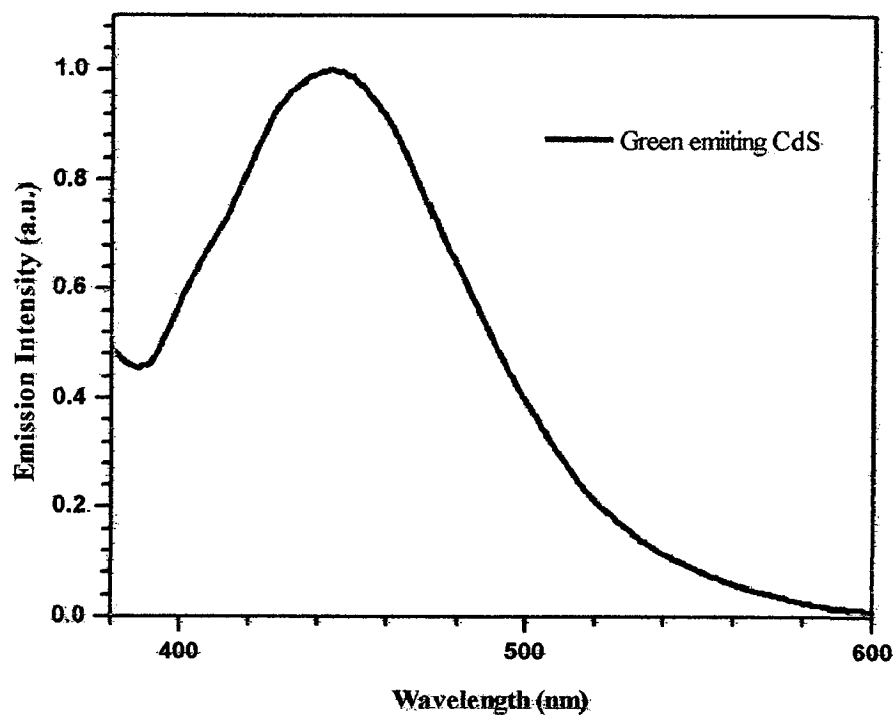


Figure 4.31 Emission spectra of the green emitting CdS quantum dots in DMF.

4.6.3 FE-SEM analysis

The green emitting CdS colloidal morphology was characterized by FE-SEM. Figure 4.32 shows that the particles are spherical and needle like in nature due to the variation in nucleation process, and the size ranges 100-500 nm due to agglomeration.²⁷



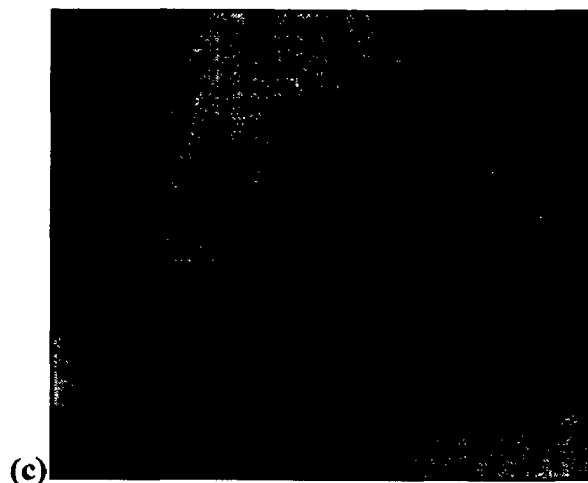


Figure 4.32 FE-SEM images of the green emitting CdS quantum dots at magnification (a) 20,000X (b) 50,000X (c) 1,00,000X

4.7 Interaction of organic dyes with green emitting CdS colloids

As the dyes studied in the present work except **D3** possess absorption profile overlapping with the emission profile of the green emitting CdS colloids, we have been interested in evaluating the energy transfer possibilities between these systems. The green emitting CdS colloids taken in dimethylformamide was treated with 1%, 2% and 5% organic dyes and their emission behavior studied by fluorescence spectroscopy. The emission data is presented in Table 4.3. The composites make a red shift due to the electron transfer from excited state dye molecules to the conduction band of colloidal CdS.³² There also occurs a red shift in the emission profile of the organic dye when the concentration of the dye was increased gradually increased to 5% as shown in the Figures 4.33, 4.34 and 4.36. However, for the **D3** and CdS mixtures a blue shifted emission profile was observed (Figure 4.35). The emission profile is reminiscent of CdS colloids rather than the dye species. It may be possible that the energy transfer from the organic dye to the CdS colloids occur in this system effectively. The above proposition is acceptable as there is sufficient overlap between the absorption spectra of the CdS colloid and the emission profile of **D3**.

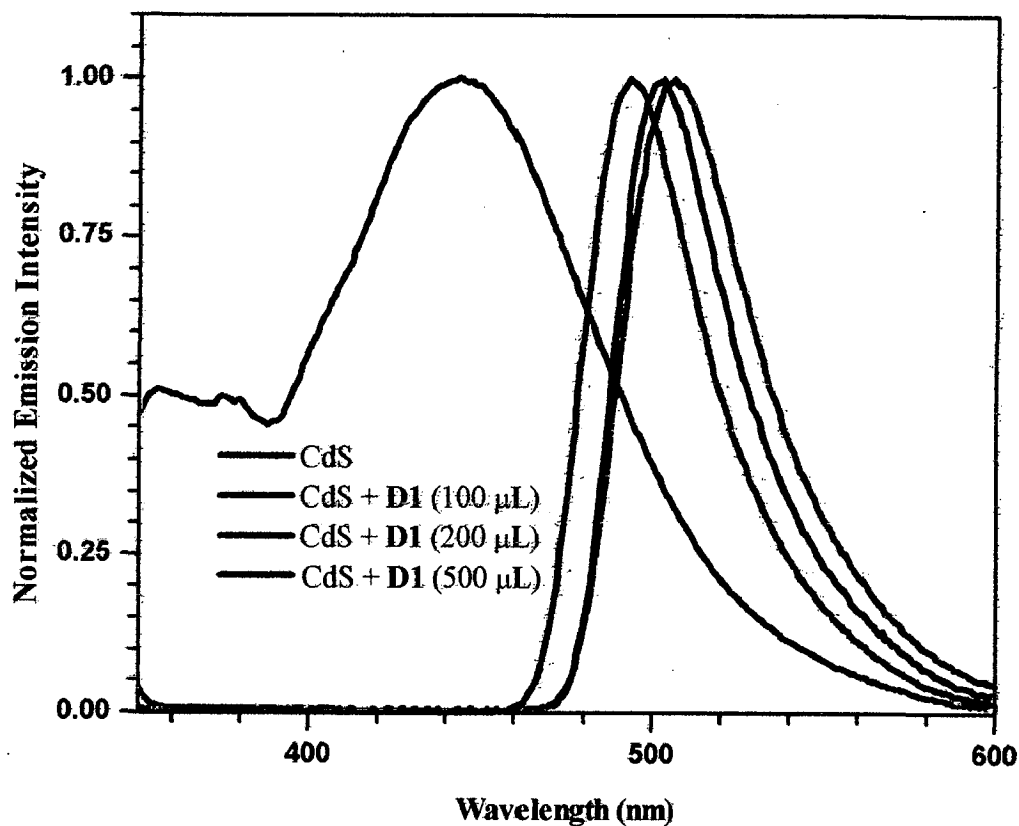


Figure 4.33 The fluorescence spectra of the green emitting CdS-D1 system.

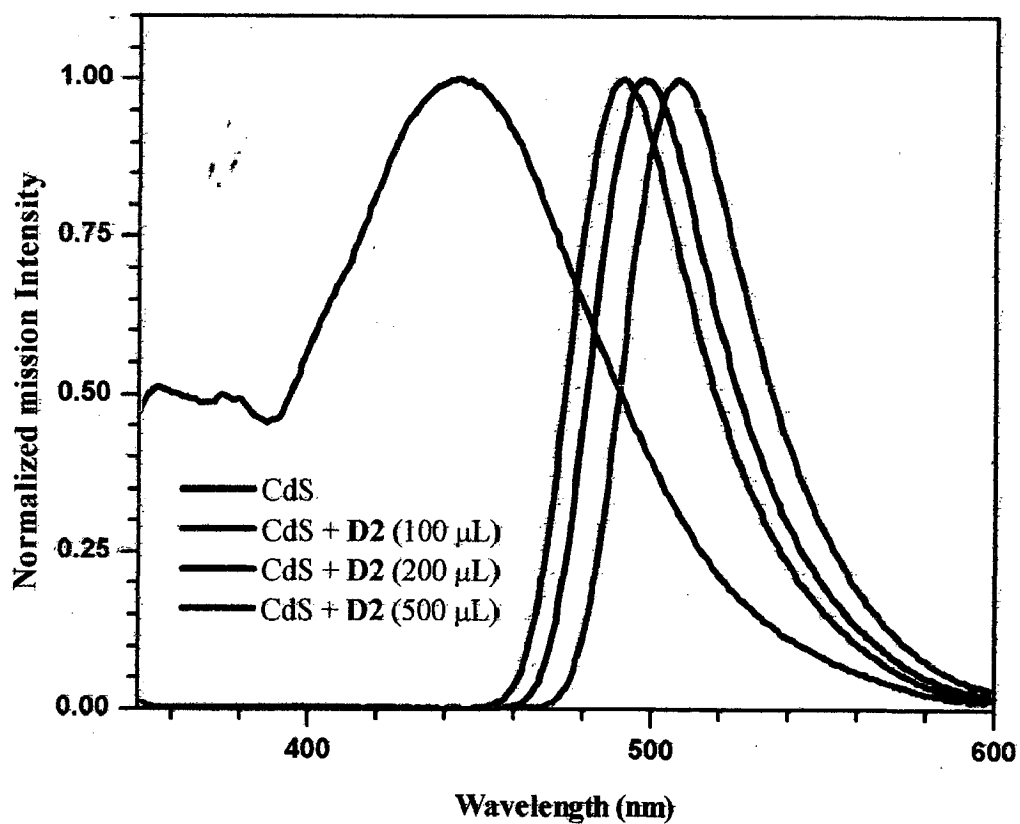


Figure 4.34 The fluorescence spectra of the green emitting CdS-D2 system.

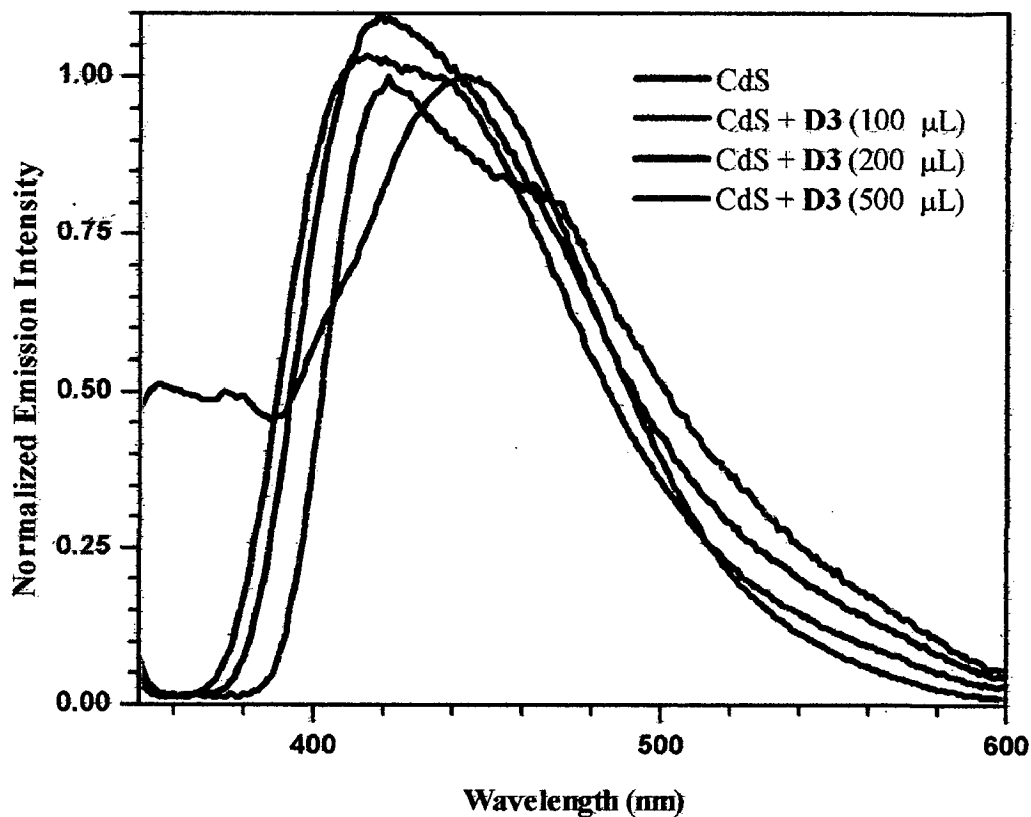


Figure 4.35 The fluorescence spectra recorded for the green emitting CdS-D3 mixture.

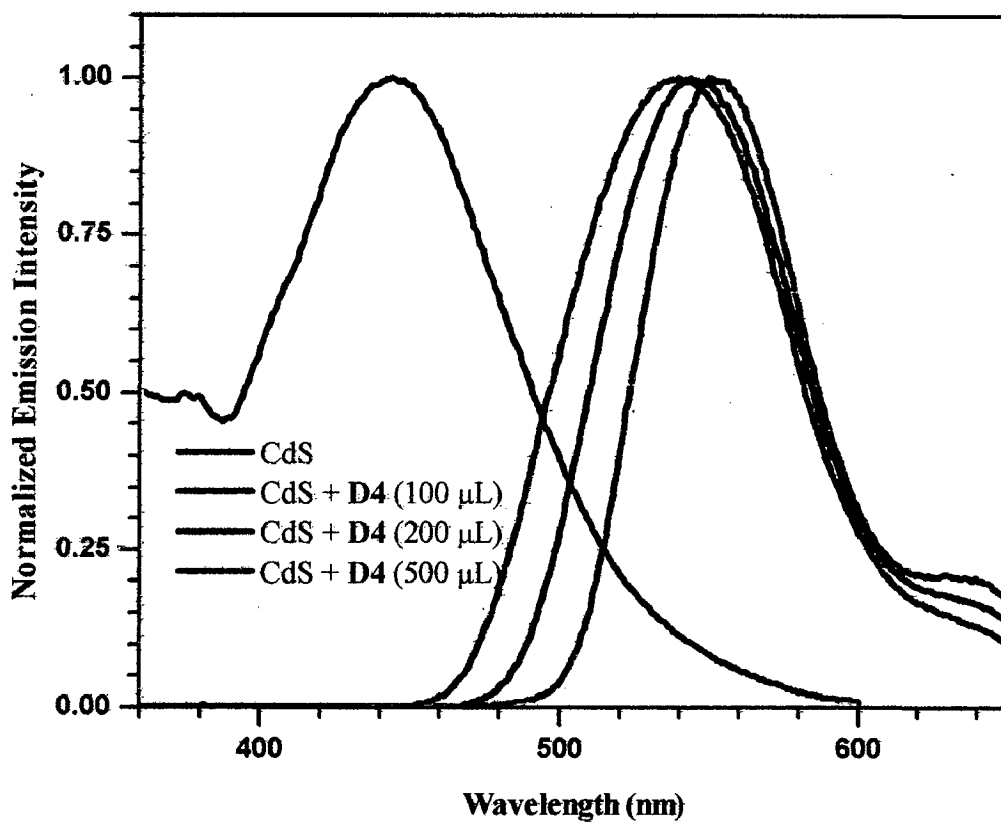


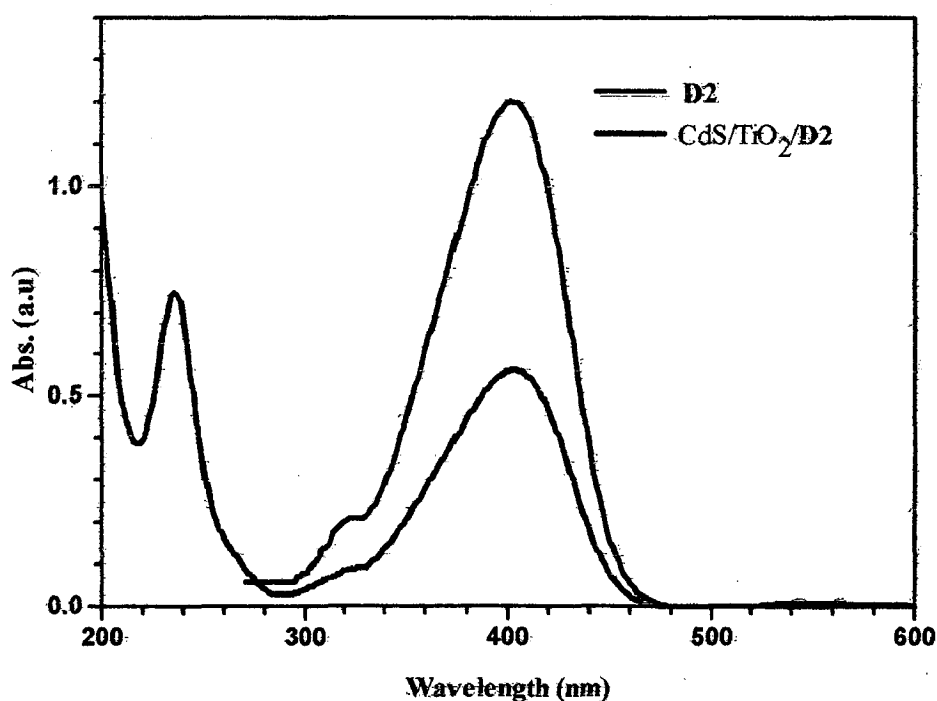
Figure 4.36 The fluorescence spectra of the green emitting CdS-D4 system.

Table 4.3 Emission data in DMF solution for green emitting (CdS + (D1-D4)).

Dye Content	1 %	2 %	5%
Compound	λ_{\max} , nm	λ_{\max} , nm	λ_{\max} , nm
CdS-D1	493	501	505
CdS-D2	490	496	507
CdS-D3	415	419	421
CdS-D4	539	544	551

4.8. Synthesis and characterization of CdS/TiO₂/D2 nanostructures

Cadmium sulphate (0.69 g) and anatase TiO₂ nanoparticles (10 mg) were mixed in a beaker. Then distilled water (25 mL) was added to this mixture and kept on stirring for 1 h. Then the pH of the solution was adjusted up to 10.5 by the addition of ammonia solution. A freshly prepared solutions of thiourea (0.069 g in 25 mL) in distilled water and dye D2 (100 mg in 25 mL) in methanol were added batch wise (2.5 mL × 10) to the above mixture sequentially. An orange emitting composite was formed, which was filtered and dried.

**Figure 4.37** Absorption spectra of the CdS/TiO₂/D2 composite and D2.

4.8.1 Absorption spectra

The absorbance spectra recorded for the organic dye **D2** and the composite CdS/TiO₂/**D2** in methanol is presented in Figure 4.37.³³ It shows a peak at 402 nm for the dye molecule and two distinctive peaks at 326 nm and 402 nm for the composite. From this it is clearly evident that the nanostructure includes the organic dye **D2** and CdS particles.

4.8.2 Emission properties

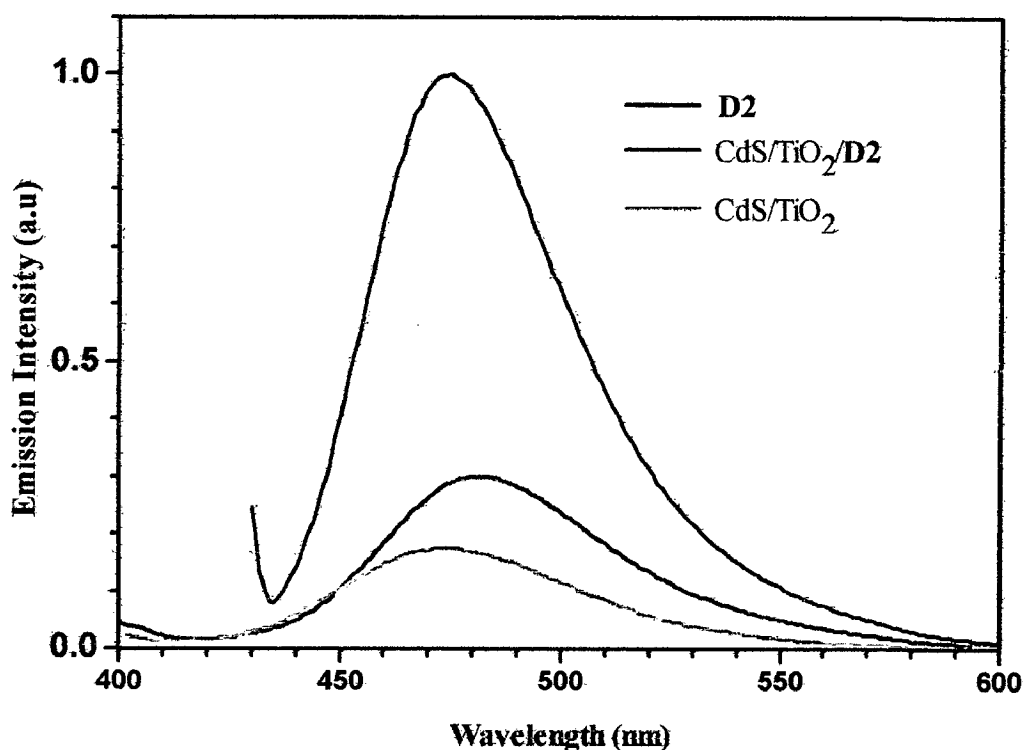


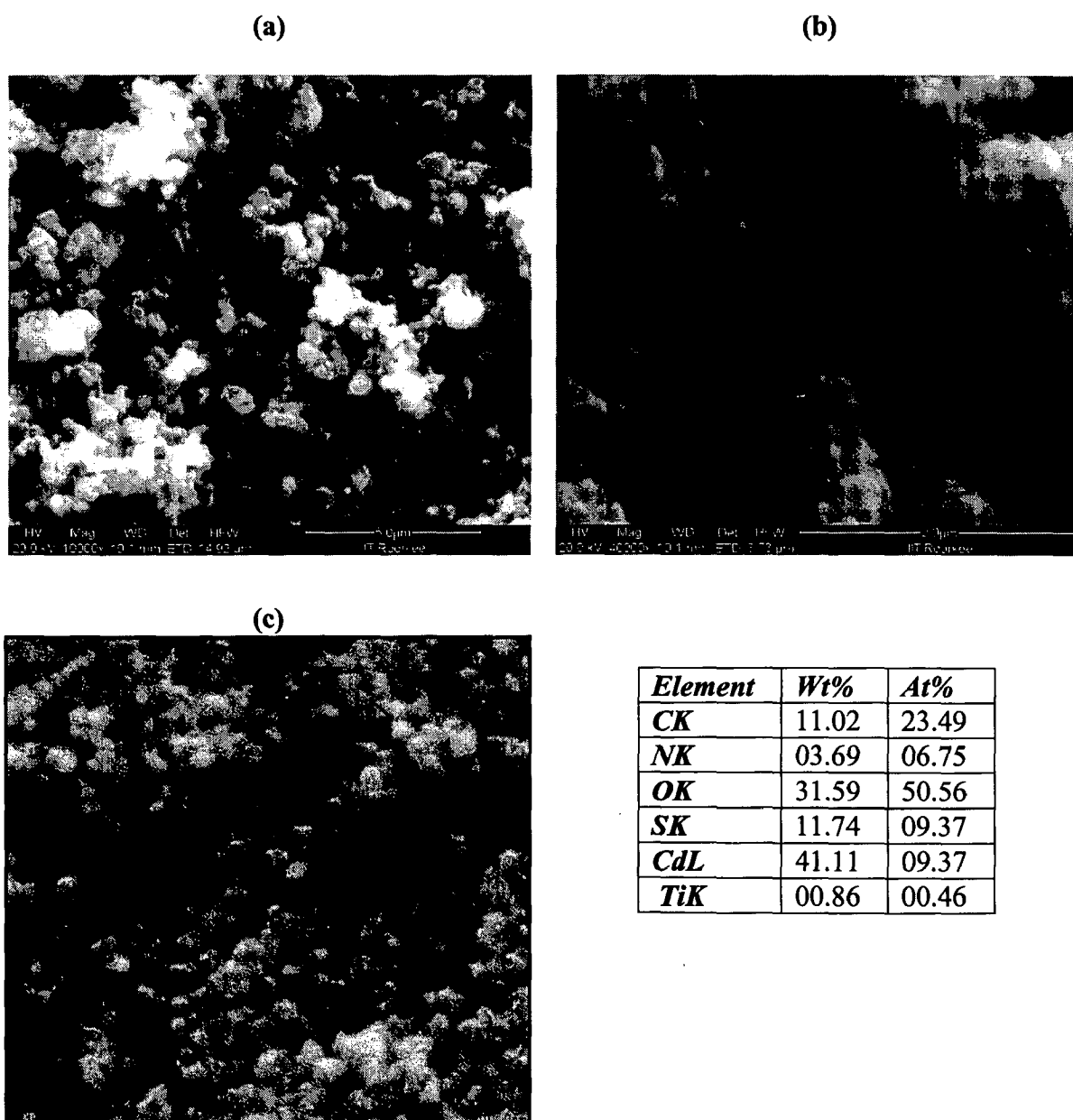
Figure 4.38 Emission spectra of CdS/TiO₂/**D2** composites.

The emission spectra recorded for the organic dye **D2** and the nanocomposites CdS/TiO₂ and CdS/TiO₂/**D2** are plotted in Figure 4.38. The dye **D2** shows an intense emission peaking at 472 nm while the nanocomposites derived from CdS and TiO₂ displays fluorescence profile centered at 336 nm. The emission of the nanocomposites probably originates from the CdS sites.³⁴ However the nanocomposites containing the organic dye **D2** exhibits a red-shifted emission profile at 483 nm. The red-shift in emission is attributed to the interaction of

the dye with the CdS sites rather than the TiO₂ sites. The interaction of TiO₂ with the organic dyes has been reported to result a blue-shift in emission due to the possible deprotonation of the carboxylic acid unit which would lead to a reduced acceptor strength.¹⁹

4.8.3 FE-SEM and EDAX analysis

The nanostructural characterization of the CdS-TiO₂ nanocomposites is carried out by scanning electron microscopy.³⁵ Figure 4.39 shows the FE-SEM image and EDAX spectrum of the CdS coupled TiO₂ nanocomposite structure.



(d)

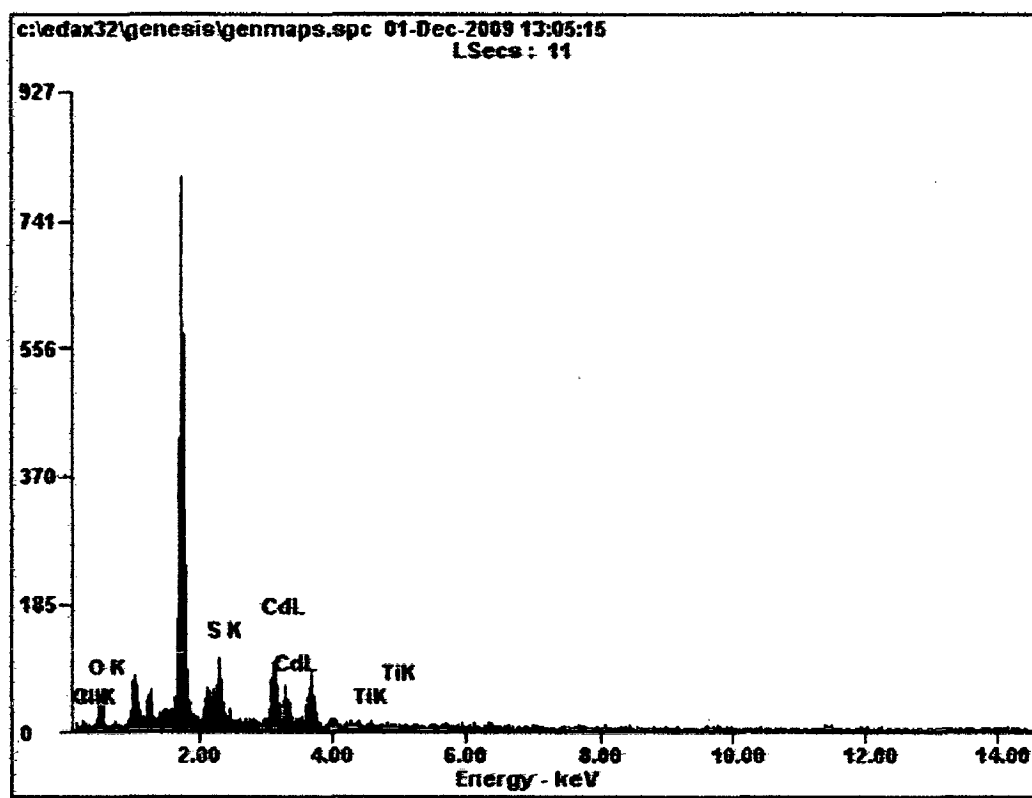


Figure 4.39 FE-SEM images (a) 10,000X (b) 40,000X (c) 1,00,00X and EDAX spectrum (d) of the CdS/TiO₂ composites.

Uniformity in the nucleation process yields homogeneous formation of particles as clearly noticed in the images with nano spherical shape of 40 nm. The atomic ratio of Cd and Ti in the nanocomposite structure was 9%:0.5% this is in agreement with the feed ratio in the synthetic procedure.

The CdS-TiO₂/Dye composites were characterized through the scanning electron microscopy and observed. The CdS-TiO₂/Dye composites exhibited generally a spherical morphology except for the one derived from the dye **D2**. The composites CdS/TiO₂/**D2** shows a change in morphology from spherical to fiber shape with a diameter of 50 nm due to the presence of lengthy alkyl group as shown in Figure 4.40. Other composites they do not

exhibit morphology changes as shown in Figure 4.41. Elemental analysis confirms the presence of organic edges coated on TiO_2/CdS composites.

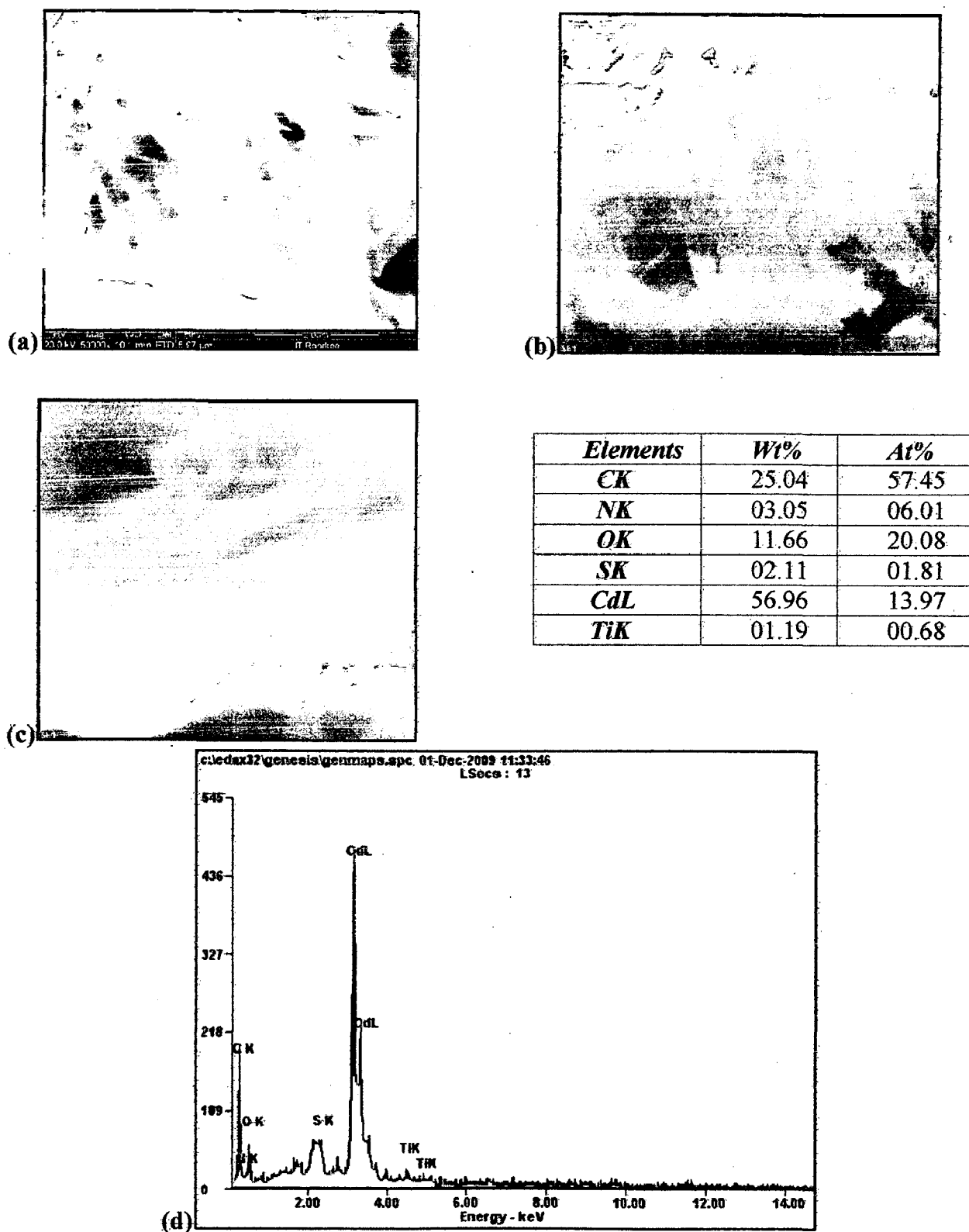


Figure 4.40 FE-SEM images (a) 50,000X (b) 70,000X (c) 1,00,00X and EDAX spectrum of $\text{CdS}/\text{TiO}_2/\text{D2}$ composites

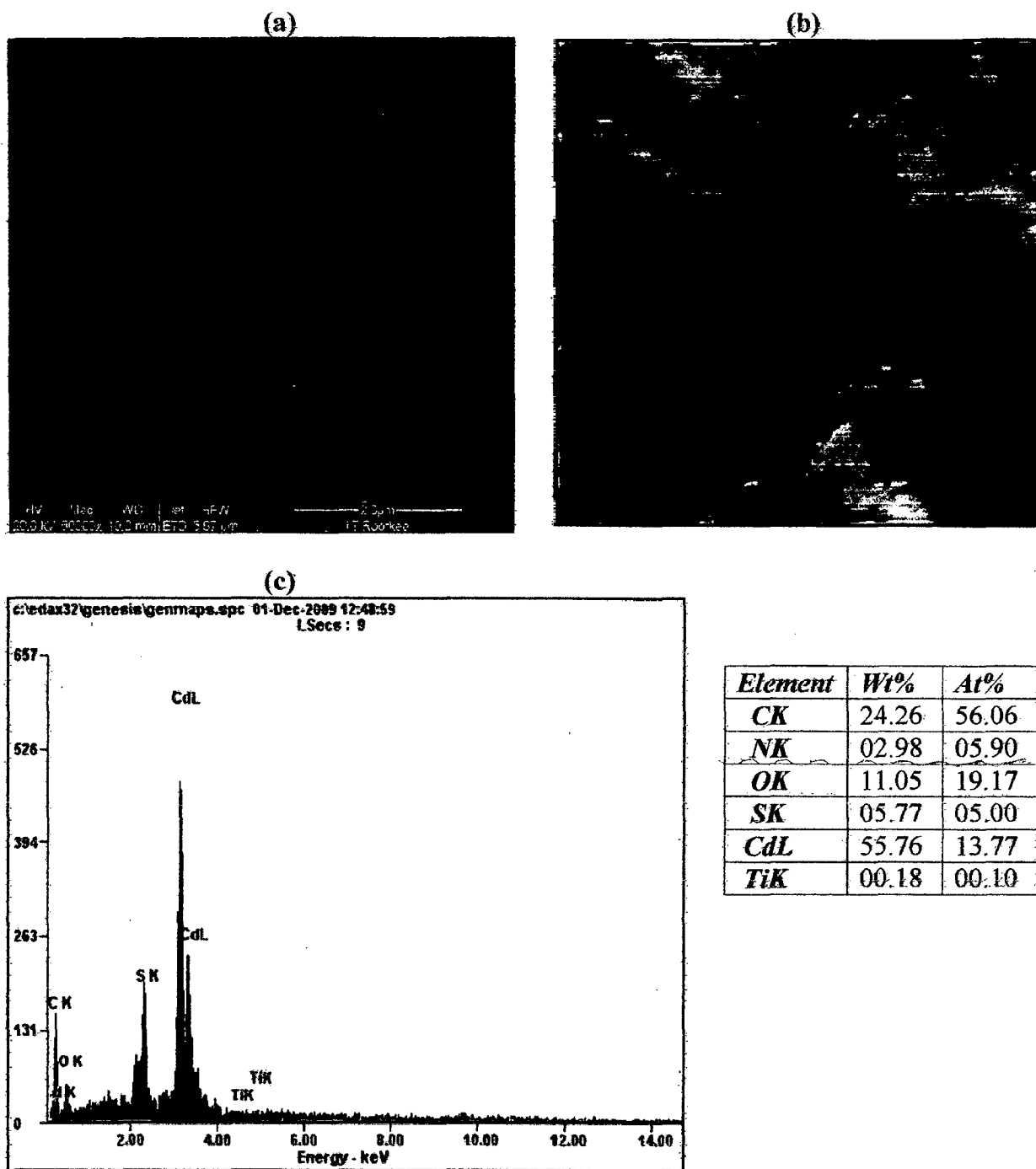


Figure 4.41 FE-SEM images (a) 50,000X (b) 70,000X (c) EDAX spectrum of CdS/TiO₂/D3 composites

4.9 Conclusions

We have successfully synthesized the semiconductor nanoparticles of anatase titanium dioxide and cadmium sulfide by simple chemical methods. Coating of the organic dyes with the semiconductor nanoparticles were also achieved by simple wet process. The

semiconductor nanoparticles and the organic dye coatings were thoroughly characterized by absorption and fluorescence spectroscopy, thermal, XRD, FE-SEM and EDAX analysis.

It has been observed that the organic dyes underwent photocatalytic degradations in the presence of TiO_2 on exposure to sun light. However dye coated TiO_2 nanostructures were accomplished by protecting the reaction mixtures from sun light. Dye **D₂** interacted with TiO_2 and induced a change in the morphology. The spherical shape of the TiO_2 nanoparticles changed to rod shape on inclusion of **D₂**. The change in the morphology may be due to presence of alkyl chain in the dye. The thermal decomposition temperature of the dye composites are higher than that of the parent dyes which indicates a firm interaction between the nanocrystalline TiO_2 and the organic dyes.

As the emission spectra of the CdS nanostructures are overlapping with the absorption profile of the dyes (**D1**, **D2** and **D4**) an efficient energy transfer from CdS to the organic dye was observed in solution. Additionally the emission due to the organic dye red-shifted slightly when compared to that of the parent dyes which indicate a chemical interaction between CdS and organic dyes. Further the red-shift observed on increasing the organic dye concentration may be due to the aggregation of the dyes on the CdS surface. As the absorption profile of **D3** is not overlapping with the emission profile of CdS no energy transfer occurred between them. The solid state structures of the CdS/ TiO_2 /**D2** composites showed a change from homogeneous spherical to fiber shape again supporting the possible role of the ethyl chains.

4.10 References

1. Kamat, P. V. *J. Phys. Chem. C* **2008**, *112*, 18737-18753.
2. Robel, I.; Subramanian, V.; Kuno, M.; Kamat, P. V. *J. Am. Chem. Soc.* **2006**, *128*, 2385-2393.
3. Ramsden, J. J.; Gratzel, M. *Faraday Trans.* **1987**, *80*, 919-933.

4. Rossetti, R.; Nakahara, S.; Brus, L. E. *J. Chem. Phys.* **1983**, *79*, 1086-1088.
5. Alivisatos, A. P. *Science* **1996**, *271*, 933-937.
6. Rajh, T.; Nedeljkovic, J. M.; Chen, L. X.; Poluektov, O.; Thurnauer, M. C. *J. Phys. Chem. B* **1999**, *103*, 3515-3519.
7. Caruso, F. *Adv. Mater.* **2001**, *13*, 11-17.
8. Torimoto, T.; Yamashita, M.; Kuwabata, S.; Sakata, T.; Mori, H.; Yoneyama, M. *J. Phys. Chem. B* **1999**, *103*, 8799-8803.
9. Dubertret, B.; Calame, M.; Libchaber, A. J. *Nat. Biotech.* **2001**, *19*, 365-370.
10. Hahlin M.; Johansson, M. J.; Plogmaker, S.; Odelius, M.; Hagberg, D. P.; Sun, L.; Siegbahn, H.; Rensmo, H. *Phys. Chem. Chem. Phys.* **2010**, *12*, 1507-1517.
11. Deki, S.; Aoi, Y.; Hiroi, O.; Kajinami, A. *Chem. Lett.* **1996**, *25*, 433-437.
12. Rajesh J. T.; Ramchandra, Kulkarni, G.; Raksh. V. J. *Ind. Eng. Chem. Res.* **2006**, *45*, 922-927
13. Hoffmann, J.; Lubbers, D.W.; Heise, H. M. *Phys. Med. Biol.* **1998**, *43*, 3571-3587.
14. Choi, T. Y.; Umebayashi, M.; Yoshikawa. *J. Mater. Sci.* **2004**, *39*, 1837-1839.
15. Kuang, D. B.; Wenger, B.; Klein, C.; Moser, J. E.; Humphry-Baker, R. *J. Am. Chem. Soc.* **2006**, *128*, 4146-4154.
16. Wu, T.; Hsiu-sao, M.; Chen, F. L.; Su, G. S.; Chang, W. C.; Wang, P. H.; Lin, C. Y.; Ou-Yang, W. C.; Sun, W. I. *J. Molec. Sci.* **2010**, *11*, 329-353.
17. Daniel, P. H.; Edvinsoon, T.; Marinado, T.; Boschloo, G.; Hagfeldt, A.; Sun, L. *Chem. Commun.* **2006**, *66*, 2245-2247.
18. Moon, J. S.; Yum, H. J.; Humphry-Baker, R.; Karlsson, M. K.; Daniel, P. H.; Marinado, T.; Hegfeldt, A.; Sun, L.; Gratzel, M.; Nazeeruddin, K. *J. Phys. Chem.* **2009**, *113*, 16816-16820.
19. Yuan, L.; Xurui, X.; Dongshe, Z.; Puhui, X.; Baowe, Z. *Chinese Sci. Bull.* **2003**, *48*, 856-858.
20. Baheti, A.; Tyagi, P.; Thomas, K. R. J.; Hsu, Ying-Chan.; Lin, J. T. *J. Phys. Chem. C* **2009**, *113*, 8541-8547.
21. Brune, A.; Jeong, G.; Liddell, P.; Sotomura, T.; Moore, T. A.; Moore, A. L.; Gust, D. *Langmuir* **2004**, *20*, 8366-8371.
22. Ziel, B.; Grzechulska, J.; Morawski, A. W. *J. Photoch. Photobio. A* **2003**, *157*, 65-70.
23. Ch, W.; Chang, H. W.; Chern, J. M. *J. Hazard. Mater.* **2006**, *137*, 336-343.
24. Yusoff, N. H.; Salleh, M.; Yahaya, M. *Sol. Sci. Technol.* **2008**, *16*, 63-74.

25. Mekprasart, W.; Jarembon, W.; Pecharapa, W. *Mater. Sci. Eng.* **2009**, *18*, 557-562.
26. Castillero, P.; Sanchez-Valencia; Cano, M.; Pedrosa, J. M.; Roales, J.; Barranco, A.; Gonzalez-Eelipe, A. R. *Appl. Mater. Interfaces.* **2010**, *2*, 712-721.
27. Khanna, P. K.; Subbarao, V. V. V. S. *Mater. lett.* **2004**, *58*, 2801-2804.
28. King, R. B. *Encyclopedia of inorganic compounds*, Wiley, **1994**.
29. Datta, A.; Chatterjee, S.; Sinha, A. K.; Bhattacharyya, N. S.; Saha, A. *J. Lumin.* **2006**, *121*, 553-560.
30. Jhonsi, A. M.; Kathiravan, A.; Renganathan, R. *J. Mol. Struct.* **2009**, *921*, 279-284.
31. Chowdhury, P. S.; Sen, P.; Patra, A. *Chem. Phys. Lett.* **2005**, *413*, 311-314.
32. Jhonsi, A. M.; Kathiravan, A.; Renganathan, R. *Spectrochim. Acta* **2008**, *71*, 1507-1511.
33. Vasileia, M.; Antoniadou, D. M.; Puma, G.; Kondarides, D. I.; Lianos, P. *Environ. Sci. Technol.* **2010**, *14*, 185-192.
34. Lee, J.; Kim, T. G.; Lee, W.; Han, S.; Sung, Y. M. *Cryst. Growth. Des.* **2009**, *9*, 4519-4523.
35. Yin, Y.; Jin, Z.; Hou, F. *Nanotechnology* **2007**, *18*, 495-501.

Chapter 5

Summary

We have synthesized and characterized composites of TiO_2/Dye , CdS/Dye , and $\text{CdS}/\text{TiO}_2/\text{Dye}$ which are useful for application in solar cells. The conjugates were characterized by different techniques like absorption spectroscopy, fluorescence spectroscopy, X-ray diffraction, field emission scanning electron microscopy, and TGA- DTA analysis.

The anatase TiO_2 nanoparticles were synthesized by a simple hydrolysis method. The XRD pattern of anatase TiO_2 nanoparticles showed the materials are in nanometric size and the FE-SEM confirms that the sizes of nanoparticles around 80 nm. We made composites of TiO_2/Dye by coating of organic dyes (**D1**, **D2**, **D3**, and **D4**) on TiO_2 nanoparticles and evaluate their interaction. Dye **D2** interacted with TiO_2 and induced a change in the morphology. The spherical shape of the TiO_2 nanoparticles changed to rod shape on inclusion of **D2**. The change in the morphology may be due to presence of alkyl chain in the dye. Thermal studies were performed and found that the stability of each composite is higher than that of parental dyes which indicates the presence of anatase TiO_2 nanoparticles.

Also, we have synthesized blue and green emitting CdS colloidal particles of sizes around 60 nm and studied their effects with organic dyes (**D1**, **D2**, **D3** and **D4**). As the emission spectra of the CdS nanostructures are overlapping with the absorption profile of the dyes (**D1**, **D2** and **D4**) an efficient energy transfer from CdS to the organic dye was observed in solution. Also the dyes are chemically interacting with the CdS nanostructures. This was confirmed by the slight red-

shift observed for the emission originating from the dyes. Further the red-shift observed on increasing the organic dye concentration may be due to the aggregation of the dyes on the CdS surface. As the absorption profile of **D3** is not overlapping with the emission profile of CdS no energy transfer occurred between them.

The composite CdS-TiO₂/**D2** was formed by co-precipitation technique. A change from homogeneous spherical (CdS-TiO₂) to fiber shape (CdS-TiO₂/**D2**) was observed which again supports the possible role of the ethyl chains in nucleation.